LEANDRO SOUZA PINHEIRO DA SILVA

NONLINEAR STOCHASTIC ANALYSIS OF WAVE ENERGY CONVERTERS VIA STATISTICAL LINEARIZATION

São Paulo

2019

LEANDRO SOUZA PINHEIRO DA SILVA

NONLINEAR STOCHASTIC ANALYSIS OF WAVE ENERGY CONVERTERS VIA STATISTICAL LINEARIZATION

Master's Thesis presented to the Polytechnic School of the University of São Paulo to obtain the title of Master of Science.

São Paulo
2019

LEANDRO SOUZA PINHEIRO DA SILVA

NONLINEAR STOCHASTIC ANALYSIS OF WAVE ENERGY CONVERTERS VIA STATISTICAL LINEARIZATION

Master's Thesis presented to the Polytechnic School of the University of São Paulo to obtain the title of Master of Science.

Concentration Area:

Hydrodynamic, Dynamic and Control of Ocean systems.

Supervisor:

Helio Mitio Morishita

São Paulo
2019

Catalogação-na-publicação

ACKNOWLEDGMENTS

"Seja você quem for, seja qual for a posição social que você tenha na vida, a mais alta ou a mais baixa, tenha sempre como meta muita força, muita determinação e sempre faça tudo com muito amor e com muita fé em Deus, que um dia você chega lá. De alguma maneira você chega lá."

-- Ayrton Senna

RESUMO

Fontes renováveis de energia desempenham um papel fundamental para atender o constante aumento da demanda de energia global. Os principais objetivos em utilizar energias renováveis são reduzir os aspectos negativos associados à utilização de combustíveis fósseis e diversificar a matriz energética. Entre as fontes renováveis, a energia das ondas oceânicas permanece insuficientemente explorada e tem a capacidade de contribuir para a produção de energia. O uso de energia das ondas tem sido promovido devido à grande e densa quantidade de energia e a regularidade na distribuição de energia. A idéia de coletar a energia das ondas existe há pelo menos dois séculos. No entanto, a extração começou principalmente após a crise do petróleo da década de 1970. Desde então, vários conversores de energia das ondas foram criados sem um design predominante, e espera-se que mais conceitos sejam criados.

Os desafios em projetar dispositivos de conversão da energia das ondas ocorre devido à dinâmica desse sistema e da natureza estocástica dos esforços ambientais. Como o dispositivo é normalmente configurado para operar próximo às condições de ressonância, os dispositivos de energia das ondas exibem grandes deslocamentos e as forças não lineares aumentam a sua contribuição na dinâmica do sistema. Com base nisto, a análise de conversores de energia das ondas é geralmente realizada usando modelos no domínio do tempo para incluir os efeitos não lineares. No entanto, o custo computacional associado a essas simulações é alto quando comparado aos modelos tradicionais no domínio da frequência. Além disso, várias condições de carregamento são necessárias para avaliar a resposta do corpo devido às características estocásticas das ondas do oceano, tornando-se indesejável a realização de simulações no domínio do tempo.

A seguinte tese enfoca na análise estocástica de conversores de energia das ondas no domínio da frequência utilizando a linearização estatística para avaliar os efeitos das forças não lineares. A técnica empregada neste trabalho oferece uma estimativa rápida e confiável da dinâmica do dispositivo. Dois conversores de energia das ondas conceitualmente diferentes são investigados: um absorvedor pontual, e uma coluna de água oscilante. Os resultados obtidos usando a linearização estatística são comparados com os seus equivalentes modelos no domínio do tempo para verificar a confiabilidade da técnica. Uma boa concordância foi obtida entre as simulações de linearização estatística e de domínio de tempo em termos de distribuição da resposta, densidade espectral, valores médios e potência média absorvida. No entanto, o custo computacional associado às simulações no domínio do tempo foi notavelmente superior à da linearização estatística como esperado. Portanto, a técnica aplicada nesta tese oferece uma abordagem valiosa para ser usada como uma ferramenta de projeto para dispositivos de energia das ondas e procedimentos de otimização para desenvolver o setor de energia das ondas.

Palavras-Chave – Energia das Ondas, Análise Estocástica, Linearização Estatística, Dinâmica Não Linear, Domínio da Frequência.

ABSTRACT

Renewable sources of energy play a fundamental role to attend the constant rising in the global energy demand. The main objectives of utilizing renewable energies are to reduce the negative aspects associated with the utilization of fossil fuels and to diversify the energy mix. Among the renewable sources, ocean wave energy remains insufficiently explored and have the capacity to contribute to energy production. The use of wave energy has been promoted due to the vast and dense amount of energy and regularity in power distribution. The idea of harvesting wave energy exists for at least two centuries. However, it mostly started after the oil crisis of the 1970s. Since then, several wave energy converters were created without a predominant design, and more concepts are expected to be created.

The challenges in the designing of wave energy converts rely on the dynamics of such systems and the stochastic nature of the environmental loads. As the device is usually set to operate near resonant conditions, wave energy devices exhibit large displacements, and nonlinear forces rise in the dynamics of the system. In this regard, the analysis of wave energy converters is usually conducted using time domain models to include the nonlinear effects. However, the computational cost associated with these simulations is high compared to traditional frequency domain models. In addition, several load conditions are necessary to evaluate the body response due to the stochastic characteristics of ocean waves, becoming undesirable to conduct time domain simulations.

This thesis focuses on the stochastic analysis of wave energy converters in the frequency domain using the statistical linearization to evaluate the effects of nonlinear forces. The technique employed in this work offers a fast and reliable estimation of the device dynamics. Two conceptually different wave energy converters are investigated: a point absorber, and an oscillating water column. The results obtained using the statistical linearization are compared with their equivalent time domain models to verify the reliability of the technique. The results obtained show a good agreement was obtained between the statistical linearization and time domain simulations in terms of response distribution, power spectrum density, mean offsets, and mean power absorbed. However, the computational cost associated with time domain simulations was remarkably superior to the statistical linearization as expected. Therefore, the technique applied in this thesis offers a valuable approach to be used as a design tool for wave energy devices, and optimization procedures to develop the wave energy sector.

Keywords – Wave Energy, Stochastic Analysis, Statistical Linearization, Nonlinear Dynamics, Frequency Domain.

LIST OF FIGURES

LIST OF TABLES

NOMENCLATURE

BEM	Boundary Element Method
CWR	Capture Width Ratio
FD	Frequency Domain
ISSC	International Ship Structures Congress
JONSWAP	Joint North Sea Wave Project
MDOF	Multi-Degrees-Of-Freedom
OWC	Oscillating Water Column
PA	Point Absorber
PDF	Probability Density Function
PM	Pierson-Moskowitz
PSD	Power Spectrum Density
PTO	Power-Take-Off
RAO	Response Amplitude Operator
SL	Statistical Linearization
TD	Time Domain
WEC	Wave Energy Converter

CONTENTS

PART I

INTRODUCTION

1   INTRODUCTION

From the economic development of countries to the quality of life of their citizens, energy drives modern society. The importance of energy is reflected in the global energy demand, which increased dramatically over the past decades and continues to rise [1]. Currently, a large amount of energy comes from fossil fuels, such as coal, oil, and natural gas. The excessive use of these fossil fuels as a source of energy has led some negative impact on the environment, ranging from the exhaustion of natural sources to air pollution, greenhouse effect, and the rise of the Earth's mean surface temperature [2]. Those adverse effects have encouraged several countries to search for sustainable sources of energy to reduce environmental impacts [3]. As a result, the energy industries and scientific communities have investigated new technologies based on renewable sources.

Renewable sources have demonstrated a feasible alternative with several advantages. Currently, the power generated from renewable sources represents approximately 10% of the total [1]. A considerable amount of this percentage comes from the past decade, which demonstrated the social acceptance and viability of renewable technologies as an alternative source of energy. There are several types of renewable sources, being the most common the solar, hydro, wind, biomass, wave, tidal. The main advantages of them range from their environmentally friendly characteristics to the vast amount of energy. Also, the use of renewable sources can diversify the energy mix and increase the reliability in the electric power supply. Within the renewable sources, ocean waves remain insufficiently explored and possess a considerable capacity to contribute to global energy production [4], in which the south of Brazil possess a good energy potential with low seasonal variations [5].

Ocean waves are a concentrated form of solar power with a substantial amount of energy. As the sun irradiates the earth's surface producing a differential heating, it generates thermal air currents. Those air currents exert tangible stress on the ocean surface resulting in a rapidly variable shear and pressure fluctuations, which transfer part of the wind energy to the ocean in the form of waves [6]. Figure 1.1 illustrates

the process of ocean waves being generated by the wind. The magnitude of ocean wave energy depends on the wind velocity, contact distance, and time interval [5]. As the energy transfer is accumulated during long distances, waves have a substantial amount of energy. According to recent estimations, the ocean wave energy in the entire planet is approximately 3.7 TW [1]. In addition, wave energy has the highest energy density [7] among the renewable sources and highest regularity in power available, up to 90 % of the time, while solar and wind energy are available up to $20-30\%$ [8]. Those benefits promote the exploitation of ocean waves as an alternative source of energy.
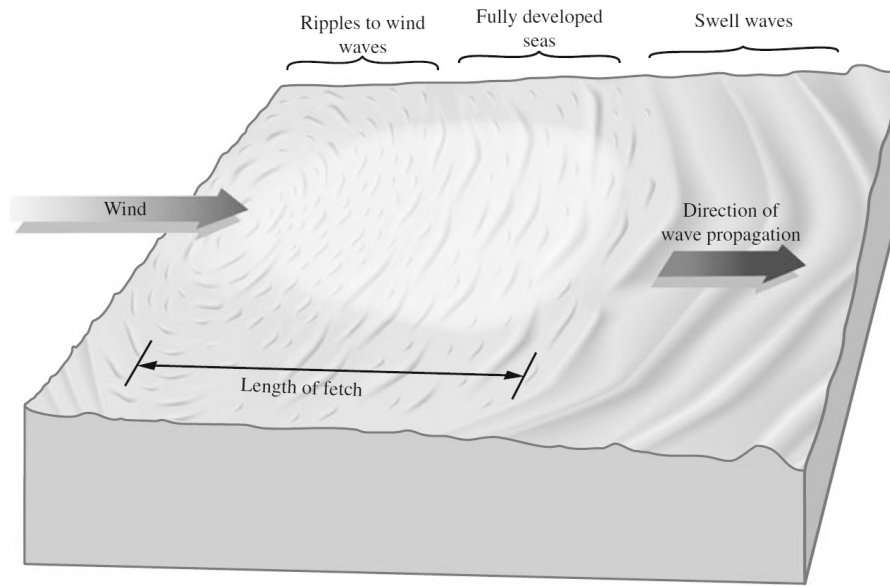
Figure 1.1: Ocean waves generation [5].

The idea of harvesting ocean energy exists for at least two centuries. The first mechanism proposed to convert the ocean waves into electricity was patented in France in 1799 by Girard and Son [9]. However, wave energy research mostly started after the oil crisis of the 1970s. Since then, several concepts were created, leading to more than one thousand patents [10]. Unlike the wind energy industry, where the predominant design is composed of a three-bladed turbine, wave energy has a wide variety of wave energy converter (WEC) concepts that differs in their wave absorption mechanism and power-take-off (PTO) system.

1.1 Wave Energy Converters

The present master dissertation focuses on the stochastic analysis of wave energy devices. The objective of this section is to provide a literature review of some of the existing

WEC technologies and their fundamental characteristics to justify the motivation behind this dissertation. Currently, several wave energy devices exist with no predominant design with demonstrated feasibility. As a result, numerous approaches have been proposed to categorize the vast amount of WECs [7, 11]. Generally, WECs are classified by their energy conversion principle, orientation and size, PTO mechanism, location, and reaction point.

1.1.1 Energy conversion principle

The incoming wave field interacts with WECs transferring part of its energy to the device. The energy conversion principle varies depending on the type of mechanism, which according to Falcão [11], can be sorted into three main categories: oscillating water column (OWC), oscillating bodies, and overtopping devices. Figure 1.2 illustrates examples of WECs for each category.

- **OWCs** produce energy due to the water oscillations inside the hollow structure that drives an air turbine generating energy. OWCs can be composed of a fixed or floating hollow structure, which acts as a cylinder/piston mechanism. As the structure is partially submerged, the wave-induced pressure leads the inner free-surface to oscillate [12]. This water column movement compresses and decompresses the trapped air, forcing it to flow through an air turbine connected to a generator. For onshore locations, the fixed OWCs are usually applied as a wave breaker to preserve the coastline [13].

- **Overtopping devices** convert the wave energy according to overtopping phenomenon driving an hydro-turbine. In those devices, the fixed or floating structure elevates the incoming waves above the sea level by an ascending ramp into a reservoir. The use of reflectors amplifies the magnitude of the incoming waves. The stored water is released back to the sea via one or mode hydro-turbines producing energy.

- **Oscillating bodies** extract the energy due to the relative motion. The structure is composed of submerged or floating structures which are exposed to the incoming wave field. The wave-induced oscillations drive the PTO mechanism that is generally hydraulic or electric. Up to date, several types of oscillating body systems exist, which is frequently divided into two main categories: pitching devices (attenuator, terminator, oscillating wave surge converter) and heaving devices (point absorber).

(a) Oscillating water column

(b) Overtopping device

(c) Oscillating bodies
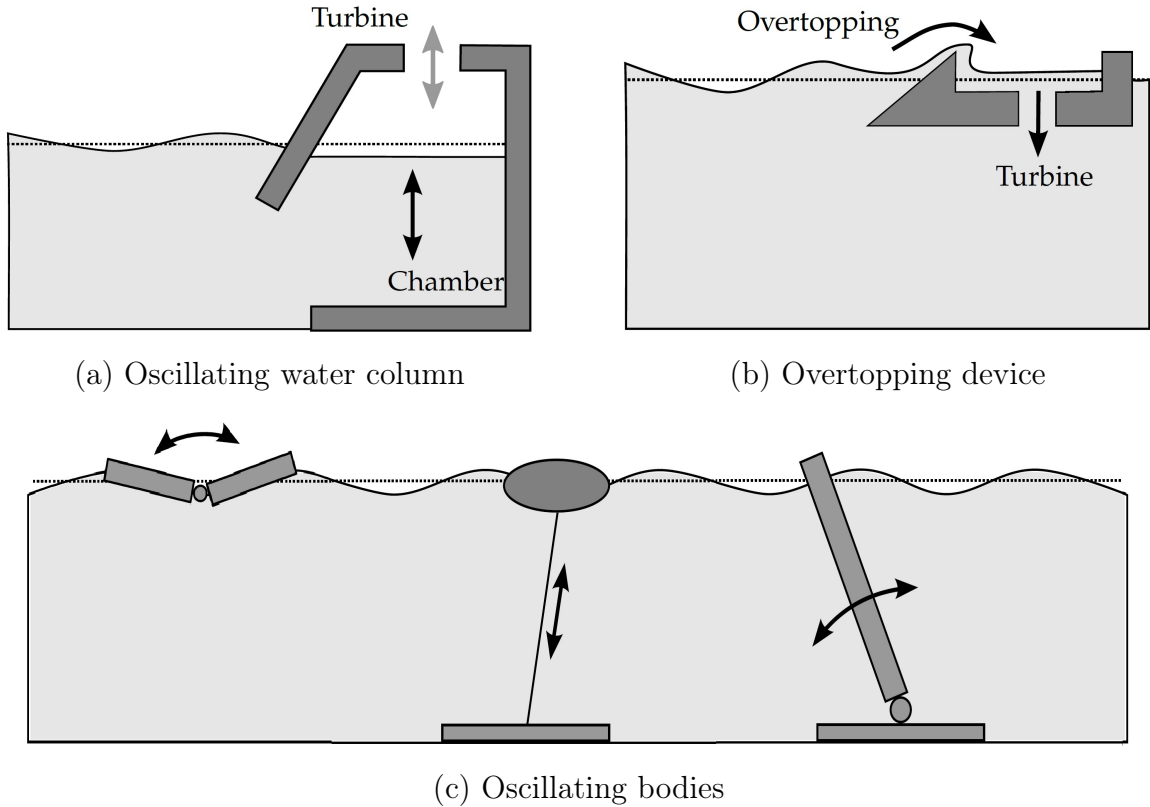
Figure 1.2: Energy conversion principle.

The efficiency of WEC changes significantly even for devices using the same energy conversion principle. For instance, as several oscillating bodies types exists, there is a broad range of efficiency for those devices. Among the categories, the overtopping device is one of the least efficient WEC [14]. Therefore, this type of device is not investigated in this master dissertation.

1.1.2 Orientation and size

Despite the variations of conversion principle, WEC can be sorted according to the relative size and orientation between the device and the incident wave field. Four categories are generally used to define the WEC regarding the orientation and size:

- **Terminators** are devices oriented in the perpendicular direction compared to the dominant wave direction, and the size comparable to the wavelength.

- **Attenuators** are devices that operate parallel to the wave propagation, and its size is superior to the dominant wavelength.

- **Point Absorbers** are devices with the dimensions considerably smaller than the dominant wavelength. Therefore, it can be assumed as a point material compared

with the wave, being insensitive to the wave direction.

- **Quasi-point absorbers** are asymmetric devices insensitive to the wave propagation. However, the structure has a dimension comparable to the dominant wavelength [15].
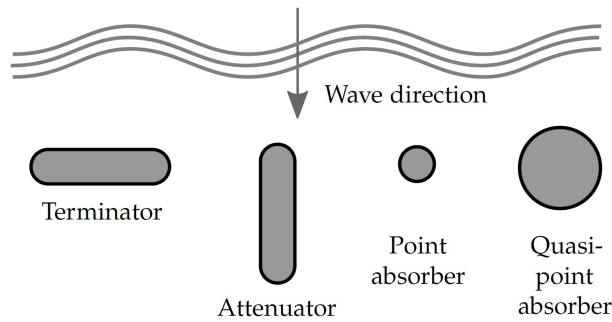
Figure 1.3: Orientation and size [16].

1.1.3   PTO mechanism

The PTO system is responsible for converting the ocean energy into an usable form of energy. There are several types of machinery, which varies with the source of power, such as mechanical, fluid, and electrical.

- **Hydraulic** PTO mechanism is driven by the moving structure that pressurizes the fluid. This fluid goes through a controlled manifold to a hydraulic motor connected to an electric generator.

- **Hydro** turbines are driven by a fluid flow, which is based on the well-establish technology employed in hydro-power plants. This type of mechanism is generally applied in overtopping WEC.

- **Pneumatic** PTO systems are composed of air-turbines driven by the oscillating pressure. The turbines are coupled to the electric generator and are applied in OWCs and pressure-differential devices.

- **Direct-drive** PTO mechanisms transform the mechanical power directly into electric power. Two main types of direct-drive mechanism can be categorized: electrical drive system where the moving part of the mechanical system is connected to a linear generator; and direct mechanical drive where an additional mechanism transfers the moving part to a rotary generator [5].
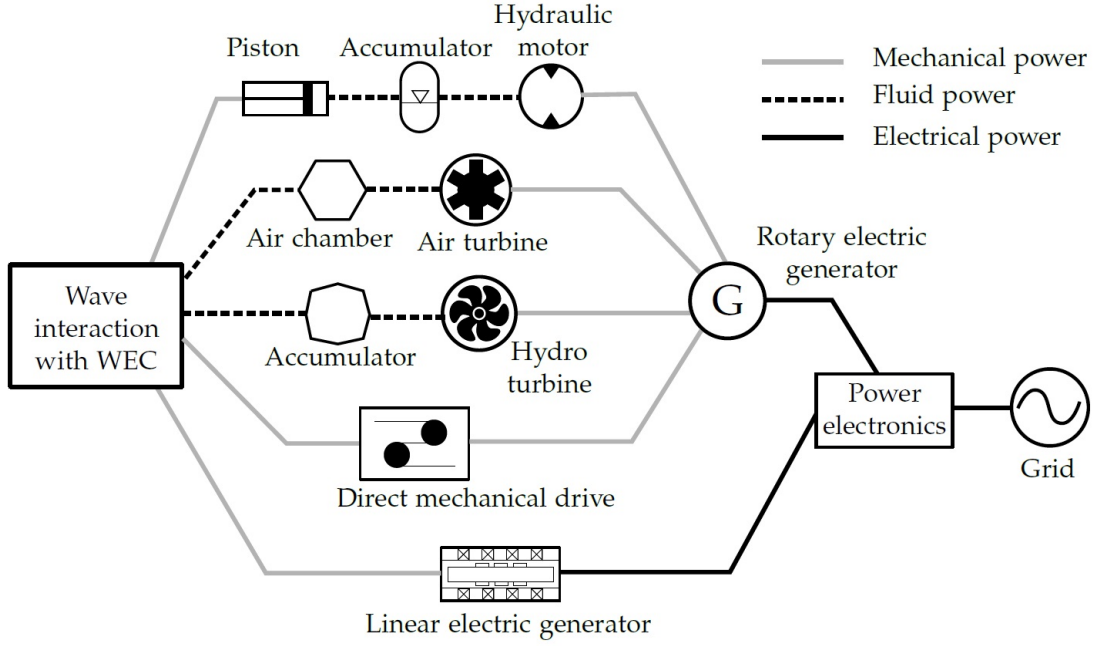
Figure 1.4: PTO mechanisms in wave energy technology, adapted from [5].

Even though direct electrical drive systems are the most efficient, hydraulic system are usually employed in wave energy devices due to the operating condition of WECs. Wave energy devices typically operate at low speed and large forces, which goes in the opposite direction of conventional electrical generators (high-speed with low torques). Conversely, hydraulic circuits are designed to work under large forces and low speeds, which attends the wave energy requirements. The efficiency can also be related to the control strategy applied, which according to the dynamic behavior of the PTO system, different approaches are used. Table 1.1 shows the indicative efficiency for several PTO systems used in wave energy.

Table 1.1: Overview of the indicative efficiency for different PTO systems [17].

PTO system	Efficiency (%)
Hydraulic	65
hydro-turbine	85
Pneumatic	55
Direct mechanical drive	90
Direct electrical drive	95

1.1.4   Location

Location is an essential criterion for the feasibility of WECs. Even though deep-water applications are attractive due to the high wave power, some challenges exist moving offshore such as installation and maintenance. Also, depending on the water depth, some types of energy conversion principles are more favorable. Therefore, a balance must be established according to the type of WEC. Generally, WECs are classified based on the location where the device installed, such as shoreline, nearshore, and offshore.

- **Shoreline** sites are easier for maintenance due to access to the wave power plant. Besides that, shoreline WECs have fewer chances to be damaged in severe wave conditions as waves are attenuated when traveling to shallow water. However, this phenomenon leads to low wave power. In addition, WECs can experience more breaking waves and nearshore related phenomena such as fouling and corrosion due to sediments. Fixed OWCs are usually employed in shoreline sites to protect the coastline.

- **Nearshore** sites are usually shallow water regions. Generally, in those locations, the WECs are attached to the seabed, which generally occurs for oscillating bodies. Like shoreline regions, wave power in nearshore is reduced compared to offshore locations. However, in some cases, the wave energy magnitude is nearly preserved when moving from deep water to transitional waters.

- **Offshore** sites are more attractive due to higher wave energy content in deep water seas [4]. However, the devices suffer greater loads in severe wave conditions. Also, as the WEC moves to deeper waters, the cost associated with installation and maintenance increases. In this case, the increase of cost can be related to the foundation, substructure, electric cable, mooring system, distance from ports and cities.

1.1.5   Reaction point

Wave energy extraction occurs due to the relative motion of two or more working parts of the WEC such as water, structure, or the seafloor. Based on this relative motion, the PTO mechanism absorbs part of the ocean wave energy generating electricity. Generally, the reaction source can be divided into three components: self-reacting, seafloor reference, and fixed structure.

- **Self-reacting** WECs use the device's inertia as a reaction point. Generally, inertial structures use heaving plates, buoyant spine, and self-rotating mechanisms.

- **Seafloor reference** is usually employed with tightly-moored WECs. The structure is tied to an anchorage system which can be composed by a dead-weight or a pile.

- The **Fixed structure** is frequently applied for onshore and near-shore installations. The structure is attached to the land, or a concrete foundation, and jack-up platform.

(a) Self-reacting (b) Seafloor reference (c) Fixed structure
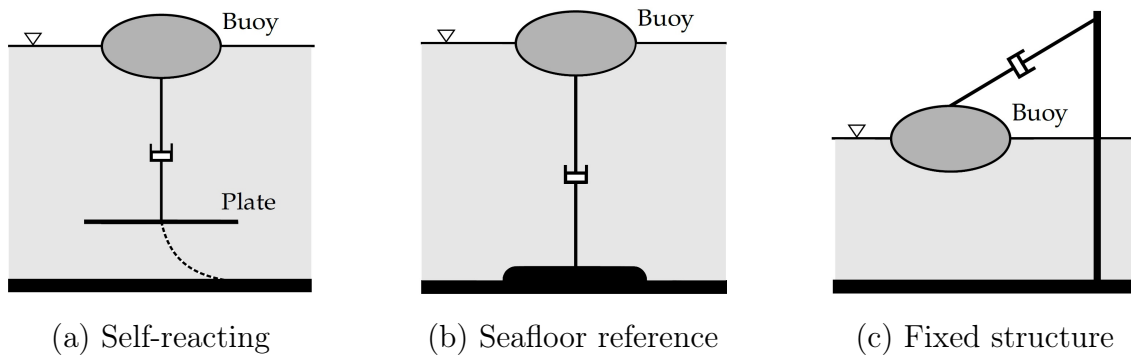
Figure 1.5: Types of reaction point [16].

1.2 Dissertation

1.2.1 Motivation

Up to date, several wave energy converters (WECs) have been proposed, and new concepts are expected to be created. However, just a few models have reached feasibility, and even fewer have produced energy for the grid [18]. WEC technology still requires some further development to become a highly competitive solution for the energy industry. The challenges in developing WEC technology are intensified as these structures are excited continuously by uncertain environmental loads from waves and ocean currents. In addition, as the system is usually set to operate next to resonant conditions to enlarge the power produced, WEC exhibits large displacements. Therefore, nonlinearities present in numerical models that represent the system dynamics plays a significant contribution. Generally, WECs are simulated using time domain (TD) models to deal with nonlinear forces. However, the computational effort related to those simulations is extremely high compared with traditional frequency domain (FD) simulations. Also, a considerable amount of environmental condition and optimization procedures must be conducted for feasibility studies, becoming undesirable to perform TD simulations.

1.2.2 Statistical Linearization (SL)

The SL technique allows to obtain a fast and realistic prediction of the system dynamics and mean power produced, which is valuable to address the challenges associated with the elevated number of simulations and computational effort. The SL uses a probabilistic model to generate an approximated solution to estimate the contribution of the nonlinear terms in the governing equations. This technique has been widely applied in several engineering fields such as aerospace and earthquake engineering to investigate the stationary random response of nonlinear systems [19, 20]. The SL consists of an iterative procedure which minimizes the error between the nonlinear system and the equivalent linear one in a mean square sense based on the stochastic response. However, despite the advantages of the technique, a limited number of papers has applied the SL for WECs [21–27]. This technique is a valuable tool for estimating the nonlinear response of the system, especially for optimizing a system with a large number of parameters [28] and several sea states [29].

1.2.3 Scope and Structure of the Dissertation

The present dissertation deals with the nonlinear stochastic analysis of WECs via statistical linearization (SL) to estimate the system dynamics, power output, spectral response, response distribution and mean offsets. Two devices are investigated to illustrate the capability of the SL technique. An oscillating body type, a Point Absorber (PA); and one OWCs type. The choice of the WEC types is based on the high efficiency of oscillating bodies and OWCs [14]. The reliability of the method is verified against their respective nonlinear TD simulation for each WEC.

The work is divided into four parts: Introduction, Background theory, Wave energy converters, and Conclusion. The introduction presents the topic and the objectives of the master's dissertation, also, it introduces some of the existing WEC technologies and their characteristics to justify the motivation behind this dissertation. In the Background theory part, the required knowledge is presented, which includes: the modeling of the ocean resource, and the statistical linearization technique. Two devices are investigated in the Wave energy converters part: a PA [30] and an OWC [31]. Finally, the conclusion part reviews some relevant results of each WEC and discuss the reliability of the SL method.

1.2.4 List of Publications

Up to date, the following master dissertation has contributed directly or indirectly to the development of the following publications:

1. da Silva, L. S. P., Tancredi, T. P., Ding, B., Sergiienko, N., and Morishita, H. M., 2017. "Fully submerged point absorber in Santa Catarina, Brazil-a feasibility study". In 24th ABCM International Congress of Mechanical Engineering (COBEM 2017).

2. da Silva, L. S. P., Morishita, H. M., Pesce, C. P., Gonçalves, R. T., 2019. "Nonlinear analysis of a heaving point absorber in frequency domain via statistical linearization". In Proceedings of the ASME 2019 International Conference on Ocean, & Offshore and Arctic Engineering (OMAE2019).

3. da Silva, L. S. P., Pesce, C. P., Morishita, H. M., Gonçalves, R. T., 2019. "Nonlinear analysis of an oscillating water column wave energy device in frequency domain via statistical linearization". In Proceedings of the ASME 2019 International Conference on Ocean, & Offshore and Arctic Engineering (OMAE2019).

PART II

BACKGROUND THEORY

2 OCEAN WAVES

Prior to the design of coastal and offshore structures, proper modeling of the environment is essential. In this regard, this section deals with the modeling of ocean waves. Firstly, the analysis of regular wave is presented based on the linear wave theory. Then, the analysis is extended to irregular waves, scatter diagram, and wave power.

2.1 Wave characteristics

Like WECs, waves are also classified based on their location. In this case, the water depth has a contribution in the wave characteristics, which affects the trajectory of the water particles, and consequently, the shape of the wave. Three regions are used to describe the influence of the water depth [32]:
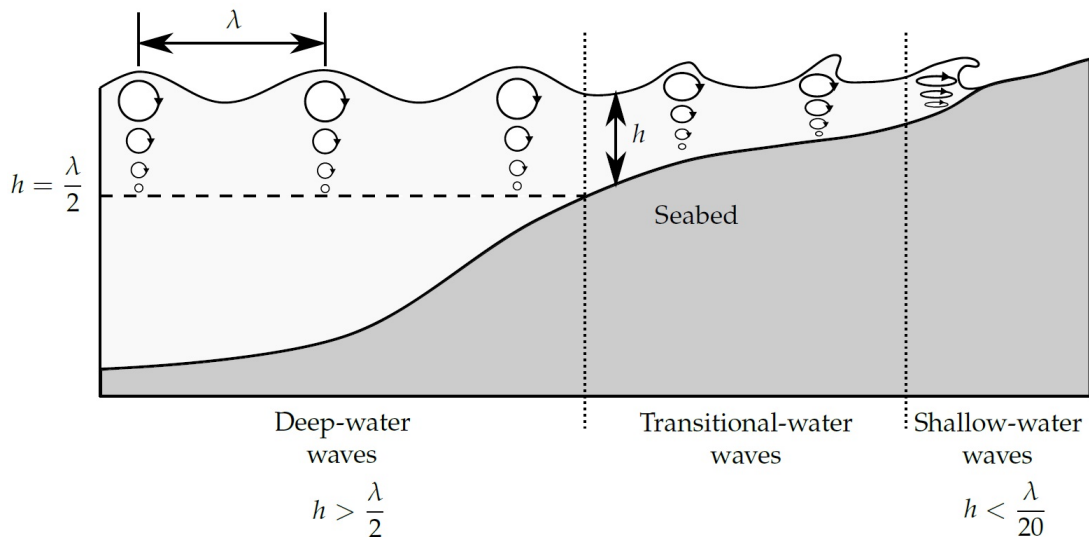
Figure 2.1: Wave classification based on water depth, adapted from [32].

- **Deep-waters** are regions deeper than half of the wavelength. For those conditions, waves are not affected by the seabed, and water particles experience a circular trajectory.

- **Transitional-waters** are regions with water depth between half to $1/20^{th}$ of the wavelength. For those regions, the seabed affects the characteristics of waves, and water particles have an elliptical trajectory.

- **Shallow-waters** are regions with water depth less than $1/20^{th}$ of the wavelength. For those regions, waves have a flattened trajectory, and depending on the wave characteristics, the wave becomes unstable and breaks.

Deep-water waves with small wave steepness are described using the linear wave theory, which considers an inviscid, irrotational, and incompressible fluid. However, as ocean waves travel to shallow water regions, the wave shape alters. Generally, when moving to the shallow-water areas, waves exhibit an increase of height and decrease of wave speed and length. Those effects lead to nonlinear wave profiles with sharper crests and flattened troughs. As the nonlinearities rise, the Stokes' wave theory offers a better description of the wave characteristics using a perturbation series approach, in which the wave steepness relates the order of nonlinearity. Figure 2.2 presents wave models according to the relative water depth and wave steepness proposed by Le Méhauté [33], where H denotes the wave height, g is the gravitational acceleration, T is the wave period, h is the water depth, and λ is the wavelength.
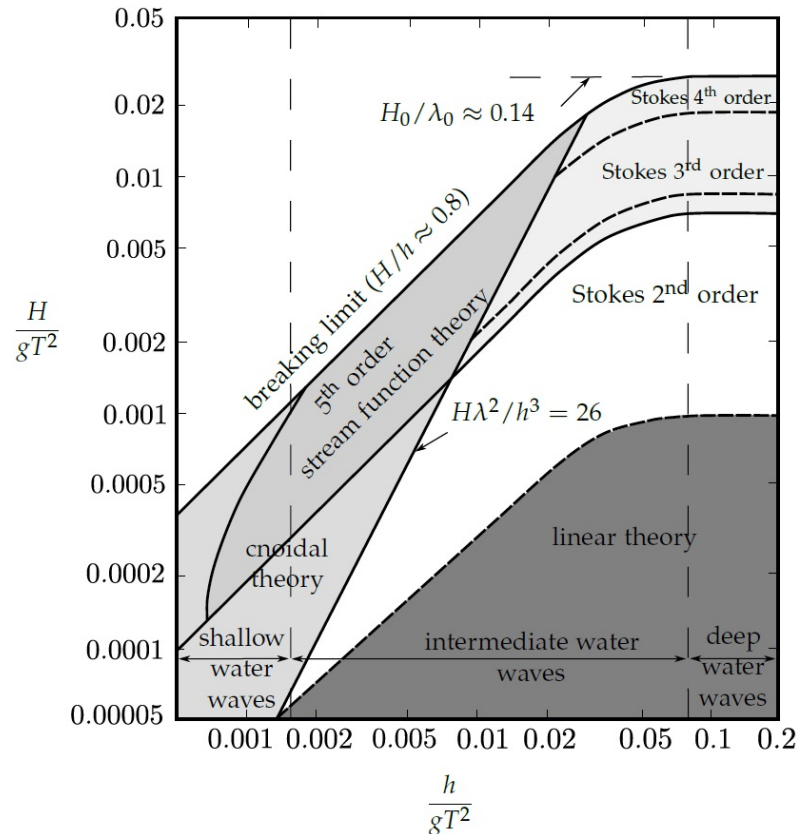
Figure 2.2: Wave models, adapted from [33].

Generally, WECs are assumed to operate in the linear wave theory range. The assumption of linear wave theory contributed to the development of WECs due to the extensive literature available of offshore structures [6]. However, during operational conditions, WECs may experience Stokes 2nd and 3rd order waves [34].

2.2 Linear wave theory

Some assumptions are adopted when dealing with the Linear theory. First, the fluid is assumed incompressible, inviscid, and irrotational [35]. The premise of incompressible is valid due to the insignificant water compressibility. Viscous effects are most critical only in a thin boundary layer near the seabed and surface. Therefore, the fluid can be treated as inviscid in the entire fluid domain. The fluid is considered irrotational owing to the inviscid flow assumption. In addition, the wave steepness is considered small, which relates the wave amplitude and wavelength. Also, no surface tension is included, only gravitational force. Based on the hypothesis adopted, two fundamental equations describe the fluid motion: Laplace equation and Bernoulli equation [15].

- **Continuity equation or Laplace's equation** is obtained from the conservation of mass applied to the fluid domain:

$$\nabla^2 \Phi = \frac{\partial^2 \Phi}{\partial x^2} + \frac{\partial^2 \Phi}{\partial y^2} + \frac{\partial^2 \Phi}{\partial z^2} = 0, \tag{2.1}$$

where Φ denotes the velocity potential.

$$\vec{v} = \vec{v}(x, y, z, t) = \nabla \Phi. \tag{2.2}$$

- **Bernoulli's equation** is derived based on Euler's equation for an unsteady flow:

$$\frac{\partial \Phi}{\partial t} + \frac{1}{2} \nabla \Phi \cdot \nabla \Phi + gz = -\frac{p - p_{atm}}{\rho}. \tag{2.3}$$

where p denotes the pressure, and p_{atm} is the atmospheric pressure.

Disregarding second-order term due to the assumption of small steepness, Equation (2.3) can be linearized to:

$$\frac{\partial \Phi}{\partial t} + gz = -\frac{p - p_{atm}}{\rho}. \tag{2.4}$$

2.2.1 Boundary conditions

Besides the governing equations, the velocity potential function must satisfy the boundary conditions. Three main boundary conditions must be fulfilled in the fluid domain: at the seabed and free surface [15]. Figure 2.3 illustrates the wave boundary conditions, where ζ represents the surface elevation.
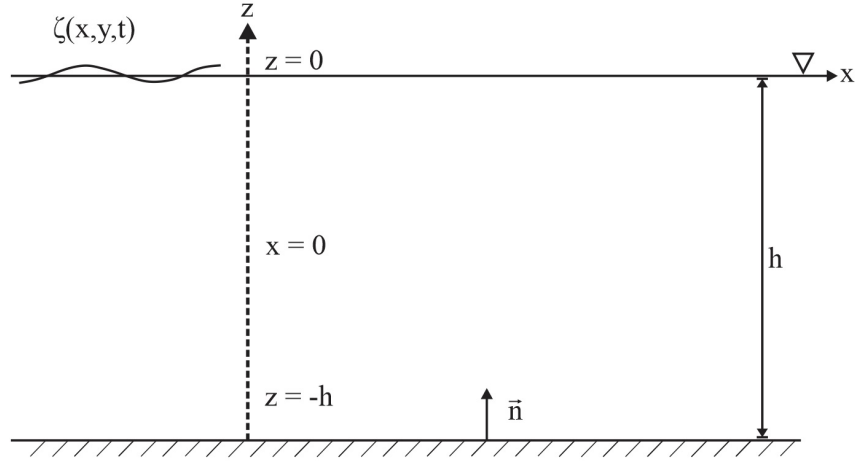
Figure 2.3: Wave boundary conditions, adapted from [15].

- **Seabed Boundary Condition** is characterized by its impermeability, which consists of zero velocity normal to the seabed surface.

$$\left[\frac{\partial \Phi}{\partial z}\right]_{z=-h} = 0. \tag{2.5}$$

- **Boundary Condition at the Free Surface** is composed of two conditions. Based on the linearized Bernoulli equation:

$$\left[\frac{\partial \Phi}{\partial t}\right]_{z=0} + g\zeta = 0, \tag{2.6}$$

and the free-surface kinematic boundary condition:

$$\left[\frac{\partial \Phi}{\partial z}\right]_{z=0} = \frac{\partial \zeta}{\partial t}. \tag{2.7}$$

Combining Equations (2.6) and (2.7), the Cauchy-Poisson condition is obtained:

$$\left[\frac{\partial^2 \Phi}{\partial t^2} + g\frac{\partial \Phi}{\partial z}\right]_{z=0} = 0. \tag{2.8}$$

2.3 Regular waves

Regular waves are generally characterized in terms of wave height ($H = 2\zeta_a$), wave period (T), and wavelength (λ), where ζ_a is the wave amplitude. Based on these characteristics, parameters such as wave steepness ($s = H/\lambda$), wavenumber ($k = 2\pi/\lambda$) and wave frequency ($\omega = 2\pi/T$) are determined. The wavenumber k refers to the geometric cyclicity, while the wave frequency ω refers to the time cyclicity. Figure 2.4 illustrates the main wave parameters.
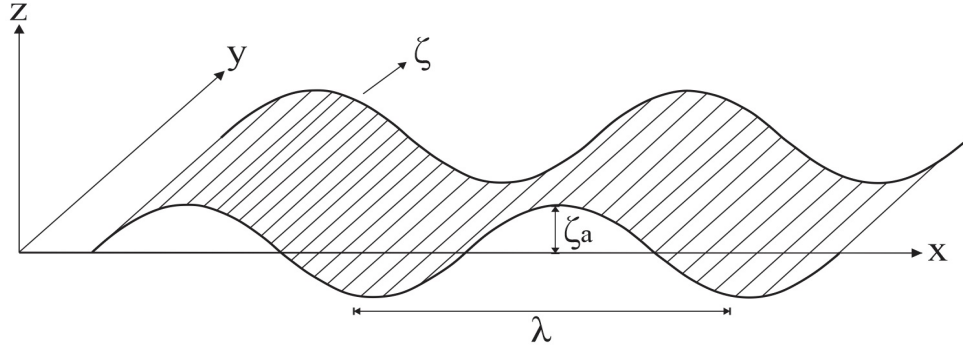
(a) Snapshot (t = fixed)
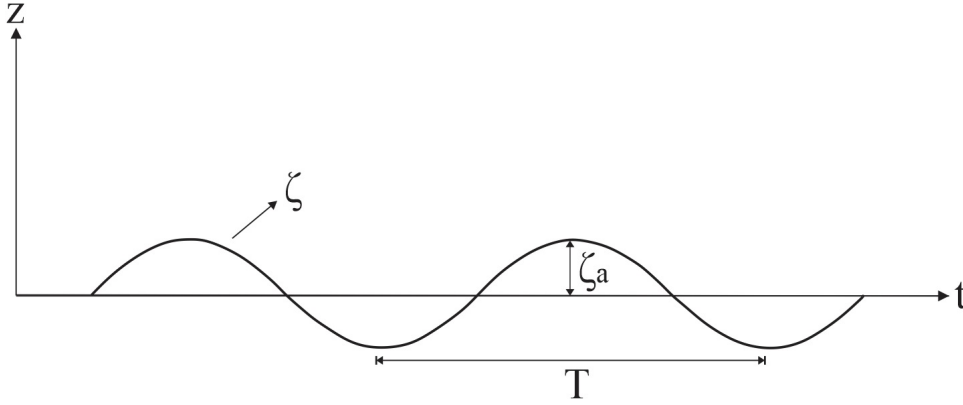
(b) Time history (x = fixed)

Figure 2.4: Wave main parameters, adapted from [36].

From the wavelength and period, the wave velocity is obtained:

$$c = \frac{\lambda}{T} = \frac{\omega}{k}.$$ (2.9)

Based on the governing equations, boundary conditions, and the wave characteristics, the following velocity potential satisfies the boundary conditions [36]:

$$\Phi = \frac{g\zeta_a}{\omega} \frac{\cosh k(z+h)}{\cosh kh} \sin(kx - \omega t).$$ (2.10)

Also, the dispersion relation must satisfy the free-surface condition:

$$k \tanh kh = \frac{\omega^2}{g}. \tag{2.11}$$

The dispersion relation determines the wavenumber and wavelength for a given frequency and water depth. From the velocity potential and free-surface dynamic boundary condition, Equation (2.6), the wave surface elevation is given by:

$$\zeta = -\frac{1}{g} \left[\frac{\partial \phi}{\partial t} \right]_{z=0} = \zeta_a \cos(kx - \omega t). \tag{2.12}$$

2.4   Irregular waves

Laplace's equation is linear and homogeneous, which allows the superposition of elementary results, such as waves superposition and potential fields. This result is essential for the characterization of real seas. Ocean waves are usually characterized by a spectral representation, which gives the energy in each frequency component [36]. The spectrum is obtained by measurements of the wave surface elevation over an extensive period of time and characterized by a stochastic process [6]. The characteristics of the spectrum depend on the formation of the sea state. Figure 2.5 illustrates a spectral representation of sea waves.
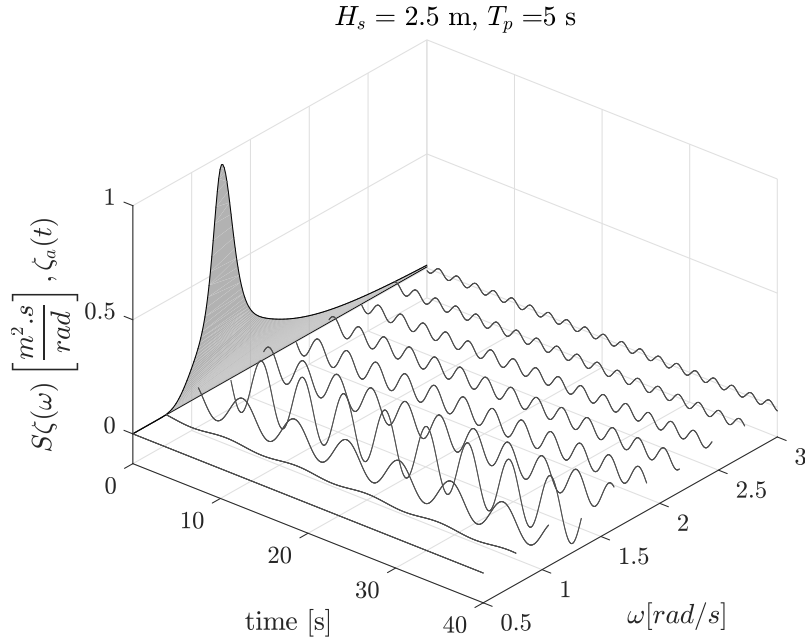
Figure 2.5: Sea spectrum representation.

Based on the statistical aspects and superposition principle, the non-deterministic behavior of seas can be modeled. Generally, sea spectrum is described based on the wave period (T_p), significant wave height (H_s), shape factors, zero-crossing period, and so forth [37]. This representation is valuable to offshore structures owing to the reduced number of sea parameters required to describe the spectrum. Several formulations are used to describe the wave spectra depending on the formation, such as the Pierson-Moskowitz (PM), Bretschneider, and JONSWAP spectrum. This work uses the JONSWAP spectrum ($\gamma = 3.3$), as it offers a better representation of the sea states at the south of the Brazilian coast.

- **Pierson-Moskowitz** spectrum was obtained initially using semi-empirical formulations based on sea registers in the Atlantic north. The spectrum is used to described fully-developed seas, in which the original formula uses the wind velocity, U, at 19.5m above the sea level as input [35].

$$S_\zeta(\omega) = \frac{0.0081g^2}{\omega^5} \exp\left[-0.74(g/U\omega)^4\right].$$

(2.13)
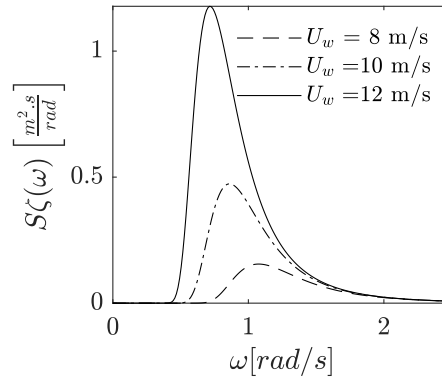
Figure 2.6: PM spectrum.

- **Bretschneider** or the generalized Pierson-Moskowitz spectrum was suggested during the International Ship Structures Congress (ISSC) of 1967 to modify the original PM spectrum. The spectrum is used to described fully-developed seas based on two input parameters, T_p and H_s. The Bretschneider spectrum is given by [36]:

$$S_\zeta(\omega) = \frac{A}{\omega^5} \exp\left(-\frac{B}{\omega^4}\right),$$

(2.14)

with:

$$A = \frac{173H_s^2}{(0.772T_p)^4}, \ B = \frac{692}{(0.772T_p)^4}.$$
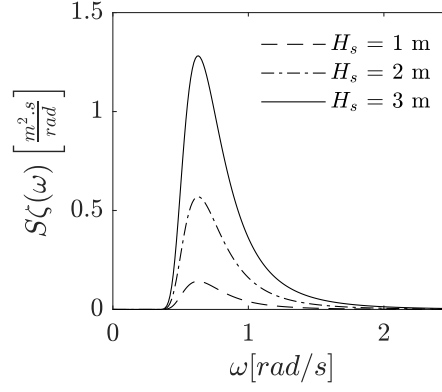
Figure 2.7: Bretschneider spectrum, $T_p = 10$ s.

- **JONSWAP** spectrum was originated during an extensive program named Joint North Sea Wave Project, which has been used to describe developing sea states. In the formulation, a peak enhancement factor introduces an additional parameter which usually goes from $1 < \gamma < 7$. For $\gamma = 1$, the JONSWAP spectrum recovers the Bretschneider spectrum. The JONSWAP spectrum is given by [36]:

$$S_\zeta(\omega) = \frac{320 H_s^2}{T_p^4 \omega^5} \exp\left(-\frac{1950}{T_p^4 \omega^4}\right) \cdot \gamma^A, \qquad (2.15)$$

with:

$$A = \exp\left[-\left(\frac{\frac{\omega}{\omega_p} - 1}{\sigma\sqrt{2}}\right)^2\right]$$

$$\sigma \begin{cases} \sigma = 0.07, & \text{for} \quad \omega < \omega_p \\ \sigma = 0.09, & \text{for} \quad \omega > \omega_p \end{cases},$$

where ω_p is the peak frequency.
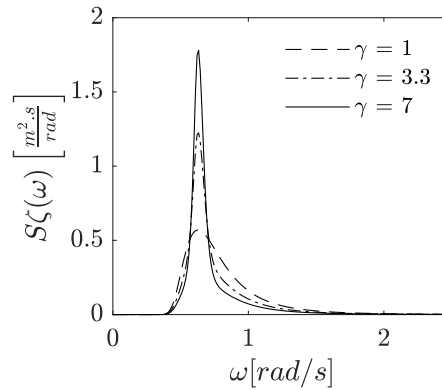
Figure 2.8: JONSWAP spectrum, $T_p = 10$ s, $H_s = 2$ m.

2.4.1 Scatter diagram

Wave spectrum represents a short-term description of the wave climate. For longer periods, a common practice is to describe the statistics of the wave climate based on scatter diagrams, which contains the probability of occurring a sea state (T_p and H_s) for a specific location. Those data are obtained monitoring several sea states over an extended period. Based on the scatter diagram, the wave resource of the site is assessed. This procedure is generally conducted during the preliminary assessment of WEC placement [6].
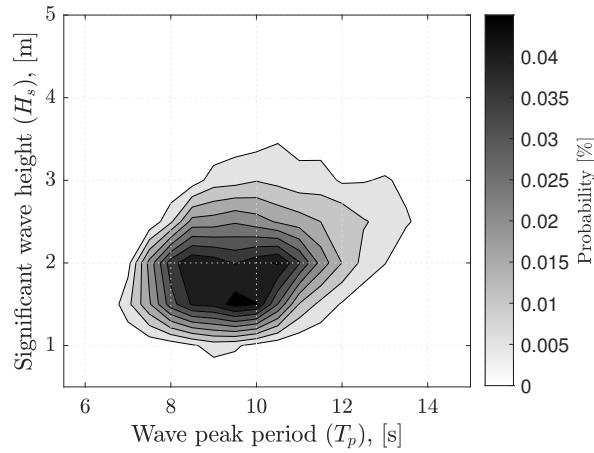
Figure 2.9: Scatter diagram of Imbituba (SC), Brazil; obtained from [38].

2.4.2 Wave power

As WECs absorbs part of the wave power, the analysis of the wave resources is a fundamental procedure to investigate the reliability of WEC installation. In addition, based on the ratio between the wave and WEC power, the efficiency of WECs are estimated. Wave power represents the amount of work delivered over a period by a vertical plane of a unit width perpendicular to the propagation direction. Each component of the wave has an energy which is transported at the wave group velocity. As the wave group, c_g, is highly dependent on the water depth, the general equation for wave power can be written as [39]:

$$\bar{P}_{wave} = \rho g \int_{-\infty}^{\infty} S_\zeta(\omega) c_g(\omega) d\omega, \tag{2.16}$$

The wave group velocity given by [35]:

$$c_g(\omega) = c(\omega) \left[\frac{1}{2} + \frac{k(\omega)h}{\sinh 2k(\omega)h} \right], \tag{2.17}$$

where the wave velocity is given in Equation (2.9), and the wavenumber is given in Equation (2.11). Note that each spectrum gives different wave power.

Figure 2.10 illustrates the wave power per meter of wave front for a site with 30 m water depth, and considering a JONSWAP spectrum with $\gamma = 3.3$.
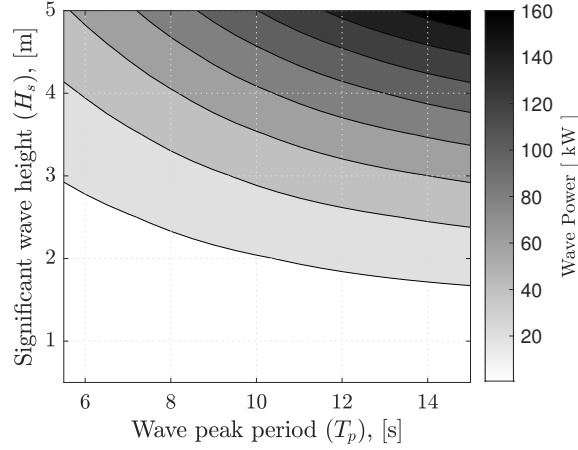
Figure 2.10: Wave power for a 30m water depth.

The wave power of a specified site is obtained summing the contributions of each sea state (Figure 2.10) multiplied by their respective probability of occurrence (Figure 2.9). Considering the scatter diagram of Imbituba (SC), Brazil, the wave power of the site is 22.53 kW per meter of wave front for a 30 m water depth considering a JONSWAP spectrum.

3   STATISTICAL LINEARIZATION

Prior to the SL technique, the FD model and the Gaussian distribution are introduced, which are essential for the derivation of the SL.

3.1   Frequency Domain Modelling

FD models are composed of a set of linearized equations, which gives a straightforward relationship between body displacement and the excitation force. In such models, the governing equations are generally linearized around mean position due to the assumption of small displacements. In this regard, consider a general multi-degree-of-freedom (MDOF) linear system described by the differential equation of the form:

$$\mathbf{M}\ddot{\mathbf{q}} + \mathbf{C}\dot{\mathbf{q}} + \mathbf{K}\mathbf{q} = \mathbf{F}(t), \tag{3.1}$$

where the vectors of generalized displacements, velocity and acceleration are given by $\mathbf{q}, \dot{\mathbf{q}}$, and $\ddot{\mathbf{q}}$; the inertia, damping and stiffness matrices are denoted by $\mathbf{M}, \mathbf{C}$, and $\mathbf{K}$; and the vector of excitation forces is represented by $\mathbf{F}(t)$.

The steady-state response of the system under stochastic loads is generally carried out based on the transfer function of the system. In this regard, the system is assumed to be excited by a harmonic load. As a result, the body tends to follow a harmonic response like the excitation force, which can be described by a complex amplitude $\hat{\mathbf{q}}$, where $\mathbf{q}(t) = \Re\{\hat{\mathbf{q}}e^{i\omega t}\}$. Based on that, the transfer function matrix between the wave force and the body displacement can be written as:

$$\boldsymbol{\alpha}(\omega) = [-\omega^2 \mathbf{M} + i\omega \mathbf{C} + \mathbf{K}]^{-1}. \tag{3.2}$$

The stochastic response is generally expressed in terms of power spectrum density (PSD), which is obtained by:

$$\mathbf{S_q}(\omega) = \boldsymbol{\alpha}(\omega)\mathbf{S_f}(\omega)\boldsymbol{\alpha}^{\mathrm{T}*}(\omega), \tag{3.3}$$

where $\mathbf{S_q}$ is the response spectrum matrix, $\mathbf{S_f}$ is the spectrum matrix of the force, and $(\ )^{\mathrm{T}*}$ denotes the transpose conjugate of the matrix. In the scalar sense, Equation (3.3) reduces to:

$$S_q(\omega) = |\alpha(\omega)|^2 S_f(\omega). \tag{3.4}$$

3.2 Gaussian Distribution

The theoretical basis of the Gaussian Distribution is grounded on the Central Limit Theorem, which states that the sum of independent random variables with arbitrary distributions tends to a Gaussian distribution as the number of independent variables becomes large [20]. In practice, environmental loads tend to a Gaussian distribution, such as wind loading, ocean waves, earthquakes, loads caused by the vehicles traveling over rough terrain, atmospheric turbulence. In the case of modeling ocean waves, the Gaussian distribution is achieved due to the random phase relationship among the irregular wave components [20]. Figure 3.1 illustrates the wave surface elevation considering an irregular wave, and its probability distribution. The wave surface elevation in the TD can be written as:

$$\zeta(t) = \sum_{k=1}^{N} \Re e \left\{ \hat{\zeta}_a(\omega_k) e^{i\omega_k t} \right\}, \tag{3.5}$$

where the complex amplitude of the surface elevation, $\hat{\zeta}_a(\omega_k)$, can be obtained from the sea spectrum using Equation (B.10).

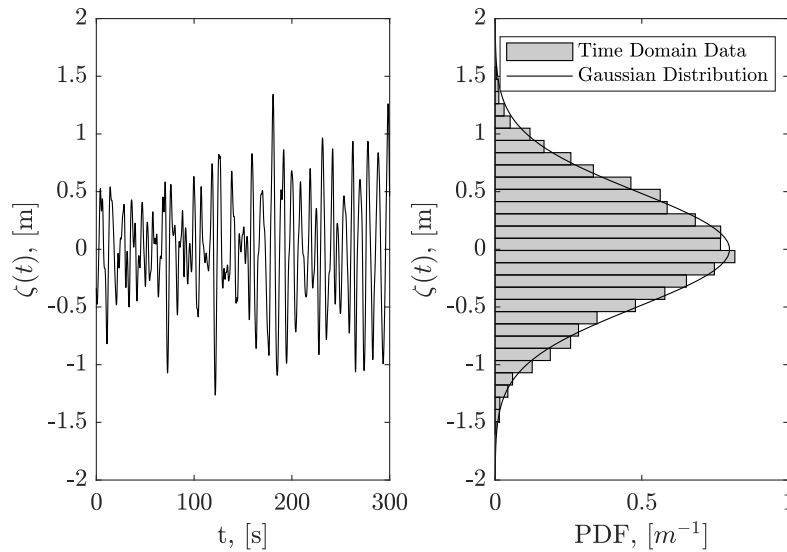
Figure 3.1: Surface elevation distribution. The TD data was acquired during a time interval of 3000s, and is given by a JONSWAP spectrum ($\gamma = 3.3$) with $T_p = 10$s and H_s = 2m.

As it can be observed in Figure 3.1, the probability distribution of the sea surface elevation recovers the Gaussian distribution. The Probability Density Function (PDF) of a Gaussian distribution for the sea surface elevation is given by:

$$f(\zeta) = \frac{1}{\sigma_{\tilde{\zeta}}\sqrt{2\pi}}\exp\left(-\frac{\zeta^2}{2\sigma_{\tilde{\zeta}}^2}\right), \tag{3.6}$$

where $\sigma_{\tilde{\zeta}}$ denotes the standard deviation of the sea surface. The TD and FD can be correlated by [20]:

$$\sigma_{\tilde{\zeta}}^2 = \int_0^\infty S_\zeta(\omega)d\omega. \tag{3.7}$$

According to the linear theory, the response processes have a Gaussian distribution whenever the excitation process is Gaussian. For a MDOF system, the Gaussian response of the displacement is written as:

$$\mathrm{f}(\mathbf{q}) = \frac{1}{(2\pi)^{n/2}|\mathbf{V}|^{1/2}}\exp\left(-\frac{1}{2}(\tilde{\mathbf{q}}-\bar{\mathbf{q}})^\mathrm{T}\mathbf{V}^{-1}(\tilde{\mathbf{q}}-\bar{\mathbf{q}})\right), \tag{3.8}$$

where $\mathbf{V}$ is the covariance matrix of $\mathbf{q}$, and $|\mathbf{V}|$ denotes the determinant of the covariance matrix, $(\tilde{\cdot})$ denotes a random zero-mean component, and $(\bar{\cdot})$ denotes a mean value component. The covariance matrix of the body response is given by:

$$\mathbf{V} = \begin{bmatrix} \sigma_{q_1}^2 & \sigma_{q_1 q_2} & \cdots & \sigma_{q_1 q_n} \\ & \sigma_{q_2}^2 & \cdots & \sigma_{q_2 q_n} \\ & & \ddots & \vdots \\ sym & & & \sigma_{q_n}^2 \end{bmatrix}, \tag{3.9}$$

where the diagonal terms $(i=j)$ are based on the auto-spectrum and calculated as:

$$\sigma_{q_k}^2 = \int_0^\infty S_{q_k}(\omega)d\omega, \tag{3.10}$$

and the non-diagonal terms $(i \neq j)$ are based on the cross-spectrum and calculated as:

$$\sigma_{q_i q_j} = \int_0^\infty S_{q_i q_j}(\omega)d\omega. \tag{3.11}$$

Considering the case of a two degrees-of-freedom (DOF) system, the covariance matrix of

the displacement and their first time derivatives can be expressed as:

$$\mathbf{V} = \begin{bmatrix} \sigma_{q_1}^2 & \sigma_{q_1 q_2} & \sigma_{q_1 \dot{q}_1} & \sigma_{q_1 \dot{q}_2} \\ & \sigma_{q_2}^2 & \sigma_{q_2 \dot{q}_1} & \sigma_{q_2 \dot{q}_2} \\ & & \sigma_{\dot{q}_1}^2 & \sigma_{\dot{q}_1 \dot{q}_2} \\ sym & & & \sigma_{\dot{q}_2}^2 \end{bmatrix}, \tag{3.12}$$

where :

$$\sigma_{\dot{q}_k q_k} = 0, \tag{3.13}$$

$$\sigma_{\dot{q}_k}^2 = \int_0^\infty \omega^2 S_{q_k}(\omega) d\omega, \tag{3.14}$$

$$\sigma_{q_i \dot{q}_j} = i \int_0^\infty \omega S_{q_i q_j}(\omega) d\omega, \tag{3.15}$$

$$\sigma_{\dot{q}_i \dot{q}_j} = \int_0^\infty \omega^2 S_{q_i q_j}(\omega) d\omega. \tag{3.16}$$

Besides the formulation of the Gaussian distribution, an important characteristic of a Gaussian vector $\mathbf{q} \in R^{1 \times n}$ is summarized by the formula given in [40]:

$$\langle f(\mathbf{q})\mathbf{q} \rangle = \langle \mathbf{q}\mathbf{q}^T \rangle \langle \nabla f(\mathbf{q}) \rangle, \tag{3.17}$$

where the gradient operator ∇ is defined as:

$$\nabla = \left[\frac{\partial}{\partial q_1}, \frac{\partial}{\partial q_2}, ..., \frac{\partial}{\partial q_n} \right]^T. \tag{3.18}$$

Equation (3.17) is essential for the derivation of the SL formulation.

3.3   Statistical Linearization Technique

In this section, the response of a nonlinear MDOF vibratory system subjected to a random excitation is investigated. As those systems suffer from a lack of exact solutions, some approximations are generally applied to estimate the body response. For instance, in the case of small nonlinearities and few DOF, the approximate solutions can be obtained by perturbation techniques and methods of energy balance [20]. However, those methods become difficult to apply for general forms of nonlinearities and MDOF systems. In this regard, this work applies the SL technique, which offers a systematic approximated solution to deals with nonlinear equations with MDOF. The SL approach used in this

dissertation follows the derivations based on Robert and Spanos [20]. Consider a general MDOF nonlinear equation given by:

$$\mathbf{M}\ddot{\mathbf{q}} + \mathbf{C}\dot{\mathbf{q}} + \mathbf{K}\mathbf{q} + \mathbf{\Theta}(\mathbf{q}, \dot{\mathbf{q}}, \ddot{\mathbf{q}}) = \mathbf{F}, \tag{3.19}$$

where $\mathbf{M}, \mathbf{B}, \mathbf{K} \in R^{n \times n}$ and denotes the mass, damping and stiffness matrices respectively, $\mathbf{\Theta}(\mathbf{q}, \dot{\mathbf{q}}, \ddot{\mathbf{q}}) \in R^{n \times 1}$ is a vector containing the nonlinear terms, which can be a function of the generalized coordinate vector $\mathbf{q}$ and its derivatives. In the linear case, $\mathbf{\Theta}$ is null/ neglected. An equivalent linear system of Equation (3.19) can be written as:

$$(\mathbf{M} + \mathbf{M}_{eq})\ddot{\mathbf{q}} + (\mathbf{C} + \mathbf{C}_{eq})\dot{\mathbf{q}} + (\mathbf{K} + \mathbf{K}_{eq})\mathbf{q} = \mathbf{F}, \tag{3.20}$$

where $\mathbf{M}_{eq}$, $\mathbf{B}_{eq}$, and $\mathbf{K}_{eq}$ are deterministic matrices that represent the equivalent linear mass, damping, and stiffness matrices. The equivalent linear terms are determined by minimizing the difference between the nonlinear system and the equivalent linear system in a statistical sense. Defining the vector difference $\boldsymbol{\varepsilon}$ as:

$$\boldsymbol{\varepsilon} = \mathbf{M}\ddot{\mathbf{q}} + \mathbf{C}\dot{\mathbf{q}} + \mathbf{K}\mathbf{q} + \mathbf{\Theta}(\mathbf{q}, \dot{\mathbf{q}}, \ddot{\mathbf{q}}) - (\mathbf{M} + \mathbf{M}_{eq})\ddot{\mathbf{q}} - (\mathbf{C} + \mathbf{C}_{eq})\dot{\mathbf{q}} - (\mathbf{K} + \mathbf{K}_{eq})\mathbf{q}, \tag{3.21}$$

$$\boldsymbol{\varepsilon} = \mathbf{\Theta}(\mathbf{q}, \dot{\mathbf{q}}, \ddot{\mathbf{q}}) - \mathbf{M}_{eq}\ddot{\mathbf{q}} - \mathbf{C}_{eq}\dot{\mathbf{q}} - \mathbf{K}_{eq}\mathbf{q}. \tag{3.22}$$

The equivalent inertia, damping, and stiffness matrix depend on the response $\mathbf{q}$. Since the solution depends on the equivalent linear system, a cyclic relationship between both can be established. Euclidean norm $\|\boldsymbol{\varepsilon}\|_2$ is used as a criterion for the minimization of the difference:

$$\|\boldsymbol{\varepsilon}\|_2 = \boldsymbol{\varepsilon}^{\mathrm{T}}\boldsymbol{\varepsilon}. \tag{3.23}$$

The minimization is performed according to:

$$\min \left\langle \boldsymbol{\varepsilon}^T \boldsymbol{\varepsilon} \right\rangle, \tag{3.24}$$

where $\langle\ \rangle$ denotes the mathematical expectation. Using the linearity property of the expectation, Equation (3.24) can be represented in the form:

$$\min \sum_{i=1}^{n} D_i^2, \tag{3.25}$$

with D defined as:

$$D_i^2 = \left\langle \varepsilon_i^2 \right\rangle, i = \{1, 2, ..., n\}. \tag{3.26}$$

Based on Equation (3.22), it is possible to write:

$$D_i^2 = \left\langle \left[\Theta_i - \sum_{j=1}^{n} (M_{eq_{i,j}} \ddot{q}_j + C_{eq_{i,j}} \dot{q}_j + K_{eq_{i,j}} q_j) \right]^2 \right\rangle, \; i = \{1, 2, ..., n\}, \qquad (3.27)$$

where $M_{eq_{i,j}}, C_{eq_{i,j}}$, and $K_{eq_{i,j}}$ are the elements of the equivalent linear mass, damping and stiffness matrices respectively, and Θ_i are the nonlinear elements of $\boldsymbol{\varepsilon}$.

The quantity D_i^2 can be minimized by solving the equations:

$$\frac{\partial}{\partial M_{eq_{i,j}}} (D_i^2) = 0, j = \{1, 2, ..., n\}, \qquad (3.28)$$

$$\frac{\partial}{\partial C_{eq_{i,j}}} (D_i^2) = 0, j = \{1, 2, ..., n\}, \qquad (3.29)$$

$$\frac{\partial}{\partial K_{eq_{i,j}}} (D_i^2) = 0, j = \{1, 2, ..., n\}. \qquad (3.30)$$

Applying the minimization procedure, the following equations are obtained:

$$\langle \ddot{q}_j \Theta_i \rangle = \sum_{s=1}^{n} \left[M_{eq_{i,s}} \langle \ddot{q}_s \ddot{q}_j \rangle + C_{eq_{i,s}} \langle \dot{q}_s \ddot{q}_j \rangle + K_{eq_{i,s}} \langle q_s \ddot{q}_j \rangle \right], \qquad (3.31)$$

$$\langle \dot{q}_j \Theta_i \rangle = \sum_{s=1}^{n} \left[M_{eq_{i,s}} \langle \ddot{q}_s \dot{q}_j \rangle + C_{eq_{i,s}} \langle \dot{q}_s \dot{q}_j \rangle + K_{eq_{i,s}} \langle q_s \dot{q}_j \rangle \right], \qquad (3.32)$$

$$\langle q_j \Theta_i \rangle = \sum_{s=1}^{n} \left[M_{eq_{i,s}} \langle \ddot{q}_s q_j \rangle + C_{eq_{i,s}} \langle \dot{q}_s q_j \rangle + K_{eq_{i,s}} \langle q_s q_j \rangle \right]. \qquad (3.33)$$

The compact form of Equations (3.31) to (3.33) is given by:

$$\left\langle \Theta_i \underset{\sim}{\mathbf{q}} \right\rangle = \left\langle \underset{\sim}{\mathbf{q}} \underset{\sim}{\mathbf{q}}^{\mathrm{T}} \right\rangle \begin{bmatrix} \mathbf{K}_{eq_i}^{\mathrm{T}} \\ \mathbf{C}_{eq_i}^{\mathrm{T}} \\ \mathbf{M}_{eq_i}^{\mathrm{T}} \end{bmatrix}, \qquad (3.34)$$

where

$$\underset{\sim}{\mathbf{q}} = [\mathbf{q}, \dot{\mathbf{q}}, \ddot{\mathbf{q}}]^{\mathrm{T}},$$

and $\mathbf{K}_{eq_i}$, $\mathbf{C}_{eq_i}$, and $\mathbf{M}_{eq_i}$ are the ith rows of the equivalent stiffness, damping and mass matrices. Under the assumption of a Gaussian approximation, the equivalent linear matrices can be determined based on Equations (3.17) and (3.34), leading to [20]:

$$M_{eq_{i,j}} = \left\langle \frac{\partial \Theta_i}{\partial \ddot{q}_j} \right\rangle, \qquad (3.35)$$

$$B_{eq_{i,j}} = \left\langle \frac{\partial \Theta_i}{\partial \dot{q}_j} \right\rangle, \qquad (3.36)$$

$$K_{eq_{i,j}} = \left\langle \frac{\partial \Theta_i}{\partial q_j} \right\rangle. \qquad (3.37)$$

Based on the equivalent terms, the equivalent linear transfer function of the nonlinear system is expressed as:

$$\boldsymbol{\alpha}_{eq}(\omega) = [-\omega^2(\mathbf{M} + \mathbf{M}_{eq}) + i\omega(\mathbf{C} + \mathbf{C}_{eq}) + (\mathbf{K} + \mathbf{K}_{eq})]^{-1}, \qquad (3.38)$$

and the response spectrum obtained as:

$$\mathbf{S_q}(\omega) = \boldsymbol{\alpha}_{eq}(\omega)\mathbf{S_f}(\omega)\boldsymbol{\alpha}_{eq}^{\mathrm{T}*}(\omega). \qquad (3.39)$$

3.3.1 Treatments of asymmetric non-linearities

Depending on the source of nonlinearity, additional treatment is required to apply the SL technique, due to a constant offset in the system solutions [20]. In this regard, the system can be written in terms of a mean value, $(\bar{\ })$ and a random zero mean component of the response $(\tilde{\ })$:

$$\mathbf{q(t)} = \bar{\mathbf{q}} + \tilde{\mathbf{q}}(\mathbf{t}). \qquad (3.40)$$

Hence, for a system with a zero-mean force, Equation (3.19) can be written as:

$$\mathbf{M}\ddot{\tilde{\mathbf{q}}} + \mathbf{C}\dot{\tilde{\mathbf{q}}} + \mathbf{K}\bar{\mathbf{q}} + \mathbf{K}\tilde{\mathbf{q}} + \boldsymbol{\Theta}(\bar{\mathbf{q}} + \tilde{\mathbf{q}}, \dot{\tilde{\mathbf{q}}}, \ddot{\tilde{\mathbf{q}}}) = \tilde{\mathbf{F}}. \qquad (3.41)$$

In this condition, the mean offset is estimated taking the expectation of Equation (3.41):

$$\mathbf{K}\bar{\mathbf{q}} + \left\langle \boldsymbol{\Theta}(\bar{\mathbf{q}} + \tilde{\mathbf{q}}, \dot{\tilde{\mathbf{q}}}, \ddot{\tilde{\mathbf{q}}}) \right\rangle = 0. \qquad (3.42)$$

Subtracting Equation (3.42) from Equation (3.41), an equivalent form of Equation (3.19) is obtained:

$$\mathbf{M}\ddot{\tilde{\mathbf{q}}} + \mathbf{C}\dot{\tilde{\mathbf{q}}} + \mathbf{K}\tilde{\mathbf{q}} + \mathbf{G}(\tilde{\mathbf{q}}, \dot{\tilde{\mathbf{q}}}, \ddot{\tilde{\mathbf{q}}}) = \tilde{\mathbf{F}}, \qquad (3.43)$$

where:

$$\mathbf{G}(\tilde{\mathbf{q}}, \dot{\tilde{\mathbf{q}}}, \ddot{\tilde{\mathbf{q}}}) = \boldsymbol{\Theta}(\bar{\mathbf{q}} + \tilde{\mathbf{q}}, \dot{\tilde{\mathbf{q}}}, \ddot{\tilde{\mathbf{q}}}) - \left\langle \boldsymbol{\Theta}(\bar{\mathbf{q}} + \tilde{\mathbf{q}}, \dot{\tilde{\mathbf{q}}}, \ddot{\tilde{\mathbf{q}}}) \right\rangle.$$

3.3.2 Statistical Linearization Procedure

According to Equations (3.35) to (3.37), the determination of the equivalent linear terms requires the knowledge of the body response distribution. Since there is no analytic solution, the technique uses an iterative procedure, which uses the linearized dynamic of the system as an initial guess until achieving predetermined criteria. The standard step-by-step procedure is given by:

Step 1: Define the linear transfer function between the system dynamics and the force, which will be used as an initial guess for the iterative procedure ($\mathbf{M}_{eq} = \mathbf{C}_{eq} = \mathbf{K}_{eq} = 0$).

Step 2: Calculate the PSD matrix of the body response based on Equation (3.3), and calculate the covariance matrix and the body response distribution (Gaussian) using Equation (3.8).

Step 3: If the system has asymmetric nonlinearities, calculate the mean offsets based on Equation (3.42).

Step 4: Calculate the equivalent linear mass, damping, and stiffness terms ($\mathbf{M}_{eq}, \mathbf{C}_{eq}$, and $\mathbf{K}_{eq}$) using Equations (3.35) to (3.37).

Step 5: Update the equivalent transfer function of the system dynamics based on Equation (3.38) and calculate the spectral response of the body using the equivalent linear system using Equation (3.39).

Step 6: Calculate the covariance matrix, the body response distribution (Gaussian) using Equation (3.8), and the mean offsets based on Equation (3.42) (in the case of asymmetric nonlinearities).

Step 7: Check the convergence of the new results obtained in Step 6. If the results did not converge, return to Step 4.

The convergence criteria can be verified comparing the body response used to estimate the equivalent linear terms and mean offsets with the results obtained using with these new equivalent linear terms, namely comparing the covariance matrix and mean offsets. In this work, the solution is considered converged when the relative error between the covariance matrix terms and the mean offset of the new values and their previous iteration results are less than 0.1%.

$$\frac{|\sigma_{i,j}{}^{it} - \sigma_{i,j}{}^{it-1}|}{|\sigma_{i,j}{}^{it}|} < 0.1\%, \tag{3.44}$$

$$\frac{\left|\bar{q}_i{}^{it} - \bar{q}_i{}^{it-1}\right|}{\left|\bar{q}_i{}^{it}\right|} < 0.1\%, \tag{3.45}$$

where it refers to the number of iteration.

Generally, the technique converges effortless and requires a few iterations depending on the system, its source of nonlinearity, and the number of DOF. For some systems, an iteration relaxation method can be used to guarantee the convergence [41], which is important for sensitive nonlinear forces and system with mean offsets. In this work, a simple solver is used for the iterative procedure.

PART III

WAVE ENERGY CONVERTERS

4 POINT ABSORBER

PAs constitute a majority of existing prototypes and are usually investigated during preliminary studies. The size of the structure is small compared to the wavelength, and the design has an axis-symmetry. Due to these characteristics, the device is insensitive to the wave direction, which is essential as the wave direction varies in offshore zones. Currently, several types of PAs exist, wherein the most common is the single floating PA. For such type, the device extracts energy mainly in heave motion. A standard configuration consists of a floating structure exposed to the incident wave field. Due to the wave loads, the structure moves and drives the power-take-off (PTO) system, which in this case is directly connected to an electric generator. The PTO system is generally anchored to the sea floor or attached to an external structure. Figure 4.1 illustrates a typical single floating PA.
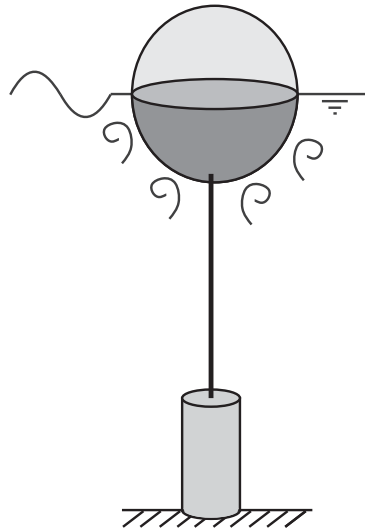

Figure 4.1: Illustration of a Point Absorber.

4.1 Governing Equation

The dynamics of the PA can be divided into linear and nonlinear terms to facilitate the development of the SL technique. Based on the illustration given in Figure 4.1 and the description above, the dynamics of the PA can be expressed as:

$$M\ddot{z} = F_r(t) + F_{hs,l} + F_s + F_{exc} - \Theta(z,\dot{z}), \qquad (4.1)$$

where M represents the mass of the structure, which comprises the floating structure and the PTO system; z denotes the heave displacement, $F_r(t)$ is the radiation force, $F_{hs,l}(t)$ indicates the linearized hydrostatic force, $F_s(t)$ is the linear mechanical restoring force, and $F_{exc}(t)$ is the excitation force; which are linear terms.

The nonlinear terms, $\Theta(z,\dot{z})$, of the PA dynamic is given by:

$$-\Theta(z,\dot{z}) = F_{hs,nl} + F_{ls} + F_{es} + F_{vd} + F_{EG}, \qquad (4.2)$$

where $F_{hs,nl}(t)$ is the nonlinear hydrostatic restoring component, $F_{ls}(t)$ is the lateral restoring force, $F_{es}(t)$ is the end-stop force, F_{vd} is the viscous drag force, and $F_{EG}(t)$ is electrical generator force. Note that the negative signal of Θ occurs to maintain the formulation described in Chapter 3.

- **Radiation Force (F_r):**

Regarding the linear terms, the first component refers to the radiation force, which according to the linear wave theory, occurs due to the own body oscillation in the absence of waves [36]. This force can be divided into two components: the first in phase with the acceleration, and the second in phase with the velocity [36]. The radiation force can be expressed in the FD as:

$$F_r(\omega) = -A_{33}(\omega)\ddot{z}_k - B_{33}(\omega)\dot{z}_k, \qquad (4.3)$$

where A_{33} and B_{33} denote the hydrodynamic added mass and radiation damping in heave respectively. Figure 4.2 shows the hydrodynamic added mass and radiation damping of a sphere half-submerged obtained based on the database available in [42].
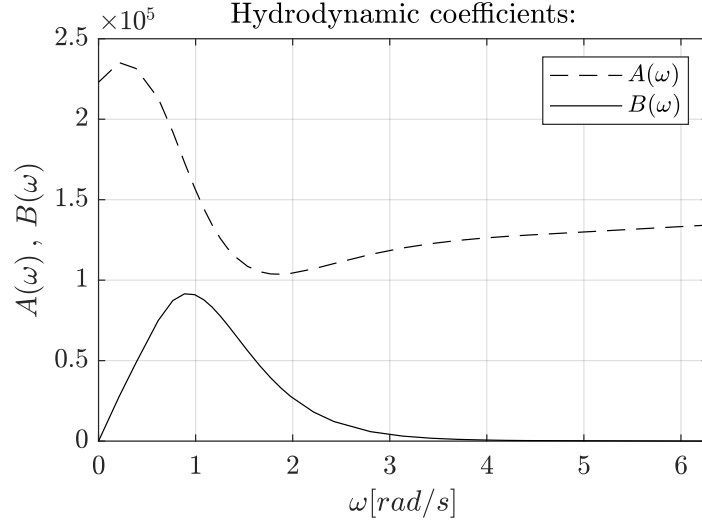
Figure 4.2: Added mass and radiation damping coefficients of a sphere ($R = 5$m).

- **Hydrostatic Stiffness, Linear ($F_{hs,l}$) and Nonlinear ($F_{hs,nl}$):**

The second linear force refers to the hydrostatic force that is caused due to the increment and decrement of the differential volume immersed. This component is also unrelated to the incident wave field according to the linear wave theory, and it can be described by:

$$F_{hs} = -\int S_{wpa}(z)\rho g dz. \tag{4.4}$$

Usually, the cross-sectional area is assumed to be constant, and the hydrostatic force can be described linearly with the body displacement. However, for some cases, the cross-section is a function of the height, and the linearization might lead to an unreliable hydrostatic force. For a sphere submerged around its center, the waterplane area S_{wpa} is given by;

$$S_{wpa}(z) = \pi \left(R^2 - z^2 \right) dz, \tag{4.5}$$

where R is the radius of the sphere. Substituting Equation (4.5) in Equation (4.4) yields:

$$F_{hs} = -\int \pi \left(R^2 - z^2 \right) \rho g dz. \tag{4.6}$$

As it can be observed, it is possible to divide the hydrostatic force into two terms, a linear and a nonlinear one as:

$$F_{hs} = F_{hs,l} + F_{hs,nl} = -\underbrace{\pi \rho g R^2}_{K_{hs,l}} z + \frac{\pi \rho g}{3} z^3, \tag{4.7}$$

where $K_{hs,l}$ refers to the linear hydrostatic restoring coefficient.

- **Mechanical Restoring Force (F_s):**

The third linear force is the mechanical restoring force caused by the mooring line that connects the buoy/PTO to the foundation. This force can be simply represented by a linear stiffness as:

$$F_s = -K_s z, \tag{4.8}$$

where K_s denotes the stiffness of the mooring line.

- **Spectrum of Excitation Force (S_f):**

The last linear force refers to the excitation force caused by the ocean waves, which is composed of two contributions: incident and diffracted waves. In the SL procedure described previously in Chapter 3, the excitation force is included in the spectrum of force $S_f(\omega)$. This force is represented by a spectrum which depends on the sea state and the excitation force per meter of wave amplitude as:

$$S_f(\omega) = |F_{exc}(\omega)|^2 S_\zeta(\omega). \tag{4.9}$$

Figure 4.3 shows the excitation force per meter of wave amplitude acting on the sphere in heave. For more information regarding the fluid-structure forces, such as radiation, hydrostatic and wave excitation forces, see Appendix A.
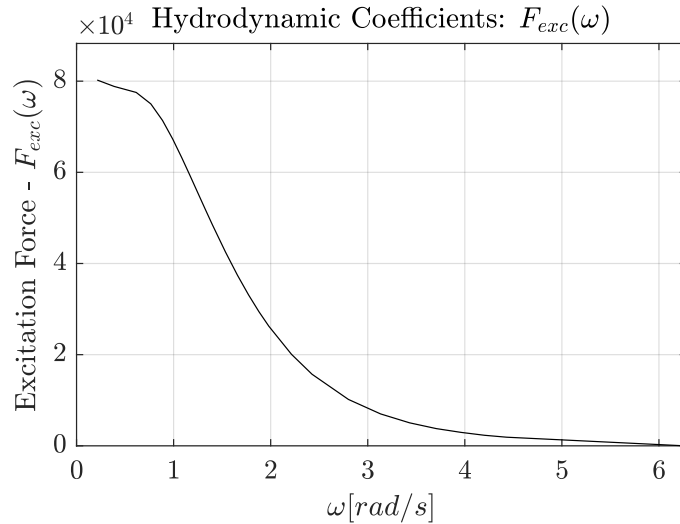

Figure 4.3: Excitation force per meter of wave amplitude in the heave direction of a sphere ($R = 5$m).

- **Lateral Stiffness (F_{ls}):**

Regarding the nonlinear forces, the first term refers to the nonlinear hydrostatic force, which was modeled for the case of a sphere in Equation (4.7). The second nonlinear force refers to some mooring systems with an additional lateral stiffness composed of two linear springs under transverse displacements, as illustrated in Figure 4.4.
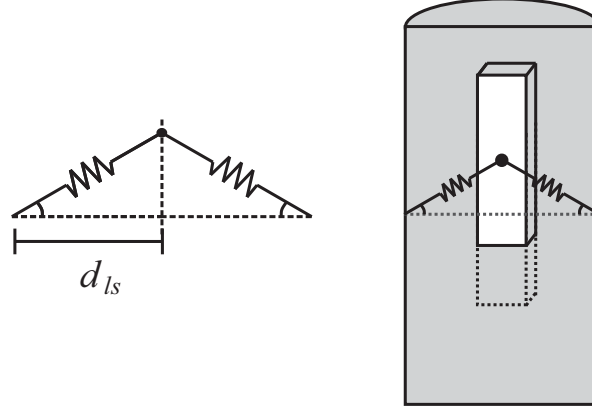

Figure 4.4: Lateral stiffness.

For such systems, the force exerted by the lateral springs in the vertical direction can be described by:

$$F_{ls} = -2K_{ls} \left(\sqrt{z^2 + d_{ls}^2} - l_{ls} \right) \sin\theta, \qquad (4.10)$$

where the projection of the spring forces is expressed as:

$$\sin\theta = \frac{z}{\sqrt{z^2 + d_{ls}^2}}. \qquad (4.11)$$

Substituting Equation (4.11) into Equation (4.10), the following nonlinear force is obtained:

$$F_{ls} = -2K_{ls} \left(1 - \frac{l_{ls}}{\sqrt{z^2 + d_{ls}^2}} \right) z. \qquad (4.12)$$

Note the length of the unstretched spring l_{ls} is smaller than the distance d_{ls}. Therefore, the system is stable at the origin, and the force increases the magnitude as the device move from the equilibrium point.

- **End-stop Mechanism (F_{es}):**

The third nonlinear force refers to the additional springs employed to the PTO system to preserve the structure from damaging when the device reaches a certain displacement. Figure 4.5 illustrates such a mechanism, which is named end-stop.
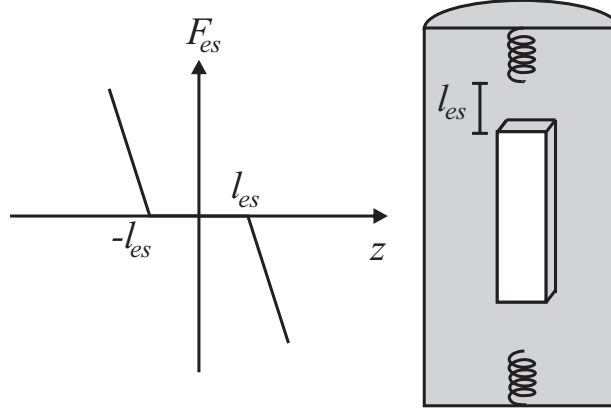

Figure 4.5: End-stop force.

Generally, the end-stop force is described by:

$$F_{es} = \begin{cases} 0, & \text{for} \quad l_{es} > |z| \\ -K_{es}(z - l_{es}), & \text{for} \quad z > l_{es} \\ -K_{es}(z + l_{es}), & \text{for} \quad -l_{es} > z \end{cases}, \qquad (4.13)$$

where K_{es} and l_{es} are the end-stop stiffness and the distance from the contact when the buoy is on its the mean position respectively.

- **Viscous Drag (F_{vd}):**

The fourth nonlinear force is a correction to the linear wave theory, which considers the inclusion of viscous drag forces. This correction is essential for a realistic estimation of the response due to the large displacements of WECs. The viscous drag contribution can be written based on Morison's equation as [43]:

$$F_{vd}(t) = -\frac{1}{2}\rho C_D S_\perp \dot{z}|\dot{z}|, \qquad (4.14)$$

where C_D is the drag coefficient, and $S_\perp$ denotes the cross-sectional area of the body perpendicular to the heave direction.

- **Electric Generator (F_{EG}):**

The last nonlinear force is to describe the PTO force. The PTO system is composed of an electric generator, which exerts a damping force associated with the electromagnetic force. The electromagnetic force can be represented as a function of the active area of the stator [44]:

$$F_{EG} = -C_{pto}A_{fac}(z)\dot{z}, \tag{4.15}$$

where C_{pto} is the magnitude of the damping, and A_{fac} denotes the active area of the stator given by:

$$A_{fac}(z) = \begin{cases} 0, & \text{for} \quad |z| \geq 1/2(l_p + l_s) \\ 1, & \text{for} \quad |z| \leq 1/2(l_p - l_s) \\ 1/l_s \left[1/2(l_p + l_s) - |z|\right], & \text{else,} \end{cases} \tag{4.16}$$

where l_s and l_p represent the length of the stator and piston respectively. Figure 4.6 illustrates the electric generator and its main dimensions.
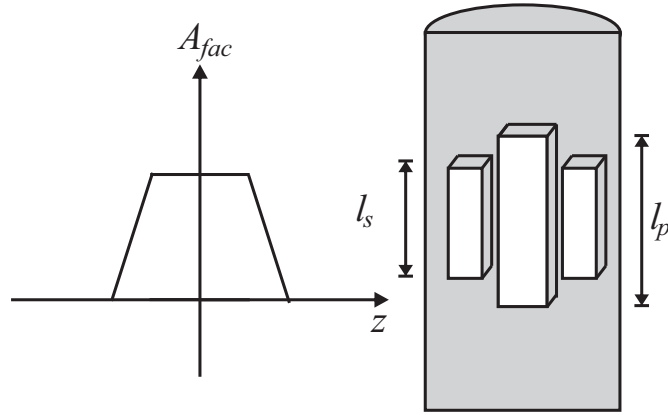
Figure 4.6: Electric generator.

Based on the electromagnetic damping force described in Equation (4.15), the instantaneous absorbed power can be obtained by:

$$P_{EG} = C_{pto}A_{fac}(z)\dot{z}^2, \tag{4.17}$$

and the mean power by:

$$\bar{P}_{EG} = \frac{1}{T} \int_0^T C_{pto}A_{fac}(z)\dot{z}^2 dt. \tag{4.18}$$

4.2 Linear System - Frequency Domain

Based on the system dynamics described above, the linearized form of Equation (4.1) can be expressed as:

$$[M + A_{33}(\omega)]\ddot{z} + [C_{pto} + B_{33}(\omega)]\dot{z} + [K_s + K_{hs,l}]z = F_{exc}(\omega). \tag{4.19}$$

Note that besides the linear forces, the damping exerted by the electric generator was linearized by neglecting the active area of the stator, while the lateral stiffness, end-stop, nonlinear hydrostatic stiffness, and viscous drag were neglected.

Based on Equation (4.19), the transfer function between the body displacement and wave excitation force can be calculated as:

$$\alpha(\omega) = [-\omega^2(M + A_{33}(\omega)) + i\omega(C_{pto} + B_{33}(\omega)) + K_s + K_{hs,l}]^{-1}. \tag{4.20}$$

Using this linear transfer function, the spectral response of the body displacement can be obtained by:

$$S_z(\omega) = |\alpha(\omega)|^2 S_f(\omega), \tag{4.21}$$

where the spectrum of the excitation force, $S_f(\omega)$ depends on the sea state condition and hydrodynamics of the buoy, namely:

$$S_f(\omega) = |F_{exc}(\omega)|^2 S_\zeta(\omega). \tag{4.22}$$

Based on Equation (4.18) and without the effect of the active area of the generator, the mean power absorbed by the linearized PTO system is given by:

$$\bar{P}_{EG} = \left\langle C_{pto}\dot{z}^2 \right\rangle, \tag{4.23}$$

which for a Gaussian distribution can be obtained as:

$$\bar{P}_{EG} = C_{pto}\sigma_{\dot{z}}^2, \tag{4.24}$$

where $\sigma_{\dot{z}}$ is the standard deviation of the body velocity.

4.3 Equivalent Linear System - Statistical Linearization

The equivalent linear transfer function between the body displacement and wave excitation force will have the form:

$$\alpha_{eq}(\omega) = [-\omega^2(M + A_{33}(\omega)) + i\omega(B_{33}(\omega) + B_{eq}) + K_s + K_{hs,l} + K_{eq}]^{-1}, \qquad (4.25)$$

where B_{eq} and K_{eq} are the equivalent linear terms of damping and stiffness given by:

$$B_{eq} = B_{eq,EG} + B_{eq,VD} = \left\langle \frac{\partial F_{EG}}{\partial \dot{z}} \right\rangle + \left\langle \frac{\partial F_{vd}}{\partial \dot{z}} \right\rangle, \qquad (4.26)$$

$$K_{eq} = K_{eq,HSNL} + K_{eq,LS} + K_{eq,ES} = \left\langle \frac{\partial F_{hs,nl}}{\partial z} \right\rangle + \left\langle \frac{\partial F_{ls}}{\partial z} \right\rangle + \left\langle \frac{\partial F_{es}}{\partial z} \right\rangle, \qquad (4.27)$$

where $B_{eq,EG}$, and $B_{eq,VD}$ denote the equivalent damping due to the electric generator and viscous drag respectively; $K_{eq,HSNL}$, $K_{eq,LS}$, and $K_{eq,ES}$ denote the equivalent stiffness due to the hydrostatic nonlinear term, lateral stiffness and end-stop respectively.

The equivalent spectral response of the body displacement is computed as:

$$S_z(\omega) = |\alpha_{eq}(\omega)|^2 S_f(\omega), \qquad (4.28)$$

where the spectrum of the wave excitation force is given by:

$$S_f(\omega) = |F_{exc}(\omega)|^2 S_\zeta(\omega). \qquad (4.29)$$

The technique initiates with an iterative procedure where the equivalent terms are calculated in each step and fed into the equivalent transfer function until the convergence. Once the results have converged, the mean power calculation via SL can be obtained taking the expectation based on Equation (4.18):

$$\bar{P}_{EG} = \left\langle C_{pto} A_{fac}(z) \dot{z}^2 \right\rangle, \qquad (4.30)$$

as the velocity and displacement are uncorrelated, it is possible to write the mean power based on the equivalent damping coefficient of the electric generator as:

$$\bar{P}_{EG} = B_{eq,EG} \sigma_{\dot{z}}^2, \qquad (4.31)$$

where $B_{eq,EG}$ accounts the effect of the active area of the stator and is obtained by the iterative approach.

4.4   Results

A nonlinear TD model is used to verify the reliability of the SL technique. In this regard, the radiation force in TD is described according to Cummins' equation, and the radiation impulse response function (memory function) was replaced by an equivalent state-space representation of order 3 via system identification (see Appendix B.1.1). Traditional FD model is used as a basis to verify the effect of the nonlinear forces.

- **Parameters:**

The spherical PA is half-submerged and excited by ocean waves described by the JONSWAP spectrum ($\gamma = 3.3$). Based on the scatter diagram of Imbituba - SC, Brazil (see in Figure 2.9), six sea states evenly spaced containing an interval of period of high probability of occurrence are simulated: $H_s = 1.75$m, and T_p from 7 to 12s. The main parameters of the simulation are given in Table 4.1. The natural frequency of the PA was set to operate between the range of higher probability of the incoming wave field to enhance the power absorption by adjusting the mechanical stiffness and the mass of the system. However, the system was not optimized.

$$\omega_n = \sqrt{\frac{K_s + K_{hs,1}}{M + A_{33}(\omega_n)}} \longrightarrow T_n \approx 9s. \tag{4.32}$$

Table 4.1: Simulation parameters of the PA.

| Property	Value	Unit
M	1.8×10^6	[kg]
R	5	[m]
K_s	200	$\left[\frac{\text{kN}}{\text{m}}\right]$
C_{pto}	50	$\left[\frac{\text{kN.s}}{\text{m}}\right]$
K_{es}	250	$\left[\frac{\text{kN}}{\text{m}}\right]$
l_{es}	1.5	[m]
K_{ls}	100	$\left[\frac{\text{kN}}{\text{m}}\right]$
d_{ls}	1	[m]
l_{ls}	1	[m]
l_p	4	[m]
l_s	3.5	[m]
C_D	0.5	[$-$]

• **Time Domain Simulation:**

Nonlinear TD simulations were used to assess the reliability of the SL technique. The total time simulated for each condition was equal to 5000s, 10 different wave phases were used in each sea state, and the wave force was discretized into 300 frequency components. Figure 4.7 illustrates the heave displacement of the PA for the sea states simulated for the first 500s.
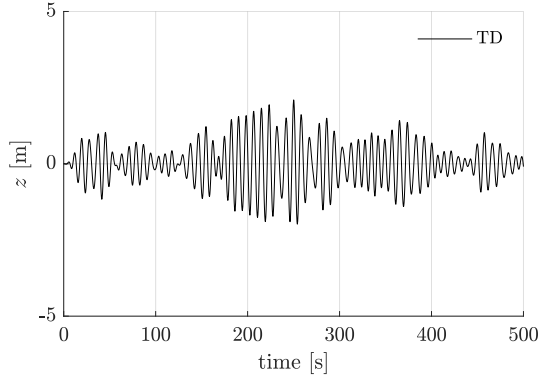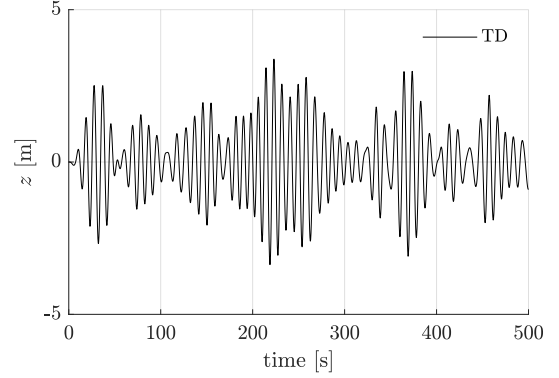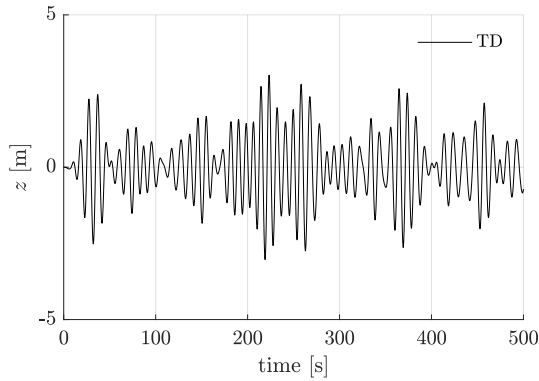

(a) 1st condition: $H_s = 1.75m; T_p = 7s$
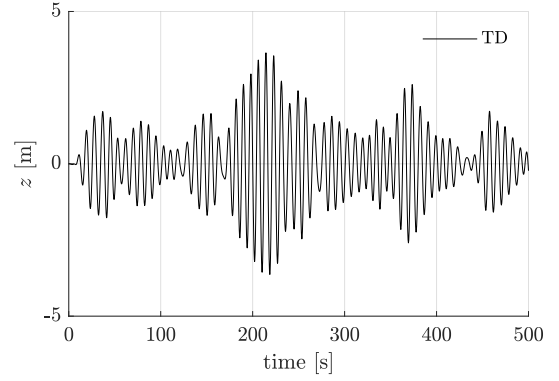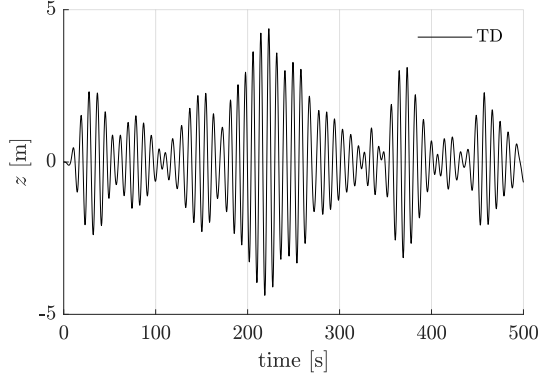
(b) 2nd condition: $H_s = 1.75m; T_p = 8s$

(c) 3rd condition: $H_s = 1.75m; T_p = 9s$

(d) 4th condition: $H_s = 1.75m; T_p = 10s$

(e) 5th condition: $H_s = 1.75m; T_p = 11s$
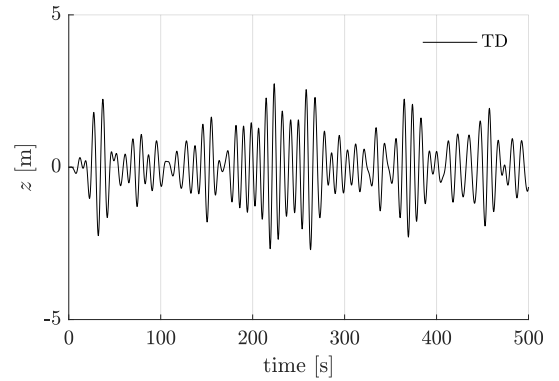
(f) 6th condition: $H_s = 1.75m; T_p = 12s$

Figure 4.7: Time series of the displacement in heave (first 500s).

• **Response Distribution:**

The SL relies on the assumption of a Gaussian distribution. Therefore, an initial procedure in the SL is the verification of the body response distribution. Based on that, the displacement distributions using nonlinear TD simulations are compared against the SL and traditional FD results based on the theoretical Gaussian distribution, which are illustrated in Figure 4.8.
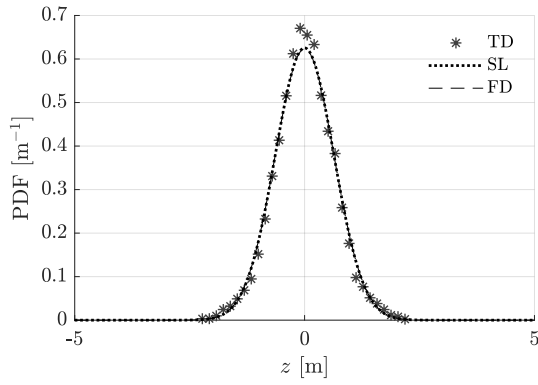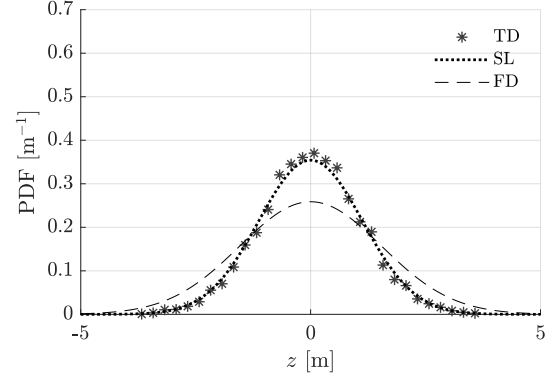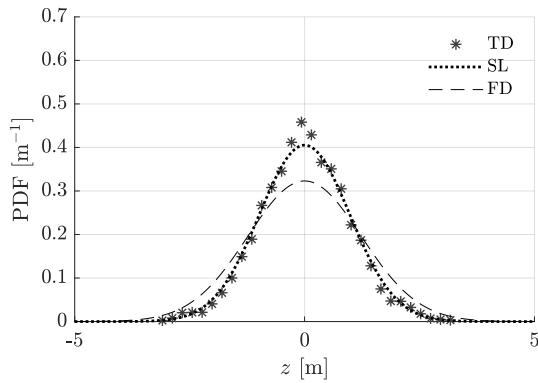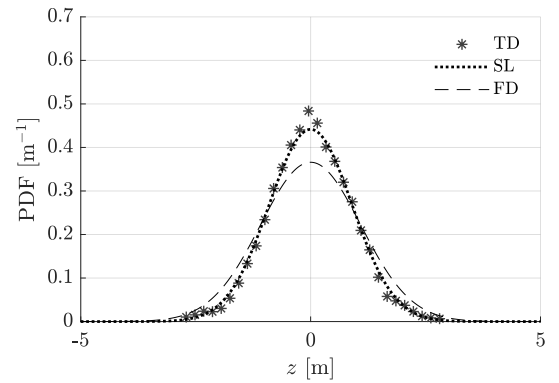

(a) 1^{st}condition: $H_s = 1.75m; T_p = 7s$
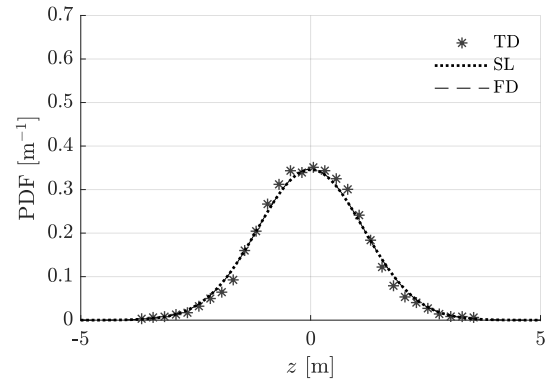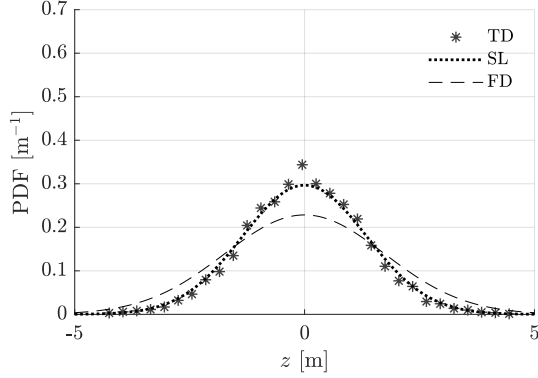
(b) 2^{nd}condition: $H_s = 1.75m; T_p = 8s$

(c) 3^{rd}condition: $H_s = 1.75m; T_p = 9s$

(d) 4^{th}condition: $H_s = 1.75m; T_p = 10s$

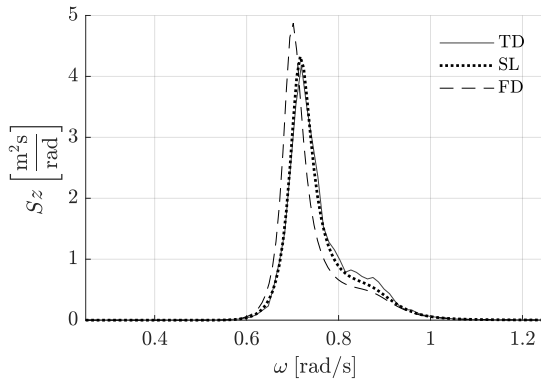(e) 5^{th}condition: $H_s = 1.75m; T_p = 11s$

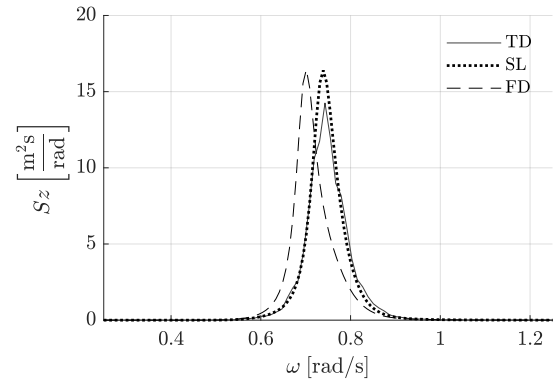(f) 6^{th}condition: $H_s = 1.75m; T_p = 12s$

Figure 4.8: Time series of the displacement in heave (first 500s).
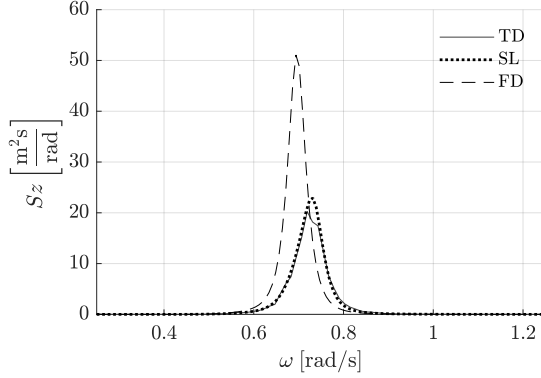
- **Spectral Response :**

Once the assumption of a Gaussian distribution of the displacement is verified, the spectral responses are analyzed. Figure 4.9 shows the PSD of the heave motion using TD, SL, and FD for all sea states. The PSDs of the nonlinear TD simulation was calculated using the *pwelch* function in MATLAB, which was calibrated using a linear TD simulation and compared with the FD results.
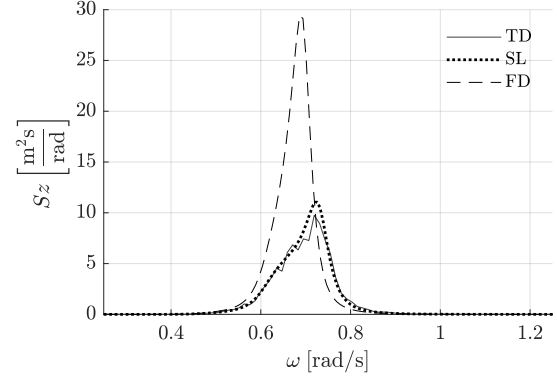

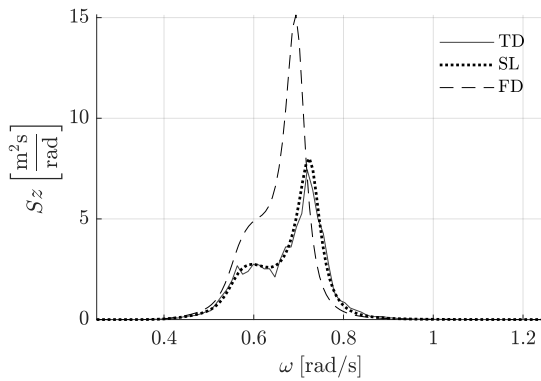(a) 1st condition: $H_s = 1.75m; T_p = 7s$

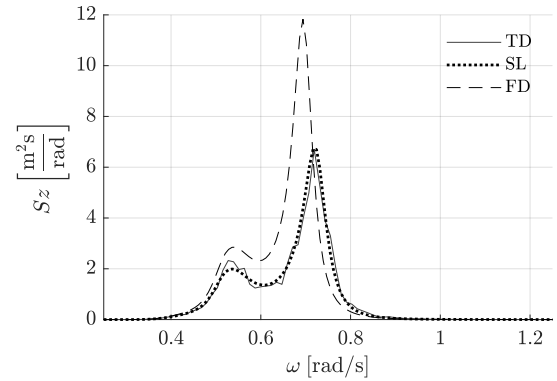(b) 2nd condition: $H_s = 1.75m; T_p = 8s$

(c) 3rd condition: $H_s = 1.75m; T_p = 9s$

(d) 4th condition: $H_s = 1.75m; T_p = 10s$

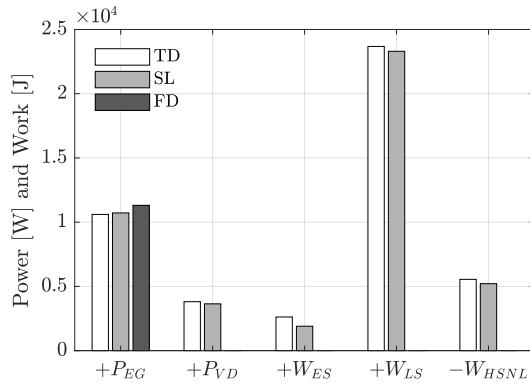(e) 5th condition: $H_s = 1.75m; T_p = 11s$
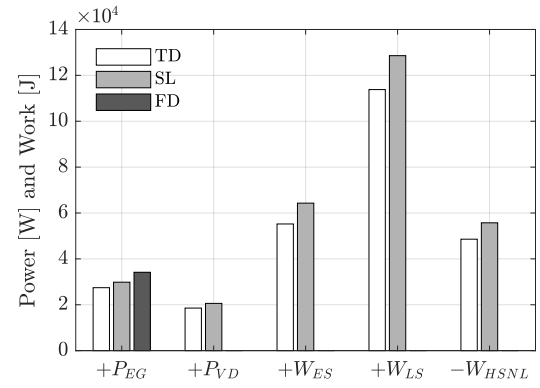
(f) 6th condition: $H_s = 1.75m; T_p = 12s$

Figure 4.9: Spectral response of the displacement of the Point Absorber.

- **Mechanical Work and Power Absorbed/Dissipated:**

For comparison purpose, the mechanical work done by the equivalent linear stiffness is compared to the mechanical work by the nonlinear term with displacement dependency using TD simulation. Similarly, the power dissipated by the equivalent linear damping is compared to the nonlinear term with velocity dependency. Figure 4.10 shows the power absorbed/dissipated, and work done by the nonlinearities for all sea states.
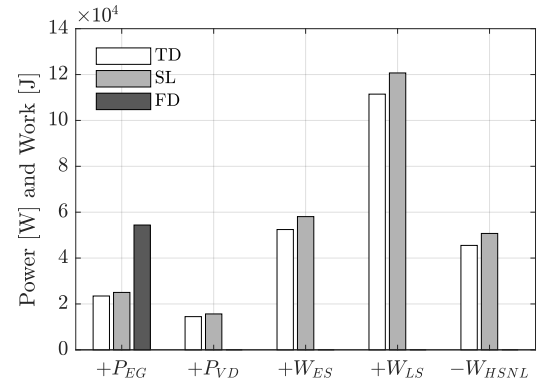

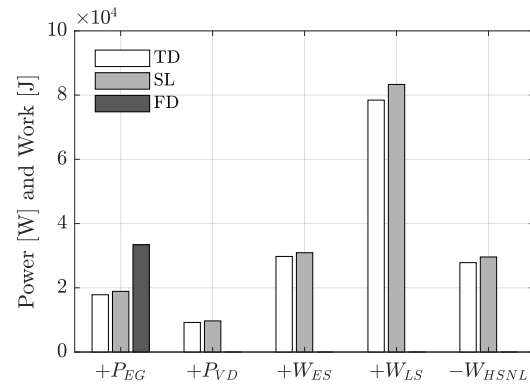(a) 1^{st}condition: $H_s = 1.75m; T_p = 7s$
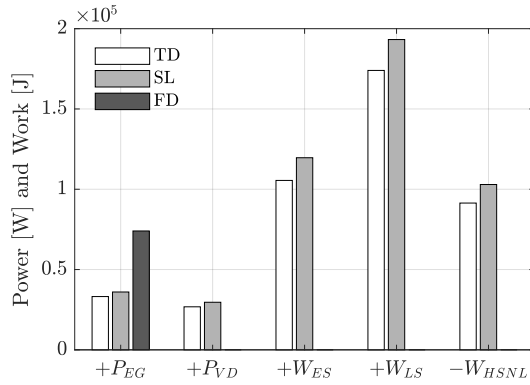
(b) 2^{nd}condition: $H_s = 1.75m; T_p = 8s$

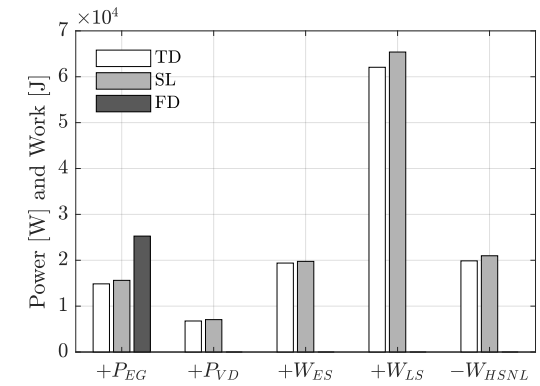(c) 3^{rd}condition: $H_s = 1.75m; T_p = 9s$

(d) 4^{th}condition: $H_s = 1.75m; T_p = 10s$

(e) 5^{th}condition: $H_s = 1.75m; T_p = 11s$

(f) 6^{th}condition: $H_s = 1.75m; T_p = 12s$

Figure 4.10: Power absorbed/dissipated and work done.

In figure 4.10, the subscripts $_{EG}$, $_{VD}$, $_{ES}$, $_{LS}$, and $_{HSNL}$, denotes the electric generator, viscous drag, end-stop, lateral stiffness, and nonlinear hydrostatic, respectively. The mechanical work by the nonlinear term using TD simulation is given by:

$$\bar{W} = \frac{1}{T} \int_0^T \Theta(z, \dot{z}) z \, dt, \tag{4.33}$$

and for SL technique, the mean mechanical work will be calculated based on the equivalent linear term as:

$$\bar{W} = K_{eq} \sigma_z^2. \tag{4.34}$$

The power exerted by the nonlinear term using TD simulation is given by:

$$\bar{P} = \frac{1}{T} \int_0^T \Theta(z, \dot{z}) \dot{z} \, dt, \tag{4.35}$$

and for the SL technique, the power exerted will be calculated based on the equivalent linear term as:

$$\bar{P} = B_{eq} \sigma_{\dot{z}}^2. \tag{4.36}$$

- **Capture Width Ratio:**

The efficiency of the device is analyzed based on the capture width ratio (CWR). The CWR is a parameter used to evaluate the WEC performance, which is the ratio between the total mean power absorbed by the device and the wave power available.

$$CWR = \frac{\bar{P}_{abs}}{\bar{P}_{wave} w}. \tag{4.37}$$

where $\bar{P}_{abs}$ is the mean power absorbed by the device, $\bar{P}_{wave}$ is the mean wave power per unit of width (as described in Equation (2.16)), and w is the width of the device. Table 4.2 shows the CWR of the PA for all sea states simulated.

Table 4.2: Capture Width Ratio of the PA using SL.

Condition	$\bar{P}_{wave}$ [kW]	$\bar{P}_{EG}$ [kW]	CWR [%]
$1^{st} : H_s = 1.75m; T_p = 7s$	9.46	10.72	11.33
$2^{nd} : H_s = 1.75m; T_p = 8s$	11.17	29.84	26.71
$3^{rd} : H_s = 1.75m; T_p = 9s$	12.92	36.01	27.88
$4^{th} : H_s = 1.75m; T_p = 10s$	14.64	25.02	17.09
$5^{th} : H_s = 1.75m; T_p = 11s$	16.27	18.89	11.61
$6^{th} : H_s = 1.75m; T_p = 12s$	17.77	15.62	8.79

- **Simulation time**

The main advantage of the SL is the low computational cost, while producing reliable estimations of the system dynamics. For the conditions simulated in this work, the SL technique required approximately 5 iterations to achieve a relative error of 0.1%. TD simulations require long periods to assume as valid the ergodicity. In addition, as the TD response depends on the wave phase components, the simulation of different incoming waves was performed for more smooth results. Table 4.3 shows the simulation time (mean) for each model. Note that the FD results denote the linear model.

Table 4.3: Simulation time - PA.

	TD	SL	FD
Time:	195.2 [s]	0.0522 [s]	0.0048 [s]

4.5   Discussion

The SL technique is based on the assumption that the excitation and distribution are stochastic processes described by Gaussian distribution, in which the displacement distribution can be verified in Figure 4.8. In general, even though the system has several nonlinearities, the results are relatively comparable with the theoretical Gaussian distribution for the case simulated and the parameters used, preserving the standard deviation. For the first and second sea states simulated, the heave distribution was comparable for all models (TD, SL and FD). For these results, the spectral moment of zero order was the same for all models; however, it was possible to verify the changes in the system dynamics based on Figure 4.9. In most cases, the SL also showed a good agreement with the PSD results using nonlinear TD simulation, preserving the spectral energy in each frequency component. The main divergences in the linear and nonlinear results occurred close to resonance when the nonlinear effects are more relevant due to the large displacements. This effect can be observed in the PDF and PSD of the response, given in Figures 4.8 and 4.9, for the cases (c) and (d).

The mechanical work and power absorbed/dissipated by the nonlinear forces were well captured by the SL technique for all nonlinearities, while the FD model was not able to capture these influence (see Figure 4.10). As expected, the nonlinear effects are more relevant for the conditions close to the resonance, where the PA experiences large

displacements. In this region, the device achieves better performance, around 27.88%, (see Table 4.2). However, note that the device is not set to operate in its highest efficiency for power production, and an optimization procedure must be performed for a more reliable estimation of the device efficiency. In addition, the overall efficiency must consider the performance of the PA in all sea states and its probability of occurrence. The main advantage of the SL is the low computational cost compared to TD simulations (see Table 4.3), while maintaining a reasonable estimation of the system response. Therefore, the SL can be used as a valuable tool for optimization routines to analyze all sea states, and select the best design parameters.

5 OSCILLATING WATER COLUMN

OWC device is WEC category that has demonstrated a high efficiency. Currently, several OWC devices/prototypes are operating in many places around the globe [12]. Typically, the structure of such devices is composed of a fixed hollow structure that acts as a chamber. The base of the structure is located below the sea level and exposed to the incident wave field. The pressure variation caused by the waves leads the inner surface to oscillate in which compresses and decompresses the air inside moving an air turbine connected to a generator. Usually, bidirectional turbines, such as Wells turbines, are employed. Figure 5.1 illustrates a typical OWC and its main components.
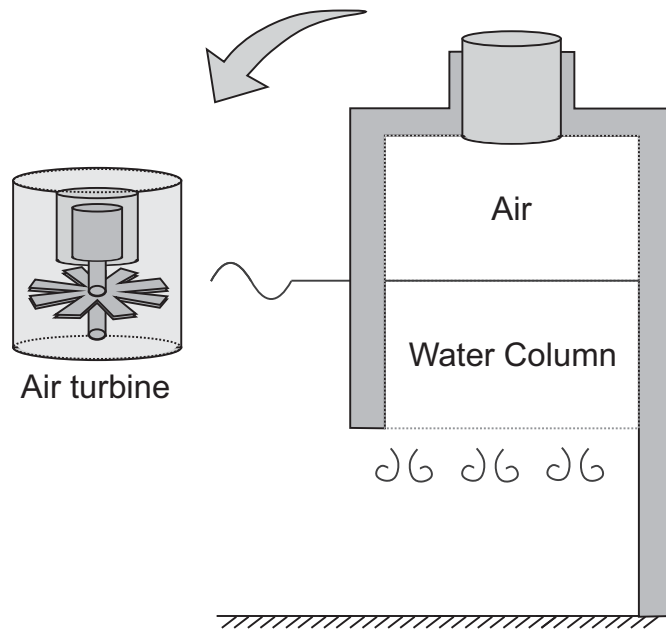
Figure 5.1: Illustration of an Oscillating Water Column.

5.1 Governing equation

Consider the OWC structure composed of a fixed box-shaped chamber that pierces a quiescent free surface. The control volume is defined as the chamber structure limits, which is composed of an air mass (m_{air}) and a water column (m_w). The mass inside this control volume varies as the inner surface is free to move. Therefore, the mass inside the chamber (m_{ch}) can be expressed as:

$$m_{ch} = m_w + m_{air}, \tag{5.1}$$

where:

$$m_w = \rho_w S(H + \xi), \tag{5.2}$$

$$m_{air} = \rho_{air} S(L - \xi). \tag{5.3}$$

where H denotes the nominal draft, L denotes the air-chamber height at the nominal position, ρ_{air} is the air density which varies due compressibility effects, $\xi(t)$, denotes the water column displacement, and S is the cross-sectional area of the chamber. Figure 5.2 illustrates the description of the control volume and the main components.
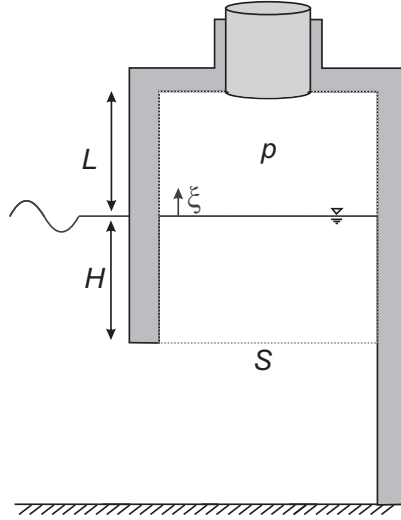

Figure 5.2: Description of the system

The mass inside the control volume has an explicit dependency on the water column displacement, as in Equations (5.2) and (5.3). Taking the first time derivative of the mass

inside the control volume, the mass flux rate is obtained.

$$\dot{m}_{ch} = \dot{m}_w + \dot{m}_{air},$$

$$\dot{m}_w = \rho_w S\dot{\xi}, \tag{5.4}$$

$$\dot{m}_{air} = -\dot{m}_{turb} = -\rho_{air}S\dot{\xi} + \dot{\rho}_{air}S(L - \xi), \tag{5.5}$$

where the mass flow rate of air is given by $\dot{m}_{air}$ and represents the air that passes through the turbine and produces energy. The negative sign occurs as the air flux is defined positive for outward flow from the chamber.

- **Air Turbine:**

The air flux and pressure are related by the air turbine via the turbine's performance in terms of dimensionless coefficients to simplify the physics behind the aerodynamics of those turbine [45]. The dimensionless parameters of: pressure head Ψ, flow rate Φ, power coefficient Π, and turbine efficiency η are given by:

$$\Phi = f_Q(\Psi), \tag{5.6}$$

$$\Pi = f_p(\Psi), \tag{5.7}$$

where

$$\Psi = \frac{p}{\rho_{in}N^2D^2}, \tag{5.8}$$

$$\Phi = \frac{\dot{m}_{turb}}{\rho_{in}ND^3}, \tag{5.9}$$

$$\Pi = \frac{P_{turb}}{\rho_{in}N^3D^5}, \tag{5.10}$$

$$\eta = \frac{\Pi}{\Psi\Phi}, \tag{5.11}$$

where N is the turbine rotational speed (rad/s), D denotes the rotor diameter, p is the manometric pressure, ρ_{in} is the air density in stagnation conditions at the turbine entrance (assumed equal to ρ_{air}), and P_{turb} is the power absorbed by the turbine. Figure 5.3 illustrates the dimensionless parameters of the air turbine used in this work.
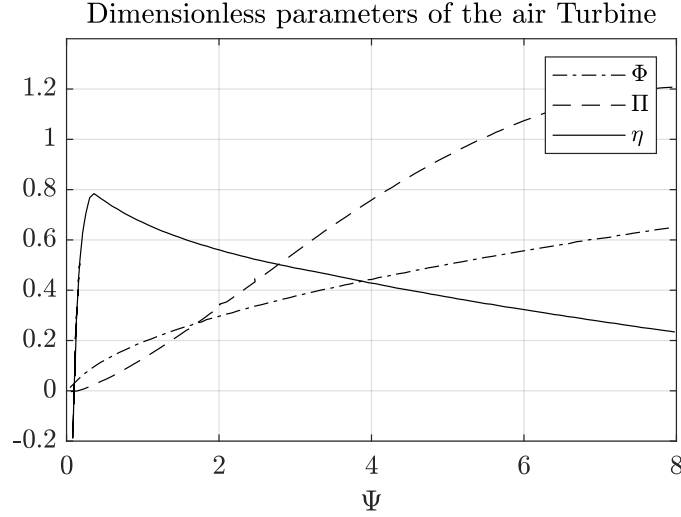
Figure 5.3: Dimensionless parameters of the air turbine, obtained from [45].

- **Air Pressure:**

Considering that the PTO system is composed of Wells turbines, a linear relationship between the mass flow rate and the pressure fluctuation can be established [46], $\Phi = K\Psi$. Therefore, the mass flow rate can be expressed in the dimensional form as:

$$\dot{m}_{turb} = \frac{KD}{N}p, \tag{5.12}$$

where K is the proportionality constant. Considering the air inside the chamber goes through an isentropic process [47], the time derivative of the density can be expressed as:

$$\dot{\rho}_{air} = \frac{1}{c_a^2}\dot{p}, \tag{5.13}$$

where c_a is the speed of sound in atmospheric conditions. Based on the previous assumptions, the air pressure inside the chamber can be expressed as:

$$\rho_{air}S\dot{\xi} = \frac{KD}{N}p + \frac{S}{c_a^2}(L - \xi)\dot{p}. \tag{5.14}$$

- **Water Column Dynamics:**

Regarding the water column dynamics, a single DOF based on the plug-flow representation is used, where the water column displacement is represented via the generalized coordinate ξ. The water column dynamic is formulated based on the derivations described in [48–50], which considered a non-forced system and without dissipative forces:

$$\rho_w S(\xi + H)\ddot{\xi} + \rho_w Sg\xi = 0. \tag{5.15}$$

Three non-conservative forces are incorporated into the governing equation of the water column dynamics:

- the excitation force caused by the wave action, f_{exc}, at the bottom of the control surface (a non-material surface).

- the force caused by the air pressure inside the chamber, f_{ch}, at the free-surface (a material interface).

- an ad-hoc force due to the viscous effects, f_v, caused by vortical flow at the mouth.

$$f^{nc} = f_{exc} + f_{ch} + f_v. \tag{5.16}$$

The excitation force is calculated by integrating the wave pressure over the bottom of the control volume. Three assumptions are considered for the excitation force, (i) the structure reflects the wave (reflective wave), (ii) the dimension of the OWC is small compared to the wavelength (uniform pressure), and (ii) the waves can be described by the linear wave theory. Based on that, the reflective wave [35] will result in an excitation force as:

$$f_{ext} = 2\zeta_a \rho_w g S \cos(kx - \omega t) \frac{\cosh(k(h - H))}{\cosh(kh)}, \tag{5.17}$$

where ζ_a represents the wave amplitude, h denotes the water depth, g is the gravitational acceleration and k is the wavenumber given by (see Equation (2.11)):

$$k = \frac{\omega^2}{g \tanh(kh)}. \tag{5.18}$$

Figure 5.4 illustrates the wave force of the OWC, as described in Equation (5.17).
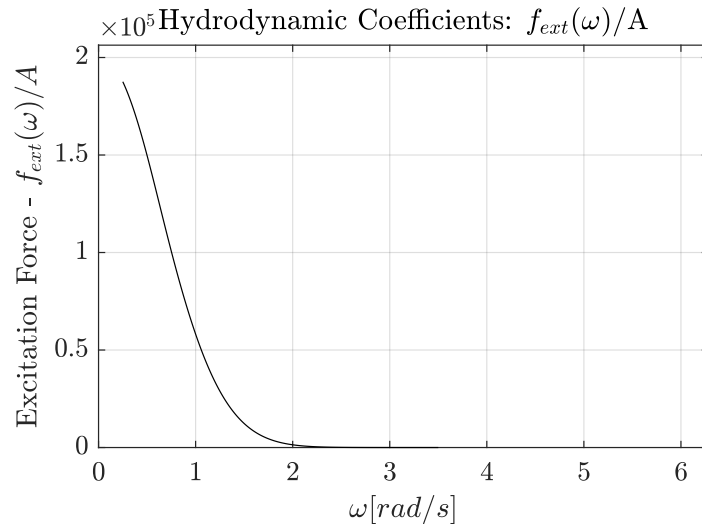

Figure 5.4: Wave excitation force per unit of wave amplitude of the OWC.

The force exerted by the air pressure inside the chamber acting on the free-surface can be modeled as:

$$f_{ch} = -Sp. \tag{5.19}$$

The ad-hoc viscous flow effects at the mouth of the structure can be expressed as:

$$f_v = -\frac{1}{2}C_v\rho_w S\dot{\xi}|\dot{\xi}|, \tag{5.20}$$

where C_v represents the viscous coefficient.

- **Governing Equations:**

Considering the non-conservative force terms described above and rearranging/simplifying the equation, the resulting governing equation for the OWC is given by:

$$(\xi + H)\ddot{\xi} + \frac{1}{2}C_v\dot{\xi}|\dot{\xi}| + g\xi + \frac{1}{\rho_w}p = F_{ext}, \tag{5.21}$$

with:

$$F_{ext} = f_{ext}/(\rho_w S).$$

For the air-chamber pressure, rearranging Equation (5.14) yields:

$$\frac{KD}{NS}p + \frac{1}{c_a^2}(L - \xi)\dot{p} - \rho_{air}\dot{\xi} = 0. \tag{5.22}$$

Besides the water column dynamics and pressure, the analysis of wave energy devices relies on the estimation of the power produced. Based on Equations (5.7) and (5.10), the instantaneous power output of the air turbine is [46]:

$$P_t(t) = \rho_{air}N^3D^5 f_p\left(\frac{p(t)}{\rho_{air}N^2D^2}\right). \tag{5.23}$$

Therefore, the mean power over a period T of time is given by:

$$\bar{P}_{turb} = \frac{\rho_{air}N^3D^5}{T}\int_{t_0}^{t_0+T} f_p\left(\frac{p(t)}{\rho_{air}N^2D^2}\right)dt. \tag{5.24}$$

where the nonlinear function, f_p, is shown in Figure 5.3.

5.2 Linear System - Frequency Domain

The SL uses the linearized system as an initial guess to start the iterative process. In addition, the mean power is calculated to compare the difference between the traditional FD results with those using SL. In this regard, the linearized form of Equations (5.21) and (5.22) are derived:

$$H\ddot{\xi} + g\xi + \frac{1}{\rho_w}p = F_{ext},\tag{5.25}$$

$$\frac{KD}{NS}p + \frac{L}{c_a^2}\dot{p} - \rho_{air}\dot{\xi} = 0.\tag{5.26}$$

The transfer function of the system response is given by:

$$\boldsymbol{\alpha}(\omega) = [-\omega^2(\mathbf{M}) + \mathbf{i}\omega(\mathbf{B}) + (\mathbf{K})]^{-1}.\tag{5.27}$$

with:

$$\mathbf{M} = \begin{bmatrix} H & 0 \\ 0 & 0 \end{bmatrix},$$

$$\mathbf{B} = \begin{bmatrix} 0 & 0 \\ -\rho_{air} & L/c_a^2 \end{bmatrix},$$

$$\mathbf{K} = \begin{bmatrix} g & 1/\rho_w \\ 0 & KD/NS \end{bmatrix}.$$

The response matrix is computed as:

$$\mathbf{S_q}(\omega) = \boldsymbol{\alpha}(\omega)\mathbf{S_F}(\omega)\boldsymbol{\alpha}^{\mathrm{T}}(\omega),\tag{5.28}$$

where $\mathbf{S_F}(\omega)$ denotes the power spectrum of the excitation, and $(\ )^{\mathrm{T}}$ is the transpose conjugate of a matrix. As the wave excites the water column, the power spectrum of the excitation force contain only the first term:

$$S_{F,11}(\omega) = |F_{ext}|^2 S_\zeta(\omega).\tag{5.29}$$

Based on the Gaussian distribution of the pressure response and the Equation (5.24), the mean power estimation in FD can be determined by taking the expectation as:

$$\bar{P}_{turb} = \rho_{air}N^3 D^5 \left\langle f_p\left(\frac{p}{\rho_{air}N^2 D^2}\right)\right\rangle,\tag{5.30}$$

where p is composed of a random zero mean component.

5.3 Equivalent Linear System - Statistical Linearization

The equivalent linear system is based on nonlinear terms, which are given by:

$$\Theta_1 = \xi\ddot{\xi} + \frac{1}{2}C_v\dot{\xi}|\dot{\xi}| \tag{5.31}$$

$$\Theta_2 = -\frac{1}{c_a^2}\xi\dot{p} \tag{5.32}$$

Unlike the PA, the OWC is characterized by a system with a constant offset due to its source of nonlinearities. Therefore, the additional procedure described in Subsection 3.3.1 is required. The mean values are obtained by taking the expectation, which for the pressure inside the chamber is given by:

$$\frac{KD}{NS}\bar{p} - \frac{1}{c_a^2}\langle\xi\dot{p}\rangle = 0, \tag{5.33}$$

and for the water column is given by:

$$\langle\xi\ddot{\xi}\rangle + g\bar{\xi} + \frac{1}{\rho_w}\bar{p} = 0. \tag{5.34}$$

The equivalent linear terms are calculated, and the equivalent linear transfer function can be expressed as:

$$\boldsymbol{\alpha}_{eq}(\omega) = [-\omega^2(\mathbf{M} + \mathbf{M}_{eq}) + i\omega(\mathbf{B} + \mathbf{B}_{eq}) + \mathbf{K}]^{-1}, \tag{5.35}$$

with:

$$\mathbf{M}_{eq} = \begin{bmatrix} \bar{\xi} & 0 \\ 0 & 0 \end{bmatrix},$$

$$\mathbf{B}_{eq} = \begin{bmatrix} \left\langle\frac{\partial}{\partial\dot{\xi}}(C_v\dot{\xi}|\dot{\xi}|/2)\right\rangle & 0 \\ 0 & \bar{\xi}/c_a^2 \end{bmatrix}.$$

Note that for these types of nonlinearities there is not an equivalent linear term for the stiffness. The equivalent response matrix is computed as:

$$\mathbf{S}_{\mathbf{q}}(\omega) = \boldsymbol{\alpha}_{eq}(\omega)\mathbf{S}_{\mathbf{F}}(\omega)\boldsymbol{\alpha}_{eq}^{\mathrm{T}}(\omega). \tag{5.36}$$

Once the iterative procedure has converged, the mean power estimation can be deter-

mined by taking the expectation as:

$$\bar{P}_{turb} = \rho_{air} N^3 D^5 \left\langle f_p \left(\frac{p}{\rho_{air} N^2 D^2} \right) \right\rangle, \tag{5.37}$$

where $p(t)$ is composed of a non-zero mean and a random zero mean component.

5.4 Results

A nonlinear TD model is used to verify the reliability of the SL results. FD results are used as a basis to analyze the nonlinear effects compared to the linear system.

- **Parameters:**

The system is considered to be excited by the same sea state condition of the PA, in which a high probability of occurrence range in Imbituba - SC, Brazil is selected ($H_s = 1.75$m, and T_p from 7 to 12s). The main parameters of the simulation are described in Table 5.1. The natural frequency of the OWC was set to operate within the range of higher probability to enlarge the power absorption. However, the system was not optimized.

$$\omega_n = \sqrt{\frac{g}{H}} \longrightarrow T_n \approx 7s. \tag{5.38}$$

Table 5.1: Simulation parameters of the OWC.

| Property	Value	Unit
ρ_w	1025	[kg/m³]
ρ_{air}	1.25	[kg/m³]
c_a	344	[m/s]
g	9.81	[m/s²]
C_v	0.5	[−]
K_T	0.28	[−]
H	12.2	[m]
D	1.75	[m]
L	9	[m]
h	50	[m]
S	10	[m²]
N	30	[rad/s]

- **Time Domain Simulation:**

Like the PA case, nonlinear TD simulations were conducted to verify the reliability of the results obtained using the SL technique. The simulation time was equal to 5000s, 10 different combinations of wave phases were used in each sea state, and the wave force was discretized into 300 frequency components. Figure 5.5 and Figure 5.6 show the first 500s of the water column elevation and the pressure inside the chamber for each sea state.
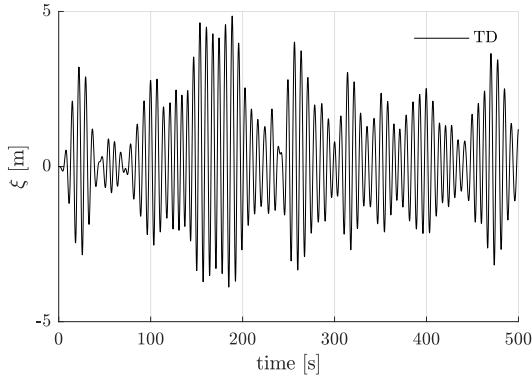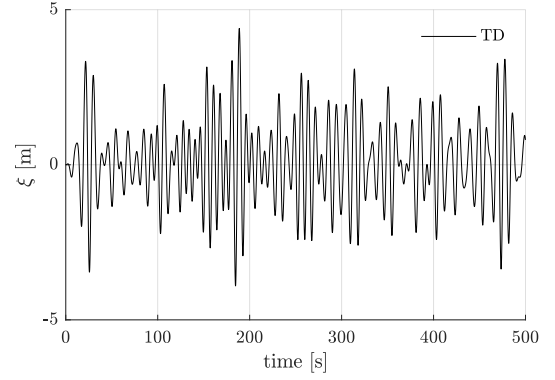

(a) 1st condition: $H_s = 1.75m; T_p = 7s$
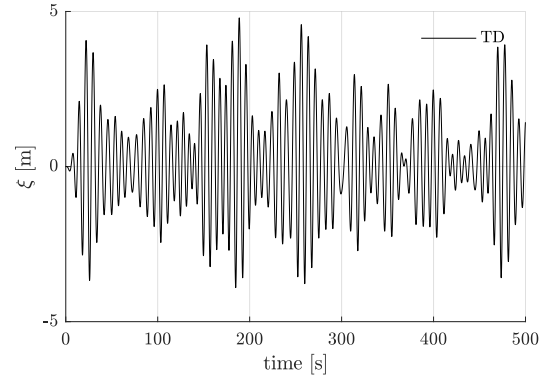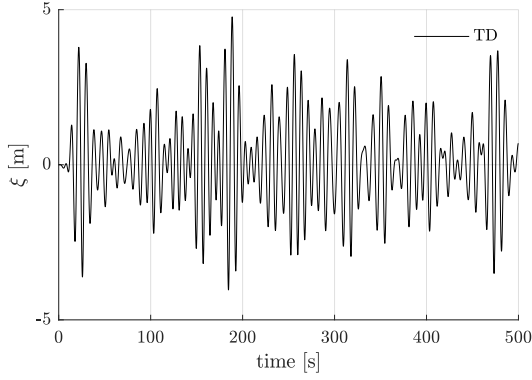
(b) 2nd condition: $H_s = 1.75m; T_p = 8s$

(c) 3rd condition: $H_s = 1.75m; T_p = 9s$

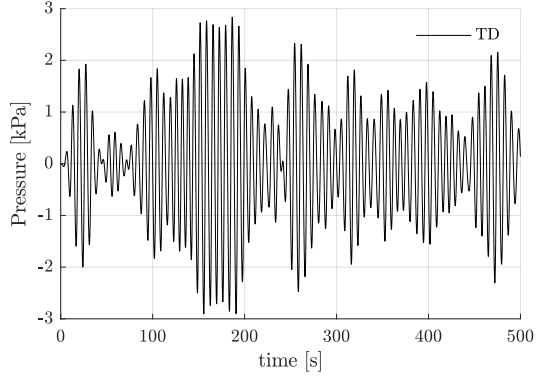(d) 4th condition: $H_s = 1.75m; T_p = 10s$
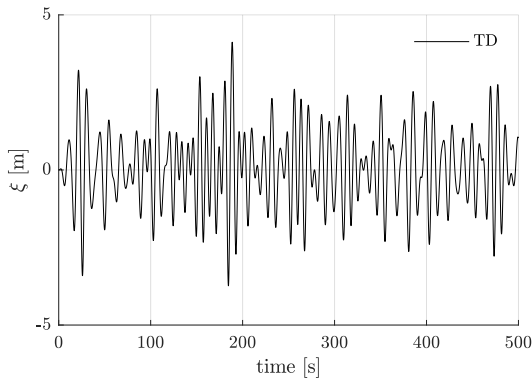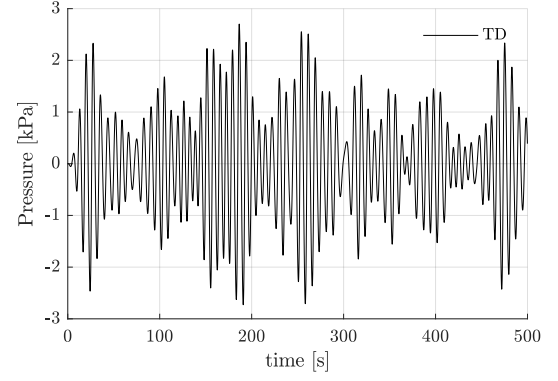
(e) 5th condition: $H_s = 1.75m; T_p = 11s$
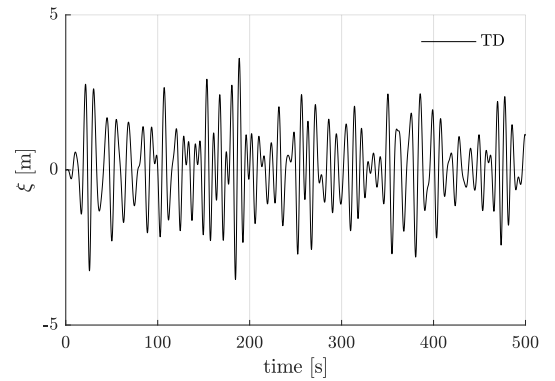
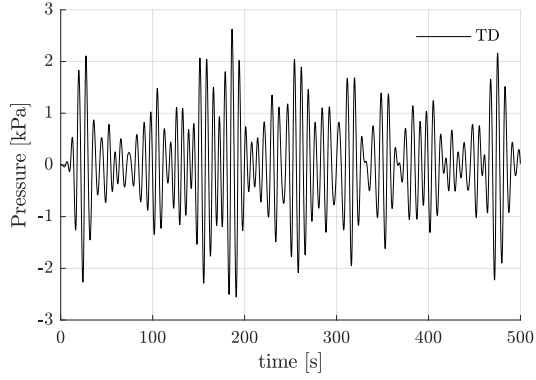(f) 6th condition: $H_s = 1.75m; T_p = 12s$

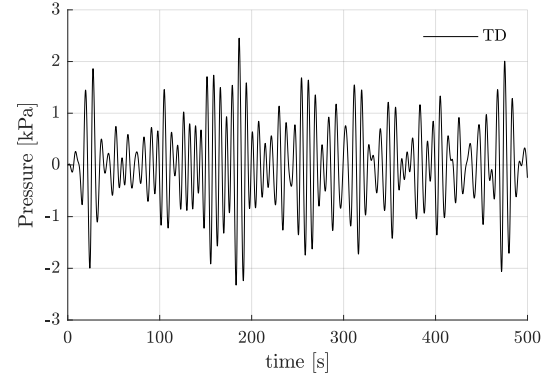Figure 5.5: Time series of the water column displacement (first 500s).
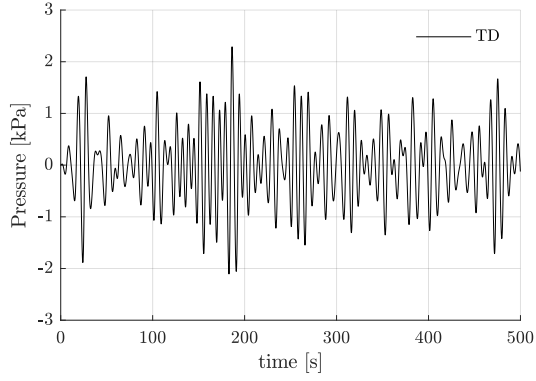
(a) 1st condition: $H_s = 1.75m; T_p = 7s$

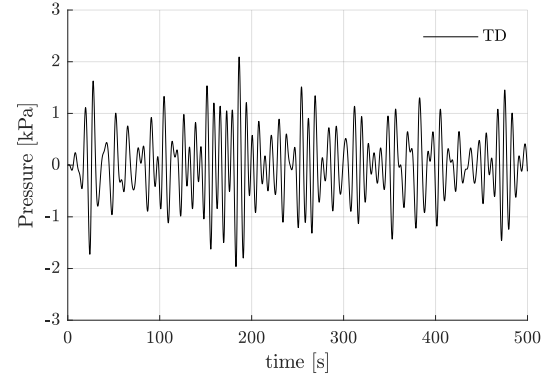(b) 2nd condition: $H_s = 1.75m; T_p = 8s$

(c) 3rd condition: $H_s = 1.75m; T_p = 9s$

(d) 4th condition: $H_s = 1.75m; T_p = 10s$
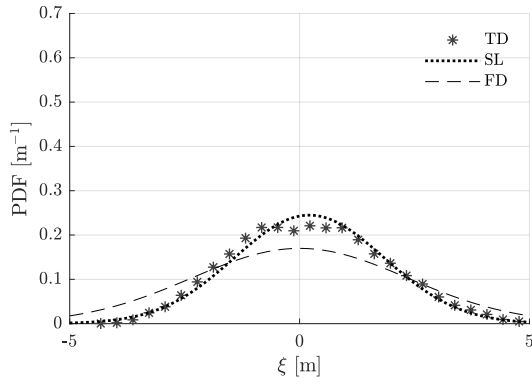
(e) 5th condition: $H_s = 1.75m; T_p = 11s$
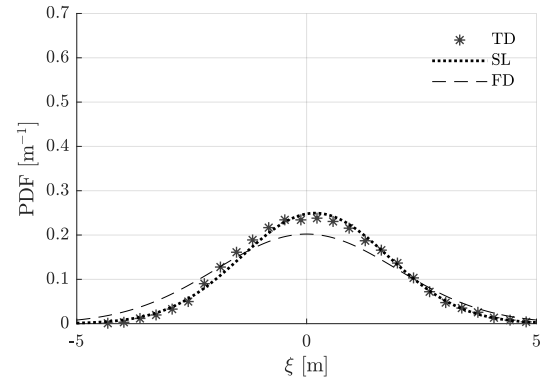
(f) 6th condition: $H_s = 1.75m; T_p = 12s$

Figure 5.6: Time series of the pressure inside the chamber (first 500s).

- **Response Distribution:**

As an initial procedure, the assumption of a Gaussian distribution must be verified for the OWC wave energy device. Based on that, the water column displacement and pressure distribution using nonlinear TD simulations are compared with the results obtained using SL and traditional FD simulations based on the theoretical Gaussian distribution, which are shown in Figures 5.9 and 5.10.

(a) 1st condition: $H_s = 1.75m; T_p = 7s$
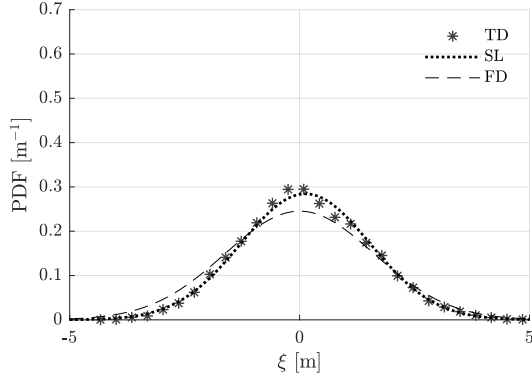
(b) 2nd condition: $H_s = 1.75m; T_p = 8s$

(c) 3rd condition: $H_s = 1.75m; T_p = 9s$

(d) 4th condition: $H_s = 1.75m; T_p = 10s$

(e) 5th condition: $H_s = 1.75m; T_p = 11s$

(f) 6th condition: $H_s = 1.75m; T_p = 12s$

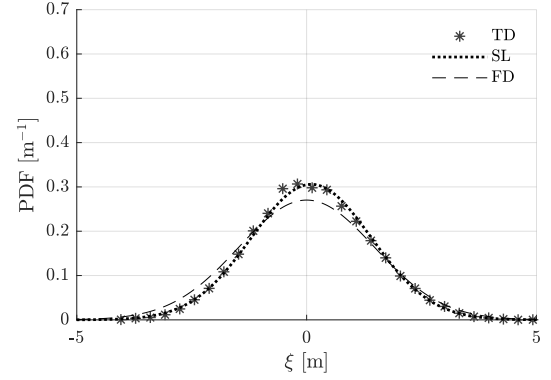Figure 5.7: Water column displacement distribution.

(a) 1st condition: $H_s = 1.75m; T_p = 7s$

(b) 2nd condition: $H_s = 1.75m; T_p = 8s$

(c) 3rd condition: $H_s = 1.75m; T_p = 9s$

(d) 4th condition: $H_s = 1.75m; T_p = 10s$

(e) 5th condition: $H_s = 1.75m; T_p = 11s$

(f) 6th condition: $H_s = 1.75m; T_p = 12s$

Figure 5.8: Chamber's pressure distribution.

- **Spectral Response:**

Once the main assumption of the SL was verified, the spectral response of the water column and pressure were analyzed. Figures 5.9 and 5.10 show the PSD of the water column displacement and pressure inside the chamber respectively for all sea states simulated.

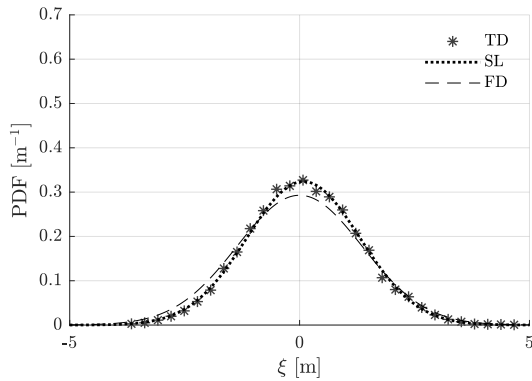(a) 1st condition: $H_s = 1.75m; T_p = 7s$
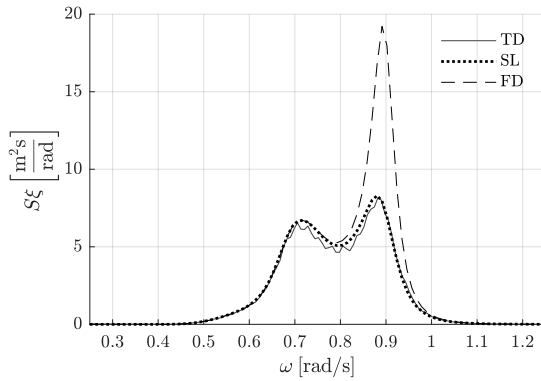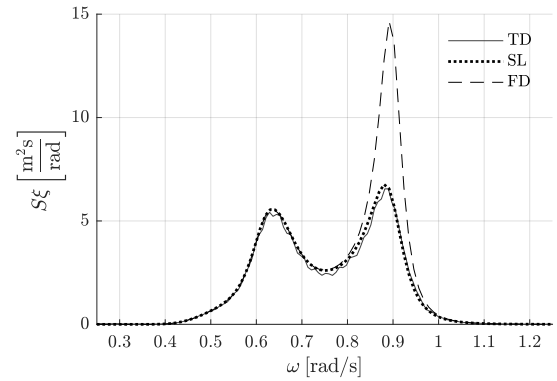
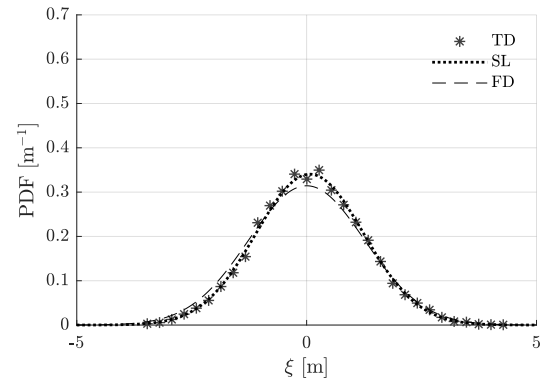(b) 2nd condition: $H_s = 1.75m; T_p = 8s$

(c) 3rd condition: $H_s = 1.75m; T_p = 9s$

(d) 4th condition: $H_s = 1.75m; T_p = 10s$
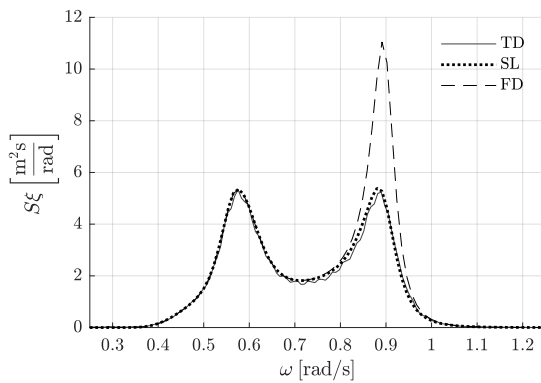
(e) 5th condition: $H_s = 1.75m; T_p = 11s$
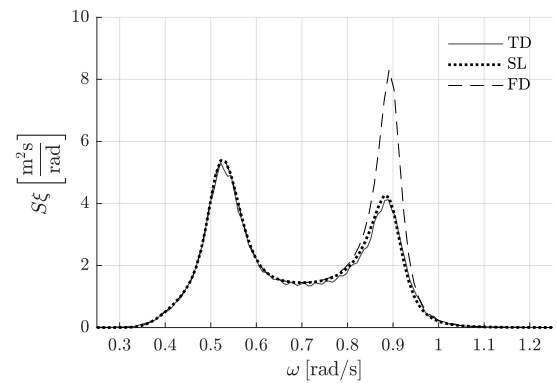
(f) 6th condition: $H_s = 1.75m; T_p = 12s$

Figure 5.9: Spectral response of the water column displacement.
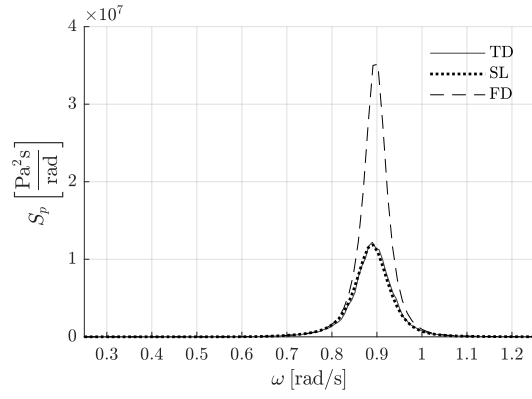
(a) 1^{st}condition: $H_s = 1.75m; T_p = 7s$
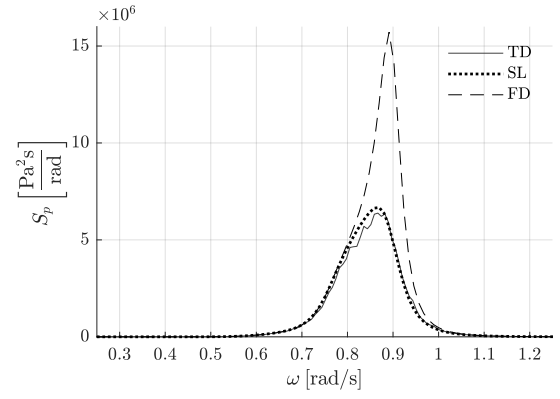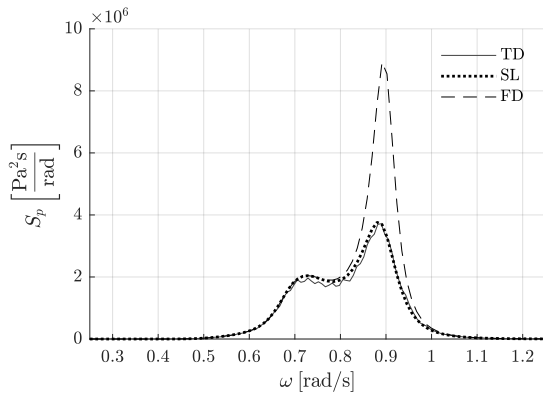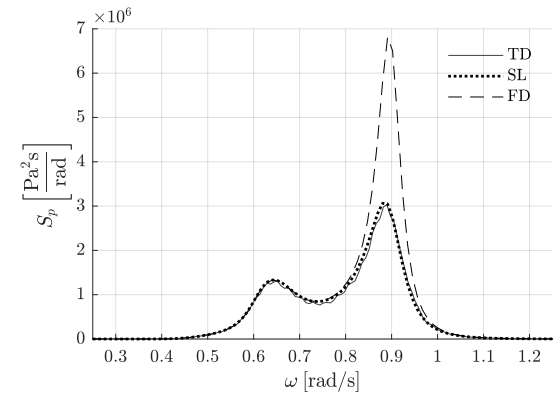
(b) 2^{nd}condition: $H_s = 1.75m; T_p = 8s$

(c) 3^{rd}condition: $H_s = 1.75m; T_p = 9s$

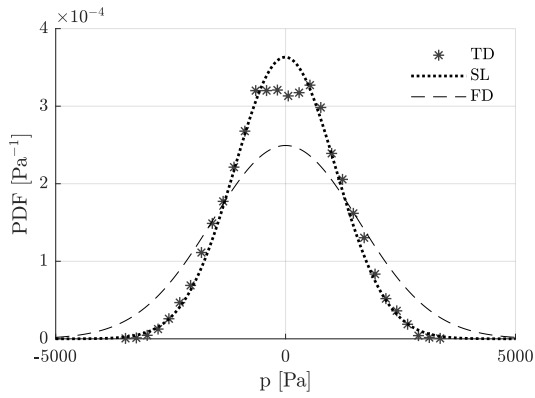(d) 4^{th}condition: $H_s = 1.75m; T_p = 10s$
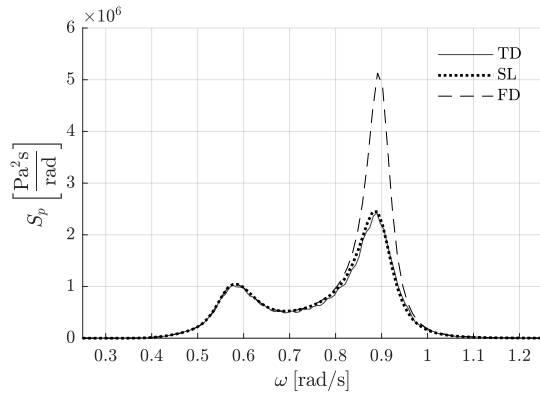
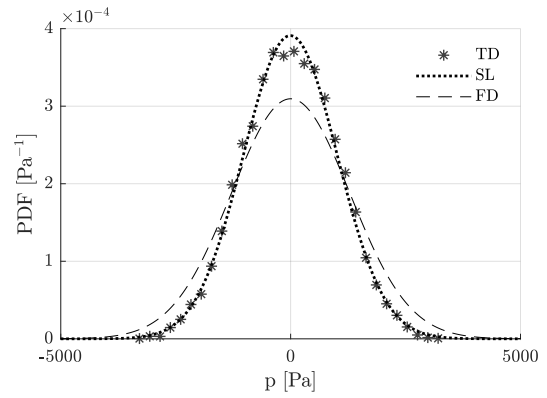(e) 5^{th}condition: $H_s = 1.75m; T_p = 11s$
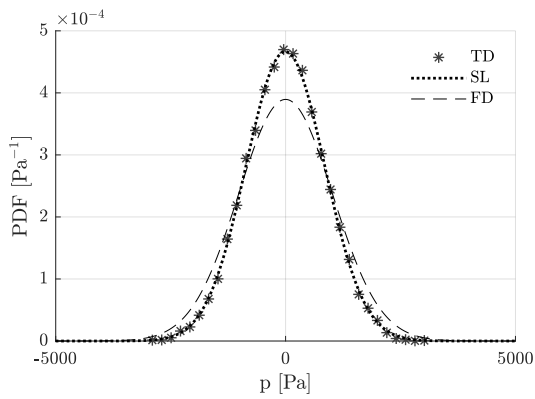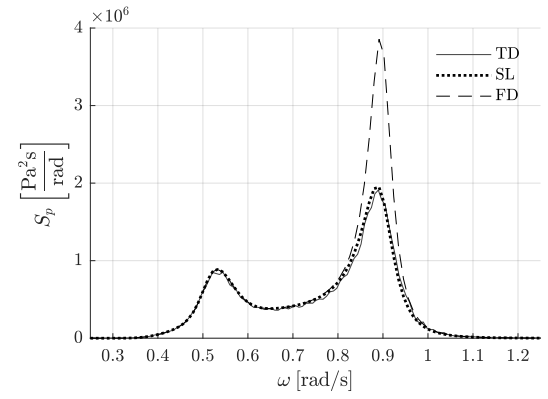
(f) 6^{th}condition: $H_s = 1.75m; T_p = 12s$

Figure 5.10: Spectral response of the pressure inside the chamber.

● **Power Absorbed and Dissipated:**

The power absorbed by the air turbine was computed based on the dimensionless parameters of the turbine described in Figure 5.3 and Equation (5.24) for the TD simulation and Equation (5.37) for the SL results. The power dissipated by the viscous flow effects at the mouth of the OWC structure were calculated based on Equations (4.35) and (4.36). Figure 5.11 shows the power absorbed and dissipated by the OWC.
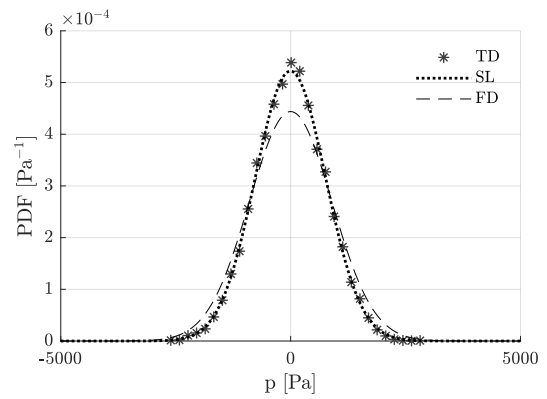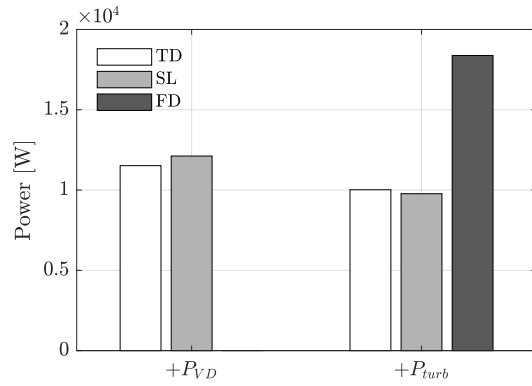

(a) 1^{st}condition: $H_s = 1.75m; T_p = 7s$
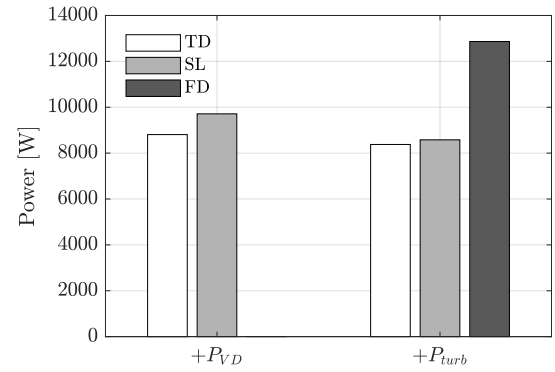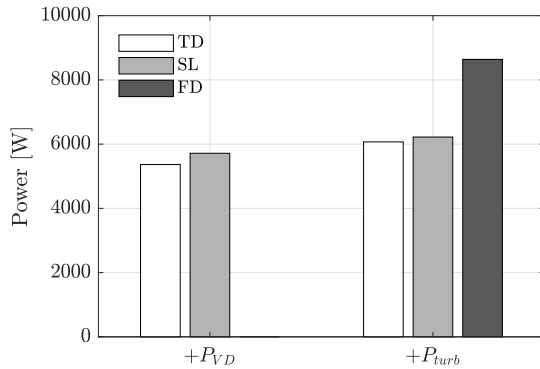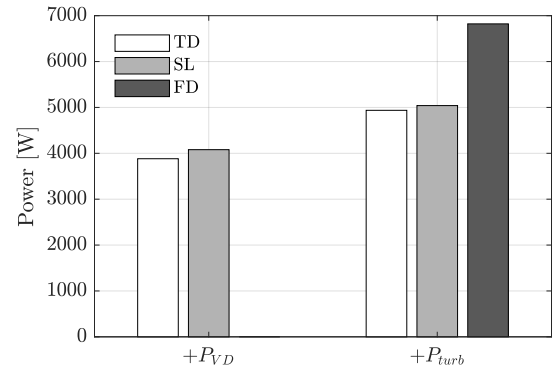
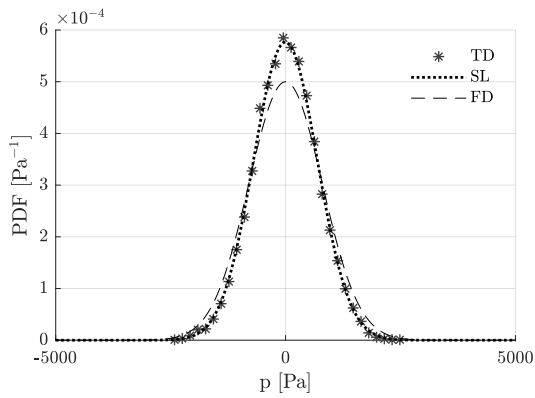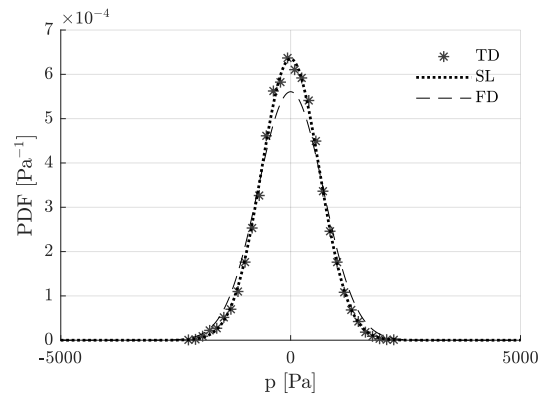(b) 2^{nd}condition: $H_s = 1.75m; T_p = 8s$

(c) 3^{rd}condition: $H_s = 1.75m; T_p = 9s$

(d) 4^{th}condition: $H_s = 1.75m; T_p = 10s$
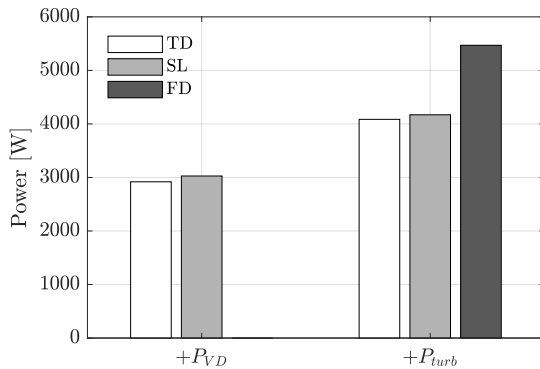
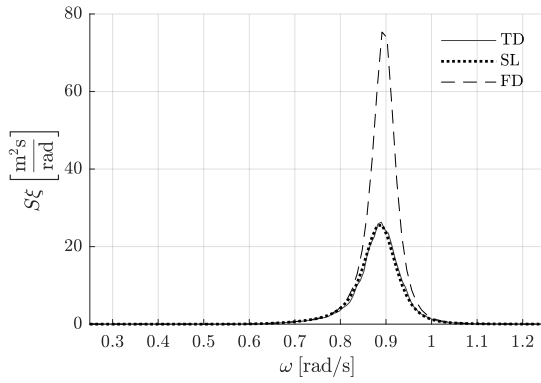(e) 5^{th}condition: $H_s = 1.75m; T_p = 11s$
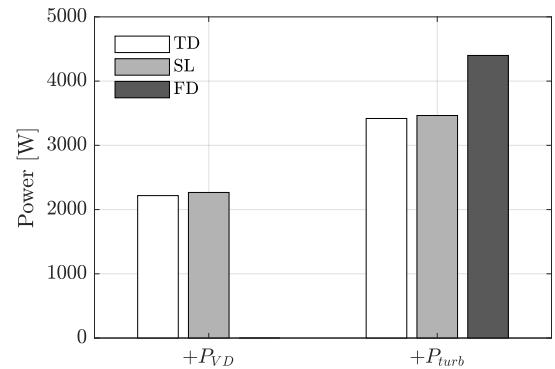
(f) 6^{th}condition: $H_s = 1.75m; T_p = 12s$

Figure 5.11: Power absorbed and dissipated - OWC

- **Mean Offsets:**

The SL technique is able to estimate the mean variables of the system, which for the pressure and water column displacement are based on Equations (5.33) and (5.34). Figure 5.12 shows the mean values for all sea states using SL and nonlinear TD simulations.
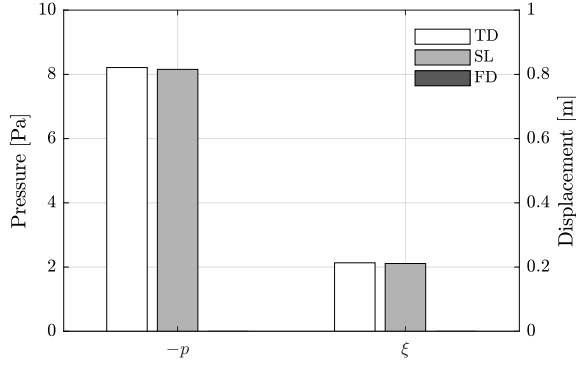
(a) 1^{st}condition: $H_s = 1.75m; T_p = 7s$
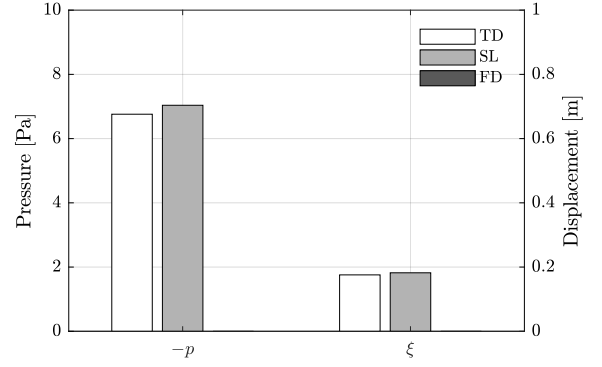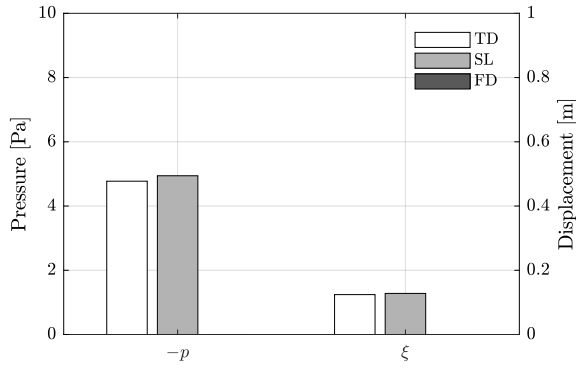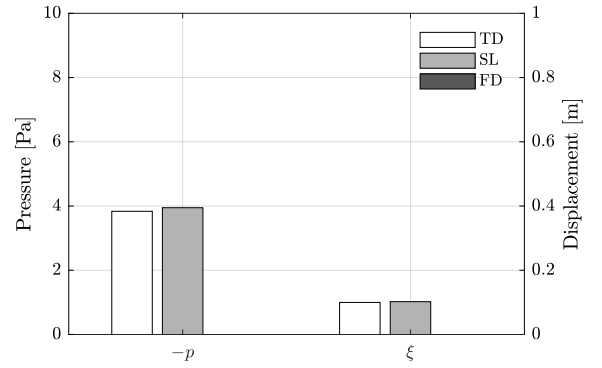
(b) 2^{nd}condition: $H_s = 1.75m; T_p = 8s$

(c) 3^{rd}condition: $H_s = 1.75m; T_p = 9s$

(d) 4^{th}condition: $H_s = 1.75m; T_p = 10s$
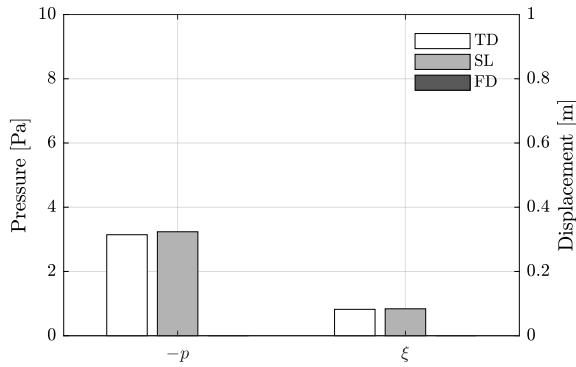
(e) 5^{th}condition: $H_s = 1.75m; T_p = 11s$
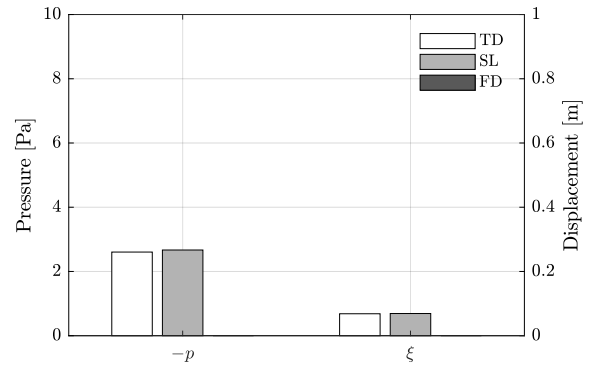
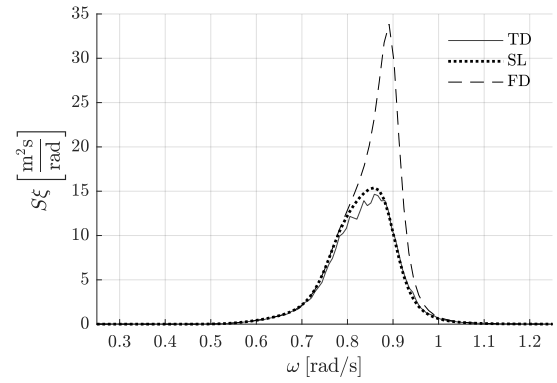(f) 6^{th}condition: $H_s = 1.75m; T_p = 12s$

Figure 5.12: Mean pressure and mean water column displacement - OWC

- **Capture Width Ratio:**

The efficiency of the OWC wave energy device is obtained based on the CWR. However, like the PA case, the device is not set to operate in its highest efficiency for power production, and an optimization procedure must be conducted to have a better estimation of the device efficiency. Table 5.2 shows the CWR of the OWC WEC considering a 3m width for all sea states investigated.

Table 5.2: Capture Width Ratio of the OWC using SL.

Condition	$\bar{P}_{wave}$ [kW]	$\bar{P}_{turb}$ [kW]	CWR [%]
$1^{st}: H_s = 1.75m; T_p = 7s$	9.46	9.76	34.40
$2^{nd}: H_s = 1.75m; T_p = 8s$	11.17	8.42	25.14
$3^{rd}: H_s = 1.75m; T_p = 9s$	12.92	6.15	15.88
$4^{th}: H_s = 1.75m; T_p = 10s$	14.64	5.00	11.39
$5^{th}: H_s = 1.75m; T_p = 11s$	16.27	4.14	8.49
$6^{th}: H_s = 1.75m; T_p = 12s$	17.77	3.44	6.46

- **Simulation time**

As stated previously, the main advantage of the SL is the low computational cost compared to TD simulations. In general, the SL technique converged in approximately 7 iterations for the OWC. The TD model required long periods of simulation to assume the ergodicity as valid, and also different wave phase components, which resulted in high computational cost compared to the SL technique. Table 5.3 shows the simulation time for each model. Note that the FD results denote the linear model.

Table 5.3: Simulation time - OWC.

	TD	SL	FD
Time:	185.5 [s]	0.1035 [s]	0.0072 [s]

5.5 Discussion

For the OWC case, the natural frequency depends only on the draft. Therefore, in order to increase the natural period of the water column, the nominal draft must increase. However, as the draft increases, the wave excitation force decays rapidly, exponentially for deep waters. Hence, the natural period was set to be inferior to the dominant period of the sea state.

For a 2 DOF system, the response distribution can be represented by a joint PDF $(\xi,\ p)$. However, the marginal PDFs were chosen to facilitate the visualization of the results. In general, despite the nonlinearities in the governing equations, the TD results were comparable to the theoretical Gaussian distribution using SL for all cases simulated, preserving the standard deviation and mean values, as observed in Figures 5.7 and 5.8. The main differences occurred at the peak of the response distribution when the incoming waves matched was next to the natural frequency of the water column, which resulted in large nonlinearities.

The SL and the nonlinear TD simulation obtained comparable results in terms of PSD, where the energy in each frequency component was correctly estimated, as shown in Figures 5.9 and 5.10. In Figure 5.10 (c) to (f), the first peak in the spectral response occurs due to the peak in the excitation force, while the second peak occurs due to the natural frequency of the water column. Note that the FD overestimates the response of the second peak due to the viscous drag term. This reduction in the peak is essential to have a better estimation of the response, as the device is usually set to operate in this region.

The mean power dissipated by the viscous drag and mean power absorbed by the air turbine were well captured using SL compared to the TD simulation, while the FD model overestimates the power absorbed by the air turbine and is not able to predict the power dissipated by the viscous drag force (see Figure 5.11). The SL technique was also able to capture accurately the mean values of pressure inside the chamber and water column displacement (see Figure 5.12). Depending on the OWC draft, the mean water column displacement can change the peak of the spectrum due to the equivalent linear mass term.

The nonlinear effects are enlarged close to the resonance due to the large displacements and pressures. In this region, the device achieves the best performance, around 34.40%, (see Table 5.2). However, as the device was not optimized, an optimization procedure must be performed for further investigations of the device efficiency. In addition, the

efficiency must consider the overall performance of the OWC, which uses the efficiency for all sea states and its probability of occurrence. This can be accomplished using the SL as a tool for fast and reliable estimation of the system response.

PART IV

CONCLUSION

6 CONCLUSION

This work investigated the nonlinear stochastic analysis of two conceptually different WECs with distinct nonlinear terms using SL. The technique consists in minimizing the difference between the equivalent linear and nonlinear dynamic equation of motion using an iterative procedure and relies on the Gaussian assumption of the underlying system response stochastic process. As an initial procedure, the response distribution was verified for both devices to check the assumption of a Gaussian distribution. This procedure must be performed before the application of the SL. In general, even though the two wave energy devices investigated have several nonlinearities, the response distributions were comparable with the theoretical Gaussian distribution. This distribution was expected due to the Gaussian excitation and the non-dominant nonlinear terms in the governing equation. Therefore, the SL technique can be applied to the cases illustrated.

The SL results were compared against nonlinear TD simulations to verify the reliability of the method, and FD results were used as a basis to verify the influence of the nonlinearities. The results have shown a good agreement between TD and SL for the nonlinearities and parameters considered of the WECs. Each nonlinearity behaved distinctly in the system dynamics, and their contributions were well captured by the equivalent linear system (SL) via the work done, power dissipated or absorbed, and mean offsets. The results have shown a considerable discrepancy with the traditional FD, which demonstrates the importance of including the nonlinear effects on the system dynamics.

Like other numerical codes, the verification and validation of the SL must be performed. This work verified the reliability of the method by comparing with nonlinear TD simulations. However, for future studies, the validation of the numerical code against experimental results must be performed. The experimental results can also be used to correct some parameters of the simulations, such as the viscous drag coefficient, wave reflection (OWC), and so on. Furthermore, experimental results can also be used to better represent the PTO mechanism, such as the electric generator, air turbine aerodynamics, and the tether.

Typically, the SL converged in a few iterations, around 5 for the PA and 7 for the OWC. The time required for the TD simulations of the nonlinear system was high to assume valid the hypothesis of ergodicity. As a result, the SL was in general 3 to 4 orders of magnitude faster, while producing comparable results. Therefore, this technique can be useful for optimization procedures and WEC farms analysis, which can facilitate the development of this technology.

The efficiency of the devices was computed for a range of each sea states with a high probability of occurrence in Imbituba (SC), Brazil. However, the devices were not optimized. For further works, the optimization considering all sea states and their probability of occurrence must be evaluated for a more realistic estimation of the device's efficiency in the specific site location.

REFERENCES

[1] BP. *Statistical review of world energy June 2017*. 2017.

[2] BOYLE, G. *Renewable energy: Power for a sustainable future*. Third. [S.l.]: Oxford University Press, 2012.

[3] KIEFFER, G.; COUTURE, T. D. Renewable energy target setting. *IRENA*, 2015.

[4] DREW, B.; PLUMMER, A. R.; SAHINKAYA, M. N. *A review of wave energy converter technology*. [S.l.]: Sage Publications Sage UK: London, England, 2009.

[5] PECHER, A.; KOFOED, J. P. *Handbook of ocean wave energy*. [S.l.]: Springer, 2017.

[6] CRUZ, J. *Ocean wave energy: current status and future prespectives*. [S.l.]: Springer Science & Business Media, 2007.

[7] FALNES, J. A review of wave-energy extraction. *Marine Structures*, Elsevier, v. 20, n. 4, p. 185–201, 2007.

[8] PELC, R.; FUJITA, R. M. Renewable energy from the ocean. *Marine Policy*, Elsevier, v. 26, n. 6, p. 471–479, 2002.

[9] CLÉMENT, A.; MCCULLEN, P.; FALCÃO, A.; FIORENTINO, A.; GARDNER, F.; HAMMARLUND, K.; LEMONIS, G.; LEWIS, T.; NIELSEN, K.; PETRONCINI, S. et al. Wave energy in europe: current status and perspectives. *Renewable and sustainable energy reviews*, Elsevier, v. 6, n. 5, p. 405–431, 2002.

[10] MCCORMICK, M. E. *Ocean wave energy conversion*. [S.l.]: Courier Corporation, 2013.

[11] ANTONIO, F. O. Wave energy utilization: A review of the technologies. *Renewable and sustainable energy reviews*, Elsevier, v. 14, n. 3, p. 899–918, 2010.

[12] FALCÃO, A. F.; HENRIQUES, J. C. Oscillating-water-column wave energy converters and air turbines: A review. *Renewable Energy*, Elsevier, v. 85, p. 1391–1424, 2016.

[13] MEDINA-LOPEZ, E.; ALLSOP, N.; DIMAKOPOULOS, A.; BRUCE, T. Conjectures on the failure of the owc breakwater at mutriku. In: *Proceedings of Coastal Structures and Solutions to Coastal Disasters Joint Conference, Boston, Massachusetts*. [S.l.: s.n.], 2015.

[14] BABARIT, A. A database of capture width ratio of wave energy converters. *Renewable Energy*, Elsevier, v. 80, p. 610–628, 2015.

[15] FALNES, J. *Ocean waves and oscillating systems: linear interactions including wave-energy extraction*. [S.l.]: Cambridge university press, 2002.

[16] SERGIIENKO, N. Y. *Three-Tether Wave Energy Converter: Hydrodynamic Modelling, Performance Assessment and Control.* Tese (Doutorado) — School of Mechanical Engineering, The University of Adelaide, February 2018.

[17] PECHER, A.; KOFOED, J. P. Introduction. In: *Handbook of Ocean Wave Energy.* [S.l.]: Springer, 2017. p. 1–15.

[18] KARIMIRAD, M. *Offshore energy structures: for wind power, wave energy and hybrid marine platforms.* [S.l.]: Springer, 2014.

[19] IWAN, W.; YANG, I.-M. Application of statistical linearization techniques to nonlinear multidegree-of-freedom systems. *Journal of Applied Mechanics,* American Society of Mechanical Engineers, v. 39, n. 2, p. 545–550, 1972.

[20] ROBERTS, J. B.; SPANOS, P. D. *Random vibration and statistical linearization.* [S.l.]: Courier Corporation, 2003.

[21] FOLLEY, M.; WHITTAKER, T. Spectral modelling of wave energy converters. *Coastal Engineering,* Elsevier, v. 57, n. 10, p. 892–897, 2010.

[22] TOM, N.; LAWSON, M.; YU, Y.-H.; WRIGHT, A. Spectral modeling of an oscillating surge wave energy converter with control surfaces. *Applied Ocean Research,* Elsevier, v. 56, p. 143–156, 2016.

[23] FOLLEY, M.; WHITTAKER, T. Preliminary cross-validation of wave energy converter array interactions. In: AMERICAN SOCIETY OF MECHANICAL ENGINEERS. *ASME 2013 32nd International Conference on Ocean, Offshore and Arctic Engineering.* [S.l.], 2013. p. V008T09A055–V008T09A055.

[24] GUNAWARDANE, P.; FOLLEY, M.; SANJAYA, S. Spectral-domain modelling of the non-linear hydrostatic stiffness of a heaving-sphere wave energy converter. In: *The 28th International Symposium on Transport Phenomena.* [S.l.: s.n.], 2017.

[25] SPANOS, P. D.; ARENA, F.; RICHICHI, A.; MALARA, G. Efficient dynamic analysis of a nonlinear wave energy harvester model. *Journal of Offshore Mechanics and Arctic Engineering,* American Society of Mechanical Engineers, v. 138, n. 4, p. 041901, 2016.

[26] FOLLEY, M.; WHITTAKER, T. Validating a spectral-domain model of an owc using physical model data. *International Journal of Marine Energy,* Elsevier, v. 2, p. 1–11, 2013.

[27] SPANOS, P. D.; STRATI, F. M.; MALARA, G.; ARENA, F. Stochastic dynamic analysis of u-owc wave energy converters. In: AMERICAN SOCIETY OF MECHANICAL ENGINEERS. *ASME 2017 36th International Conference on Ocean, Offshore and Arctic Engineering.* [S.l.], 2017. p. 1–8.

[28] SCIALÒ, A.; MALARA, G.; ARENA, F. Geometrical optimization of u-oscillating water columns in random waves. In: AMERICAN SOCIETY OF MECHANICAL ENGINEERS. *ASME 2019 38th International Conference on Ocean, Offshore and Arctic Engineering.* [S.l.], 2019.

[29] SILVA, L. S. P.; TANCREDI, T. P.; DING, B.; SERGIIENKO, N.; MORISHITA, H. M. Fully submerged point absorber in Santa Catarina, Brazil - a feasibility study. In: *24th ABCM International Congress of Mechanical Engineering (COBEM 2017)*. [S.l.: s.n.], 2017.

[30] SILVA, L. S. P.; MORISHITA, H. M.; PESCE, C. P.; GONÇALVES, R. T. Nonlinear analysis of a heaving point absorber in frequency domain via statistical linearization. In: AMERICAN SOCIETY OF MECHANICAL ENGINEERS. *ASME 2019 38th International Conference on Ocean, Offshore and Arctic Engineering*. [S.l.], 2019.

[31] SILVA, L. S. P.; PESCE, C. P.; MORISHITA, H. M.; GONÇALVES, R. T. Nonlinear analysis of an oscillating water column wave energy device in frequency domain via statistical linearization. In: AMERICAN SOCIETY OF MECHANICAL ENGINEERS. *ASME 2019 38th International Conference on Ocean, Offshore and Arctic Engineering*. [S.l.], 2019.

[32] GARRISON, T. S. *Oceanography: an invitation to marine science*. [S.l.]: Cengage Learning, 2012.

[33] HUNTLEY, D. *LE MÉHAUTÉ, B. 1976. An introduction to hydrodynamics and water waves. Springer-Verlag, New York, viii+ 323 p. 24.80.* [S.l.]: Wiley Online Library, 1977.

[34] PENALBA, M.; GIORGI, G.; RINGWOOD, J. V. Mathematical modelling of wave energy converters: a review of nonlinear approaches. *Renewable and Sustainable Energy Reviews*, Elsevier, v. 78, p. 1188–1207, 2017.

[35] NEWMAN, J. N.; LANDWEBER, L. *Marine hydrodynamics*. [S.l.]: American Society of Mechanical Engineers, 1978.

[36] JOURNÉE, J.; MASSIE, W.; HUIJSMANS, R. *Offshore Hydromechanics: Course OE4630*. [S.l.]: TU Delft, 2000.

[37] CHAKRABARTI, S. K. Hydrodynamics of offshore structures 1987. *Computational Mechanics*.

[38] WAVE energy resource along the coast of Santa Catarina (B.

[39] MULTON, B. *Marine renewable energy handbook*. [S.l.]: John Wiley & Sons, 2013.

[40] KAZAKOV, I. Generalization of the method of statistical linearization to multidimensional systems. *Automation and Remote control*, v. 26, p. 1201–1206, 1966.

[41] FOLLEY, M. *Numerical modelling of wave energy converters: State-of-the-art techniques for single devices and arrays*. [S.l.]: Academic Press, 2016.

[42] HULME, A. The wave forces acting on a floating hemisphere undergoing forced periodic oscillations. *Journal of Fluid Mechanics*, Cambridge University Press, v. 121, p. 443–463, 1982.

[43] MORISON, J.; JOHNSON, J.; SCHAAF, S. et al. The force exerted by surface waves on piles. *Journal of Petroleum Technology*, Society of Petroleum Engineers, v. 2, n. 05, p. 149–154, 1950.

[44] ERIKSSON, M.; WATERS, R.; SVENSSON, O.; ISBERG, J.; LEIJON, M. Wave power absorption: Experiments in open sea and simulation. *Journal of Applied Physics*, AIP, v. 102, n. 8, p. 084910, 2007.

[45] HENRIQUES, J.; PORTILLO, J.; GATO, L.; GOMES, R.; FERREIRA, D.; FALCÃO, A. Design of oscillating-water-column wave energy converters with an application to self-powered sensor buoys. *Energy*, Elsevier, v. 112, p. 852–867, 2016.

[46] FALCÃO, A. de O.; RODRIGUES, R. Stochastic modelling of OWC wave power plant performance. *Applied Ocean Research*, Elsevier, v. 24, n. 2, p. 59–71, 2002.

[47] MARTINS-RIVAS, H.; MEI, C. C. Wave power extraction from an oscillating water column at the tip of a breakwater. *Journal of Fluid Mechanics*, Cambridge University Press, v. 626, p. 395–414, 2009.

[48] PESCE, C. P.; CASETTA, L. Systems with mass explicitly dependent on position. In: *Dynamics of mechanical systems with variable mass*. [S.l.]: Springer, 2014. p. 51–106.

[49] PESCE, C. The application of Lagrange equations to mechanical systems with mass explicitly dependent on position. *Journal of Applied Mechanics*, American Society of Mechanical Engineers, v. 70, n. 5, p. 751–756, 2003.

[50] PESCE, C. P.; TANNURI, E. A.; CASETTA, L. The Lagrange equations for systems with mass varying explicitly with position: some applications to offshore engineering. *Journal of the Brazilian Society of Mechanical Sciences and Engineering*, SciELO Brasil, v. 28, n. 4, p. 496–504, 2006.

[51] NEWMAN, J. The interaction of stationary vessels with regular waves. In: *Proceedings of the 11th Symposium on Naval Hydrodynamics, London, 1976*. [S.l.: s.n.], 1976.

[52] BABARIT, A.; DELHOMMEAU, G. Theoretical and numerical aspects of the open source bem solver nemoh. In: *11th European Wave and Tidal Energy Conference (EWTEC2015)*. [S.l.: s.n.], 2015.

[53] ANSYS, A. *Theory manual*. [S.l.]: Release, 2014.

[54] LEE, C.-H. *WAMIT theory manual*. [S.l.]: Massachusetts Institute of Technology, Department of Ocean Engineering, 1995.

[55] CUMMINS, W. *The impulse response function and ship motions*. [S.l.], 1962.

[56] PEREZ, T.; FOSSEN, T. I. A Matlab toolbox for parametric identification of radiation-force models of ships and offshore structures. 2009.

APPENDIX A – FLUID-STRUCTURE INTERACTION

This Appendix deals with the fluid-structure interaction of floating and submerged structures. In this regard, the linear wave theory described previously is extended to capture the influence of the wave in the rigid body and vice-versa. The analysis and concepts of this chapter are fundamental to the development of this work.

A.1   Linear wave theory

Based on the derivations in section 2.2 and their respective boundary conditions (see in subsection 2.2.1), the linear wave theory can be extended to capture the fluid-structure interaction. In this regard, an additional boundary condition associated with the floating or submerged structure is included. Figure A.1 illustrates the fluid domain considered and their boundary conditions.
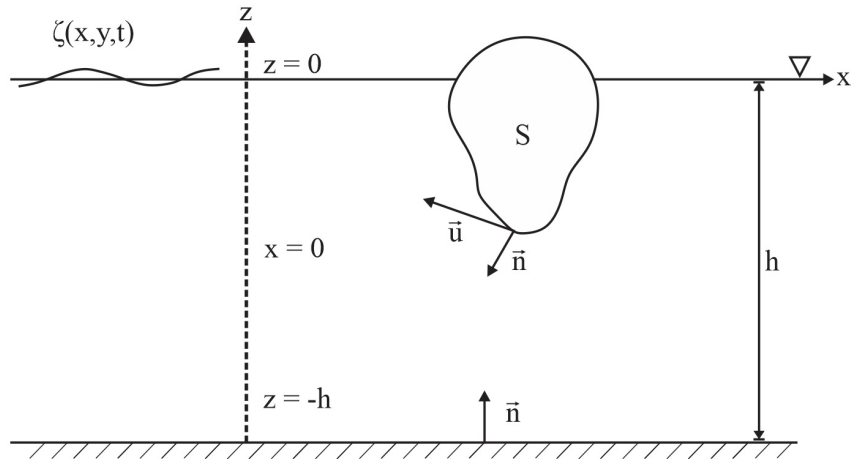

Figure A.1: Body boundary conditions, adapted from [15].

Like the seabed condition, the body surface is characterized by the impermeability condition. For a moving body surface with velocity $\vec{u}$, the fluid velocity normal to the

body surface must be equal to the body velocity [15]. Therefore, the following boundary condition must be satisfied:

$$\frac{\partial \Phi}{\partial n} = \vec{n} \cdot \vec{u}, \quad \text{on S.} \tag{A.1}$$

If the body is considered fixed, then:

$$\frac{\partial \Phi}{\partial n} = 0, \quad \text{on S.} \tag{A.2}$$

A more general velocity potential is defined in this chapter to describe the fluid-structure interaction. The linear wave theory permits to decompose the wave field into two components: radiated and scattered (wave and diffracted) [36].

$$\Phi(x, y, z, t) = \Phi_r + \underbrace{\Phi_w + \Phi_d}_{scattered}, \tag{A.3}$$

where Φ_r refers to the radiation potential from the oscillatory motion of the body considering still water, Φ_w denotes the incident undisturbed wave potential, Φ_d denotes the diffraction potential of the wave about the restrained fixed body.

A.1.1   Forces and Moments

The fluid-structure interactions generate loads in the immersed body due to the pressure from the surrounding fluid. These forces and moments are obtained by integrating the pressure over the submerged wetted area [51]:

$$\vec{F} = -\iint_S (p \cdot \vec{n}) \cdot dS, \tag{A.4}$$

$$\vec{M} = -\iint_S p \cdot (\vec{r} \times \vec{n}) \cdot dS, \tag{A.5}$$

where $\vec{n}$ is defined as the normal outward vector on surface dS, and the position vector of the surface is denoted as $\vec{r}$ in the $O(x, y, z)$ coordinate system.

The amplitude of the motion and velocities of the body are considered small enough to neglect second-order terms from Bernoulli's equation [36]. Therefore, the pressure can be written in terms of the linearized Bernoulli equation described in Eq. (2.4). Hence, the pressure can be written based on the velocity potential as:

$$p = p(x, y, z, t) \approx -\rho \frac{\partial \Phi}{\partial t} - \rho g z. \tag{A.6}$$

Based on the velocity potential in Eq. (A.3), the pressure is given by:

$$p = -\rho \left(\frac{\partial \Phi_r}{\partial t} + \frac{\partial \Phi_w}{\partial t} + \frac{\partial \Phi_d}{\partial t} \right) - \rho g z. \tag{A.7}$$

Therefore, the resulting forces and moments acting on the surface of the rigid body are given by:

$$\vec{F} = \rho \iint_S \left(\frac{\partial \Phi_r}{\partial t} + \frac{\partial \Phi_w}{\partial t} + \frac{\partial \Phi_d}{\partial t} + g z \right) \vec{n} \cdot dS, \tag{A.8}$$

$$\vec{M} = \rho \iint_S \left(\frac{\partial \Phi_r}{\partial t} + \frac{\partial \Phi_w}{\partial t} + \frac{\partial \Phi_d}{\partial t} + g z \right) \cdot (\vec{r} \times \vec{n}) \cdot dS, \tag{A.9}$$

or:

$$\vec{F} = \vec{F}_r + \vec{F}_w + \vec{F}_d + \vec{F}_s, \tag{A.10}$$

$$\vec{M} = \vec{M}_r + \vec{M}_w + \vec{M}_d + \vec{M}_s, \tag{A.11}$$

where the subscript r denotes the radiated waves from the oscillating body, which considers still water; w denotes the incident waves; d denotes the diffracted waves of the body, which assumes the body fixed; and the s denotes the hydrostatic buoyancy of the body in still water.

- **Radiation Loads**

Radiation loads refer to the forces experienced by the body due to its own oscillatory movement, which radiate waves. In this regard, radiation boundary condition states that as the distance from the oscillating body increases significantly, the potential tends to zero [36]. This boundary condition is valuable for the Green's Second Theorem.

$$\lim_{R \to \infty} \Phi_r = 0. \tag{A.12}$$

The radiation potential is not influenced by the incident wave field. However, some relationships between the radiation and the wave pressure can be established via Haskind relations [35]. The radiation force and moment are given by:

$$\vec{F}_r = \rho \iint_S \left(\frac{\partial \Phi_r}{\partial t} \right) \vec{n} \cdot dS, \tag{A.13}$$

$$\vec{M}_r = \rho \iint_S \left(\frac{\partial \Phi_r}{\partial t} \right) \cdot (\vec{r} \times \vec{n}) \cdot dS. \tag{A.14}$$

The radiation potential, Φ_r, can be written in 6 components for each degree of freedom, and separated into spatial and temporal variables [36]:

$$\Phi_r(x,y,z,t) = \sum_{j=i}^{6} \phi_j(x,y,z) \cdot v_j(t). \tag{A.15}$$

The forces and moments can be written as:

$$\{\vec{F}_r; \vec{M}_r\} = \rho \iint_S \left(\frac{\partial}{\partial t} \sum_{j=i}^{6} \phi_j \cdot v_j \right) \frac{\partial \phi_k}{\partial n} \cdot dS, \tag{A.16}$$

or:

$$\{\vec{F}_r; \vec{M}_r\} = \frac{\partial v_j}{\partial t} \rho \iint_S \left(\sum_{j=i}^{6} \phi_j \frac{\partial \phi_k}{\partial n} \right) \cdot dS. \tag{A.17}$$

Due to the complex magnitude of the potential, the radiation forces and moments can be divided into two components, one in-phase with the acceleration, named hydrodynamic added mass; and one in-phase with the velocity, named hydrodynamic radiation damping [15]. The added mass and radiation damping are defined as:

$$M_{k,j} = -\Re e \left\{ \rho \iint_S \phi_j \frac{\partial \phi_k}{\partial n} .dS \right\}, \tag{A.18}$$

$$B_{k,j} = -\Im m \left\{ \rho \omega \iint_S \phi_j \frac{\partial \phi_k}{\partial n} .dS \right\}, \tag{A.19}$$

where the body oscillates in the direction j with a velocity potential ϕ_j. Considering body oscillations in the k direction with a velocity potential ϕ_k, the added mass and radiation damping are given by:

$$M_{j,k} = -\Re e \left\{ \rho \iint_S \phi_k \frac{\partial \phi_j}{\partial n} .dS \right\}, \tag{A.20}$$

$$B_{j,k} = -\Im m \left\{ \rho \omega \iint_S \phi_k \frac{\partial \phi_j}{\partial n} .dS \right\}. \tag{A.21}$$

The determination of the added mass and radiation damping coefficients analytically are restricted to simple geometries. Generally, those coefficients are solved numerically using boundary element methods (BEM) such as NEMOH[52], ANSYS AQWA[53], or WAMIT[54]. Those software solve the radiation and scattering problems based on Green's Second Theorem over the discretized wetted surface of the body.

- **Scattered Loads**

The wave and the diffraction potential in the hydrodynamic forces and moments can be treated simultaneously. The wave component refers to the undisturbed wave potential, which was derived in chapter 2. However, the diffraction potential must be determined. The wave contribution is associated with the Froude-Krylov force [6]. For cases where the structure has a small length compared to the wavelength, the diffraction component can be neglected. The scattered loads are given by:

$$\vec{F}_w + \vec{F}_d = \rho \iint_S \left(\frac{\partial \phi_w}{\partial t} + \frac{\partial \phi_d}{\partial t} \right) \vec{n} \cdot dS, \tag{A.22}$$

$$\vec{M}_w + \vec{M}_d = \rho \iint_S \left(\frac{\partial \phi_w}{\partial t} + \frac{\partial \phi_d}{\partial t} \right) \cdot (\vec{r} \times \vec{n}) \cdot dS. \tag{A.23}$$

Based on the principle of linear superposition, the determination of these loads is defined considering the body fixed in its nominal position. Therefore, the potential must satisfy the kinematic boundary condition of the body surface:

$$\frac{\partial \Phi}{\partial n} = \frac{\partial \Phi_w}{\partial n} + \frac{\partial \Phi_d}{\partial n} = 0, \quad \text{on S}, \tag{A.24}$$

Rewriting the potentials based on a spatial and temporal dependent potentials:

$$\Phi_w(x, y, z, t) = \phi_w(x, y, z) e^{-i\omega t}, \tag{A.25}$$

$$\Phi_d(x, y, z, t) = \phi_d(x, y, z) e^{-i\omega t}. \tag{A.26}$$

From the boundary condition described in Eq. (A.24) follows:

$$\frac{\partial \phi_w}{\partial n} = -\frac{\partial \phi_d}{\partial n}, \quad \text{on S}. \tag{A.27}$$

Based on Eqs. (A.22) and (A.23) , the forces and moments can be written as:

$$\{\vec{F}_w + \vec{F}_d; \vec{M}_w + \vec{M}_d\} = -i\rho \, e^{-i\omega t} \iint_S (\phi_w + \phi_d) \frac{\partial \phi_k}{\partial n} \cdot dS, \tag{A.28}$$

where ϕ_k is the radiation potential in direction k. Using Green's second theorem and the boundary condition described in Eqs. (A.27) and (A.12), the diffraction potential can be

written based on the wave potential as:

$$\iint\limits_{S} \phi_d \frac{\partial \phi_k}{\partial n} dS = - \iint\limits_{S} \phi_k \frac{\partial \phi_w}{\partial n} dS. \tag{A.29}$$

This result leads to the Haskind relation [36]:

$$\{\vec{F}_w + \vec{F}_d; \vec{M}_w + \vec{M}_d\} = -i\rho \, e^{-i\omega t} \iint\limits_{S} \left(\phi_w \frac{\partial \phi_k}{\partial n} + \phi_k \frac{\partial \phi_w}{\partial n} \right) \cdot dS. \tag{A.30}$$

- **Hydrostatic Loads**

Hydrostatic loads can be distinguished into two components: the hydrostatic stiffness, and the buoyancy. The hydrostatic stiffness refers to the increase-decrease of buoyancy around its equilibrium position due to the variation of submerged volume. In the case of a submerged body, no hydrostatic stiffness occurs, and the buoyancy is constant. As the linear wave theory neglects the effect of the wave surface elevation, the hydrostatic loads are unrelated to the incident wave field. The hydrostatic loads are given by [36]:

$$\vec{F}_s = \rho g \iint\limits_{S} z\vec{n} \cdot dS, \tag{A.31}$$

$$\vec{M}_s = \rho g \iint\limits_{S} z(\vec{r} \times \vec{n}) \cdot dS. \tag{A.32}$$

A.1.2 Limitations of the linear theory

The Linear wave theory is grounded on the assumption of small wave steepness, and small amplitude and velocity of body oscillations. However, wave energy devices usually operate in severe wave conditions and in a resonant condition. The linear theory valid range is illustrated in Fig. A.2, which uses as parameters the wave height (H), the characteristic dimension of the body (D), and the wavelength (λ) [37]. For Regions I, III, and V, the ratio between the characteristic dimension of the body and the wavelength are small. Therefore, the body has a minor effect on the wave field, and wave diffraction is negligible. However, for higher ratios, the wave field is influenced by the body, and wave diffraction becomes relevant. When the values of the ratio H/D exceed the limits of the diffraction region (Region IV), the potential flow loads and viscous loads must be considered. At Region VI, viscous effects dominate the response, and the dynamics cannot be described via linear theory. Therefore, linear wave theory is valid for Regions II and IV.
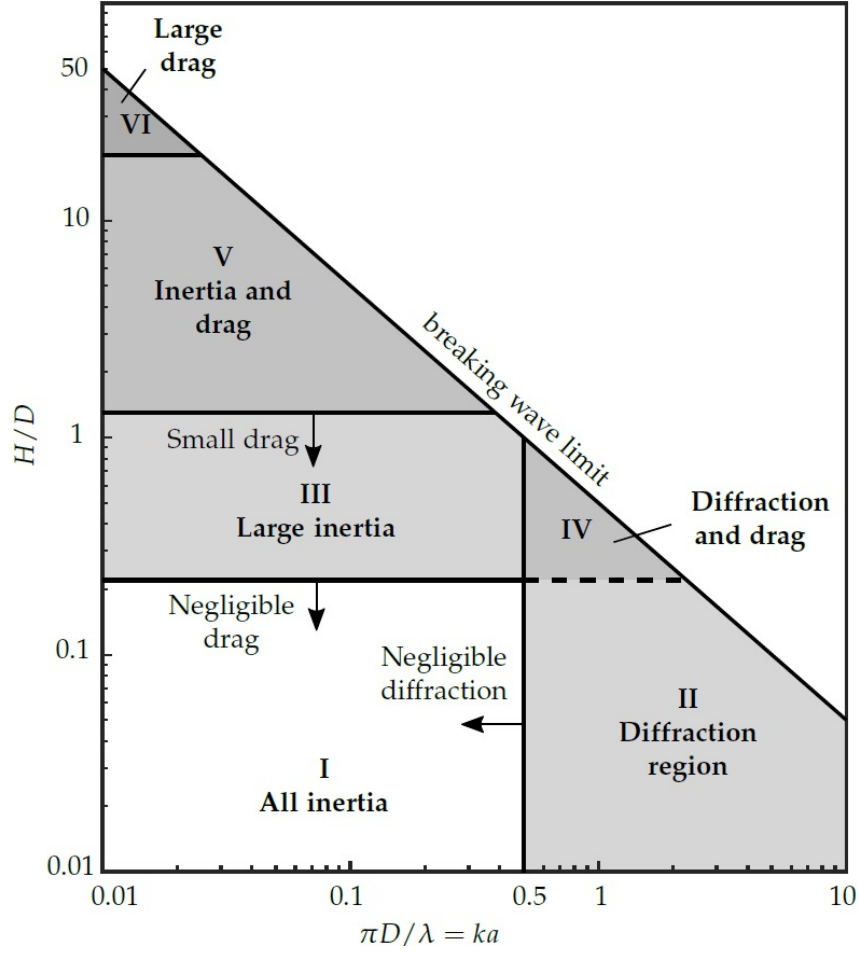
Figure A.2: Regions of importance for diffraction and viscous forces, adapted from [37].

Generally, the influence of viscous loads is determined by the Keulegan-Carpenter number, KC, given by [37]:

$$KC = \frac{u_0 T}{D},$$
(A.33)

where u_0 denotes the amplitude of the relative velocity between the body and fluid, and T is the period of the oscillation. Usually, for $KC > \pi$, viscous losses have a significant impact on system response.

APPENDIX B – TIME-DOMAIN MODELING

This Appendix deal with the hydrodynamic and hydrostatic forces of floating structures in TD.

B.1   Time-Domain Modeling

The modeling of floating rigid structures can be adequately described using 6 DOF, three translational modes (surge, sway, and heave), and three rotational modes (roll, pitch, and yaw). Figure B.1 illustrates the modes of motion for a typical PA. However, a common approach in the wave energy field is to describe the dynamics in the vertical plane of motion, or focused on a specific motion, such as heave, surge, or pitch [6].
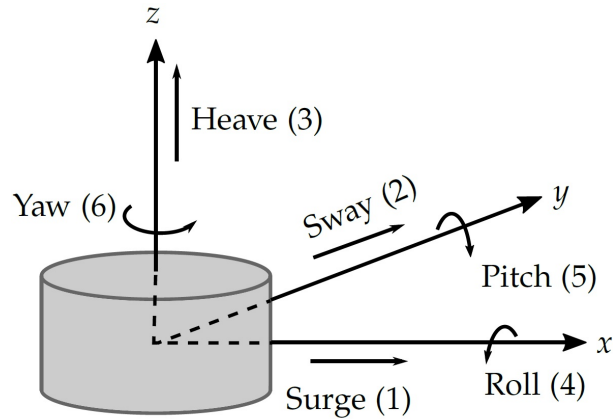

Figure B.1: Rigid body dynamics in 6 DOF [16].

The complete dynamic motion of the system can be written as:

$$\mathbf{M}\ddot{\mathbf{x}}(t) = \mathbf{F}_r(t) + \underbrace{\mathbf{F}_w(t) + \mathbf{F}_d(t)}_{\mathbf{F}_{exc}(t)} + \mathbf{F}_s(t) + \mathbf{F}_{visc}(t) + \mathbf{F}_{pto}(t), \qquad (\text{B.1})$$

where $\mathbf{M}$ denotes the inertia (mass) matrix defined by $\mathbf{M} \in R^{6 \times 6}$, $\mathbf{x}$ denotes the position vector defined by $\mathbf{x} \in R^{6 \times 1}$, and $\mathbf{F}_r(t), \mathbf{F}_w(t), \mathbf{F}_d(t), \mathbf{F}_s(t), \mathbf{F}_{visc}, \mathbf{F}_{pto}(t) \in R^{6 \times 1}$ are the radiated, wave, diffracted, hydrostatic, viscous, and PTO forces and moments acting on the body, and the excitation force $\mathbf{F}_{exc}(t)$ comprises the wave and diffracted forces. The hydrodynamic and hydrostatic forces in TD are given in the following subsections.

B.1.1   Radiation Loads

Radiation loads are usually described in FD as the magnitude of the load varies according to the frequency of oscillation. The FD representation of the radiation force is given by [15]:

$$\hat{\mathbf{F}}_r(\omega) = -\mathbf{A}(\omega)\hat{\ddot{\mathbf{x}}} - \mathbf{B}(\omega)\hat{\dot{\mathbf{x}}}, \tag{B.2}$$

where $\mathbf{A} \in R^{6 \times 6}$ is the matrix of hydrodynamic added mass, $\mathbf{B} \in R^{6 \times 6}$ is the hydrodynamic radiation matrix, $\hat{\dot{\mathbf{x}}}$ and $\hat{\ddot{\mathbf{x}}}$ are complex amplitudes of velocity and acceleration. The radiation force in the j mode due to body oscillations in the k direction is given by:

$$\hat{F}_{r,jk}(\omega) = -A_{jk}(\omega)\hat{\ddot{x}}_k - B_{jk}(\omega)\hat{\dot{x}}_k, \tag{B.3}$$

where j and $k = \{1, 2, ..., 6\}$.

In the TD, radiation loads are usually described by means of Cummins Equations given by [55]:

$$F_{r,jk}(t) = -A_{\infty,jk}\ddot{x}_k - \int_0^t k_{jk}(t - \tau)\dot{x}_k(\tau)d\tau, \tag{B.4}$$

where $A_{\infty,jk} = \lim_{\omega \to \infty} A_{jk}(\omega)$ is the infinite frequency hydrodynamic added mass, and k_{jk} denotes the retardation function, also known as the radiation impulse response.

The fluid memory term in Eq. (B.4) can be approximated to a state-space model [41]:

$$F_{fm}(t) = \int_0^t k_{jk}(t - \tau)\dot{x}_k(\tau)d\tau \approx \begin{aligned} \dot{\boldsymbol{q}}(t) &= \mathbf{A}_r\boldsymbol{q}(t) + \mathbf{B}_r\dot{x}_k(t) \\ F_{fm}(t) &= \mathbf{C}_r\boldsymbol{q}(t), \end{aligned} \tag{B.5}$$

where the body velocity $\dot{x}_k$ in the direction k is taken as input, and $\boldsymbol{q}$ is an auxiliary state vector without physical meaning. The approximate state space of the radiation force can be obtained using a MATLAB MSS FDI toolbox [56], which uses pre-calculated values of the radiation damping and added mass. This toolbox guarantees the convergence and quality of the fit by changing the order of the model.

In this work, the fluid memory term of the spherical floating PA is approximated to a state-space model of order 3 based on the hydrodynamic coefficients described in Figure 4.2. The space-state results are given by:

$$A = \begin{bmatrix} -1.449 & -1.496 & -0.114 \\ 1 & 0 & 1 \\ 0 & 1 & 0 \end{bmatrix},$$ (B.6)

$$B = \begin{bmatrix} 1 \\ 0 \\ 0 \end{bmatrix},$$ (B.7)

$$C = \begin{bmatrix} 1.378e5 & 1.495e4 & 0 \end{bmatrix}.$$ (B.8)

B.1.2 Excitation Loads

The excitation forces and moments comprise the wave and the diffraction contributions, which according to the linear theory is dependent on the surface elevation. The force can be represented in the FD as [41]:

$$\hat{F}_{exc,j}(\omega) = \hat{H}_{F_j}(\omega)\hat{\zeta}_a(x_0, y_0, \omega),$$ (B.9)

where $\hat{H}_{F_j}$ is the force response amplitude operator in the mode j, (x_0, y_0) is the reference point which coincides with the body mean position or the projection of the center of mass on the water plane.

Even though the TD equivalent force can be written by convolution operation based on the surface elevation, this work uses the excitation force as an input signal. Based on the power spectrum density of the wave, the complex amplitude of the surface elevation can be written as:

$$\hat{\zeta}_a(\omega_k) = \sqrt{2S_\zeta(\omega_k)\Delta\omega_k} \, e^{i\theta_\zeta(\omega_k)},$$ (B.10)

where θ_ζ is a phase angle obtained from real data or generated randomly based on a uniform distribution within $[0, 2\pi]$ radians. The complex wave amplitude is fed into the complex amplitude of the wave excitation by:

$$\hat{F}_{exc,j}(\omega_k) = \hat{H}_{F_j}(\omega_k)\hat{\zeta}_a(\omega_k),$$ (B.11)

and the input force in TD composed of N frequencies is given by [41]:

$$F_{exc,j}(t) = \sum_{k=1}^{N} \Re e \left\{ \hat{F}_{exc,j}(\omega_k) e^{i\omega_k t} \right\}. \tag{B.12}$$

B.1.3 Hydrostatic Loads

The hydrostatic loads are independent of the incident wave field. Therefore, the pressure field is caused due to the water column pressure. Applying the Gauss theorem in Eq. (A.31), it follows:

$$\vec{F}_s = \rho g \iiint\limits_{V} (\nabla z) dz = \rho g V \vec{k}, \tag{B.13}$$

where V denotes the volume of water displaced by the structure. This force is associated with the buoyancy component of the hydrostatic force.

The hydrostatic stiffness is obtained via Gauss theorem considering small displacements around the equilibrium position. Considering the case where the center of mass is located at the reference system, the hydrostatic loads are written in the TD as:

$$\mathbf{F}_s(t) = \mathbf{K}_s \mathbf{x}(t), \tag{B.14}$$

where the non-null terms of the hydrostatic stiffness matrix, $\mathbf{K}_s$, are given by:

$$\begin{aligned}
K_{s,33} &= -\rho g A_w \\
K_{s,44} &= -mg(z_b + S_{22}/V) \\
K_{s,55} &= -mg(z_b + S_{11}/V),
\end{aligned} \tag{B.15}$$

where the hydrostatic stiffness $\mathbf{K}_s \in R^{6\times 6}$, A_w denotes the cross-sectional area of the structure at the water plane, z_b is the distance from the center of buoyancy, S_{11} and S_{22} are the second moment of area, given by:

$$S_{11} = \iint\limits_{Aw} x^2 dS, \tag{B.16}$$

$$S_{22} = \iint\limits_{Aw} y^2 dS. \tag{B.17}$$